論文 / 著書情報
Article / Book Information

題目(和文)	
Title(English)	Study on Enhancement Mechanism of Thermal Conductivity in Main Main -Chain Liquid Crystalline Polyesters and their Composites
著者(和文)	吉原秀輔
Author(English)	Syusuke Yoshihara
出典(和文)	学位:博士(工学), 学位授与機関:東京工業大学, 報告番号:甲第9276号, 授与年月日:2013年9月25日, 学位の種別:課程博士, 審査員:渡辺 順次,芹澤 武,安藤 慎治,森川 淳子,戸木田 雅利
Citation(English)	Degree:Doctor (Engineering), Conferring organization: Tokyo Institute of Technology, Report number:甲第9276号, Conferred date:2013/9/25, Degree Type:Course doctor, Examiner:,,,,
学位種別(和文)	博士論文
Type(English)	Doctoral Thesis

平成２５年度　学位論文

Study on Enhancement Mechanism of Thermal Conductivity in Main-Chain Liquid Crystalline Polyesters and their Composites

（主鎖型液晶性ポリエステルおよび複合材料の高熱伝導率発現機構に関する研究）

By

Shusuke Yoshihara

Department of Organic and Polymeric Materials,

Tokyo Institute of Technology, 2013

Acknowledgements

I would like to express my sincere gratitude to my advisor, Professor Junji Watanabe and Associate Professor Masatoshi Tokita, Tokyo Institute of Technology, for their constant guidance, stimulating discussion, and hearty encouragement throughout my doctoral program from 2010 to 2013. Never could this study have been completed without their supervision.

I also thank to Associate Professor Koichi Sakajiri, Assistant Professor Sungmin Kang, Ms. Mami Hida, and members of Prof. Watanabe's and Assoc. Prof. Tokita's laboratory for their useful advice, valuable suggestion, and kind help.

I would like to thank Dr. Kazuaki Matsumoto and Mr. Masashi Sakaguchi, managers of Frontier Materials Development Laboratories, Kaneka Corporation, for their kind supports throughout my doctoral program.

Help from my colleagues of Frontier Materials Development Laboratories, Shoji Ubukata, Toshiaki Ezaki, and Mitsuru Nakamura, has been irreplaceable.

Eminently worthy of thanks is Masayuki Honda at Kaneka Techno Research for assisting with observations of materials. Never could this study have been completed without his assistance.

Finally, I express my heartfelt thanks to my wife, my son, my daughter, my parents and my parents-in-law for their continuous supports and encouragements.

September, 2013

Shusuke Yoshihara

Table of Contents

Chapter 1

General Introduction for Thermally Conductive Polymers

Chapter 2

Identifying Smectic I Phase of Main-Chain PB-10 Polyester Consisting of 4,4′-Biphenol and 1,10-Dodecanoic acid by Fibre X-ray Diffraction

Chapter 3

Enhanced Thermal Conductivity of Thermoplastics by Lamellar Crystal Alignment of Polymer Matrices

Chapter 4

Influence of Molecular Orientation Direction on the In-plane Thermal Conductivity of Polymer/Hexagonal Boron Nitride Composites

Chapter 5

Main-Chain Smectic Liquid Crystalline Polymer Exhibiting Unusually High Thermal Conductivity in an Isotropic Composite

Chapter 6

General Conclusion

List of Publications

Chapter 1

General Introduction for Thermally Conductive Polymers

1. Introduction

The continuous increase in power outputs along with the reduction of overall size of components in the computer, microelectronics, lighting, automotive and aerospace industries have resulted in the need for materials with multifunctional properties. These materials are desired to have thermal, electrical, and mechanical properties that are suitable for the application-specific electronic components to provide higher efficiency without compromising their performance. The high power density of electronic components results in rapid heat generation. Therefore, it is necessary to dissipate heat away from the components sufficiently fast enough in order to keep their temperatures below critical values and prevent the device from permanent damage. Metal-based heat sinks and heat spreaders have conventionally been used to dissipate the excess heat and maintain the device's temperature to an acceptable value. Due to metal’s high mass-density, their uses are limited to heat sink applications for electronic components. Many portable systems such as laptop computers, mobile phones, and avionics require low mass-density to minimize the damaging stresses resulting from shock loads during

shipping and handling. In addition, a very common disadvantage of metals is that they are electrically conductive, which may not be suitable for many applications in electronic devices due to the possibility of having short-circuits. Therefore, thermally conductive, electrically insulating materials have attracted attention as useful substances for heat dissipation in electronic devices. Polymers are lightweight electrical insulators; however, their thermal conductivity (TC) is typically lower than those of other materials (0.1–0.5 W m^{-1} K^{-1})[1-3] because of strong phonon scattering by various defects,[4] (Table 1 and 2).

Table 1. TC of selected polymers[1]

Material	TC at 25°C [W m^{-1} K^{-1}]
Low density polyethylene (LDPE)	0.30
High density polyethylene (HDPE)	0.44
Polypropylene (PP)	0.11
Polystyrene (PS)	0.14
Nylon-6 (PA6)	0.25
Poly(butylene terephthalate) (PBT)	0.29
Polycarbonate (PC)	0.20
Polyetheretherketone (PEEK)	0.25
Polyphenylene sulfide (PPS)	0.30
Polyvinyl chloride (PVC)	0.19
Polyvinylidene difluoride (PVDF)	0.19
Poly(dimethylsiloxane) (PDMS)	0.25
Epoxy resin	0.19

Table 2. TC of selected materials[1]

Material	TC at 25°C [W m^{-1} K^{-1}]
Graphite	100~400 (in-plane)
Carbon black (CB)	6~174
Carbon Nanotubes (CNT)	2000~6000
Diamond	2000
PAN-based Carbon Fibre	8~70 (along the axis)
Pitch-based Carbon Fibre	530~1100 (along the axis)
Copper (Cu)	483
Silver (Ag)	450
Gold (Au)	345
Aluminum (Al)	204
Nickel (Ni)	158
Boron Nitride (BN)	250~300
Aluminum nitride (AlN)	200
Aluminum oxide (Al_2O_3)	20~29

For improving the TC of polymeric material, usually, polymer matrices are highly filled with the thermally conductive fillers like metal particles, ceramic particles and carbon-based materials. A continuous conductive network of particles throughout the matrix can improve the TC (Figure 1).

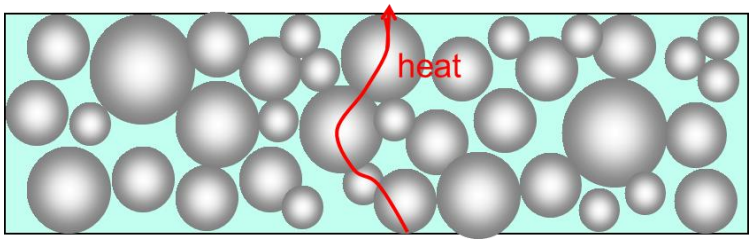

Figure 1. Thermally conductive polymer composites at high filler loading.

Polymer composites have a number of advantages, including their low mass-density and the ability to be injection molded into complex shapes with tight tolerances. Due to their multifunctionality, which includes enhanced TC, these composites are gaining traction in a number of markets such as aerospace, automotive, microelectronics, and thermal management industries.

One of the issues to develop the polymeric materials is difficulty for enhancing the composite TC even with large concentrations of thermally conductive fillers. Moreover, a high filler content leads to undesirable weight gain and poor processability. To solve these issues, a possible solution is to enhance the polymer matrix TC. However, no such matrices have been reported so far. A lot of researchers have tried to decrease percolation threshold using other techniques.

2. Literature survey for reduction of percolation threshold

2-1. Use of filler having high aspect ratio

The percolation threshold becomes extremely low when filler particles having high aspect ratio. Y-P. Sun and coworkers reported that carbon-nanosheet-based materials were used as fillers in polymeric nanocomposites that exhibited ultrahigh thermal conductivities.[5] For the epoxy nanocomposites with 33 vol% carbon nanosheets, the

in-plane TC value was close to 80 W m^{-1} K^{-1}, whereas the composites remained elastic (Figure 2a). In similar case, hexagonal boron nitride (h-BN) nanosheets were dispersed in epoxy matrices to give nanocomposite films with superior thermal transport performance.[6] The in-plane TC was higher than 30 W m^{-1} K^{-1} in the films with 50 vol% h-BN (Figure 2b). This technique is easy and enables to increase composite TC significantly, especially in the in-plane direction due to in-plane oriented filler particles.

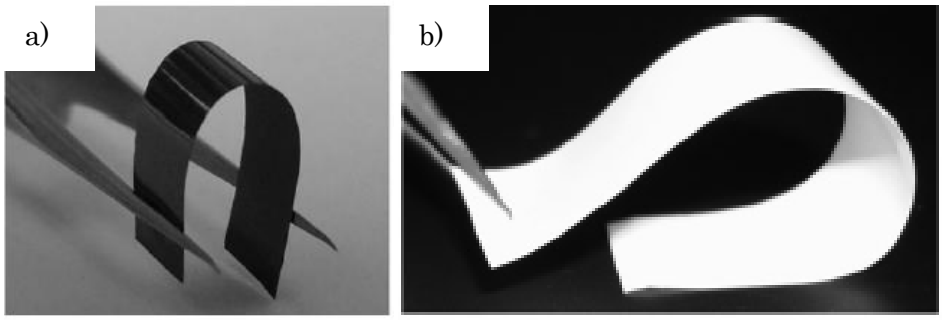

Figure 2. a) Photographs of an epoxy nanocomposite thin film (35 vol% carbon-nanosheet loading) showing that the film is still flexible (reprinted from Ref. [5]). b) Photoof a piece of film with 50% BN loading (reprinted from Ref. [6]).

2-2. Low melting point alloy-loaded polymer composite

Since the contact between filler particles in a composite is point contact, the heat pass between the particles is not efficient. To solve this issue, Y. Agari reported that low melting point alloy (LMPA) helped filler particles connect each other effectively (Figure

3).[7] The composite TC exhibits dramatic enhancement with small amount of LMPA loading, resulting in isotropic high TC of 28.5 W m^{-1} K^{-1}. This technique always leads to electrical conductive composites.

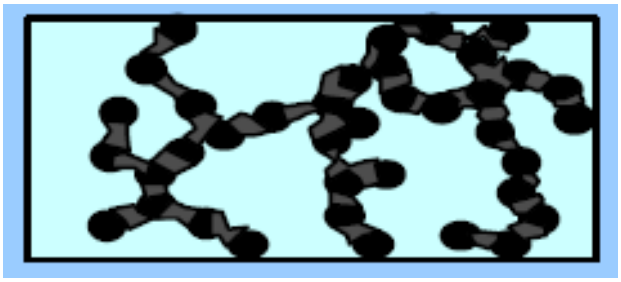

Figure 3. Heat conductive network formation using LMPA

Table 3. Effect of incorporation of LMPA

Composition	TC at 25°C [W m^{-1} K^{-1}]
Composition A	1.5
Composition A + LMPA	13.9
Composition A + LMPA + further filler loading	28.5

2-3. Double percolation technique

This technique has been used to lower the percolation threshold of electrical conductivity in conductive polymer hybrid materials.[8-10] S. Ando and coworker applied the technique to enhance TC of polymer composites.[11] Two-phase immiscible

polyimide blends, in which at least one phase is continuous, can be used as a polymer matrix, and conducting fillers are selectively and preferentially localized only in the continuous phase (Figure 4). The double percolation structures effectively function as ideal thermal conductive pathways. In polyimide/zinc oxide composite system (27.1 vol%), the largest TC value of 1.54 W m^{-1} K^{-1} was achieved in the out-of-plane direction. D. Yorifuji reported that combination with other techniques such as orientation of filler particles are required to further enhance TC.[12]

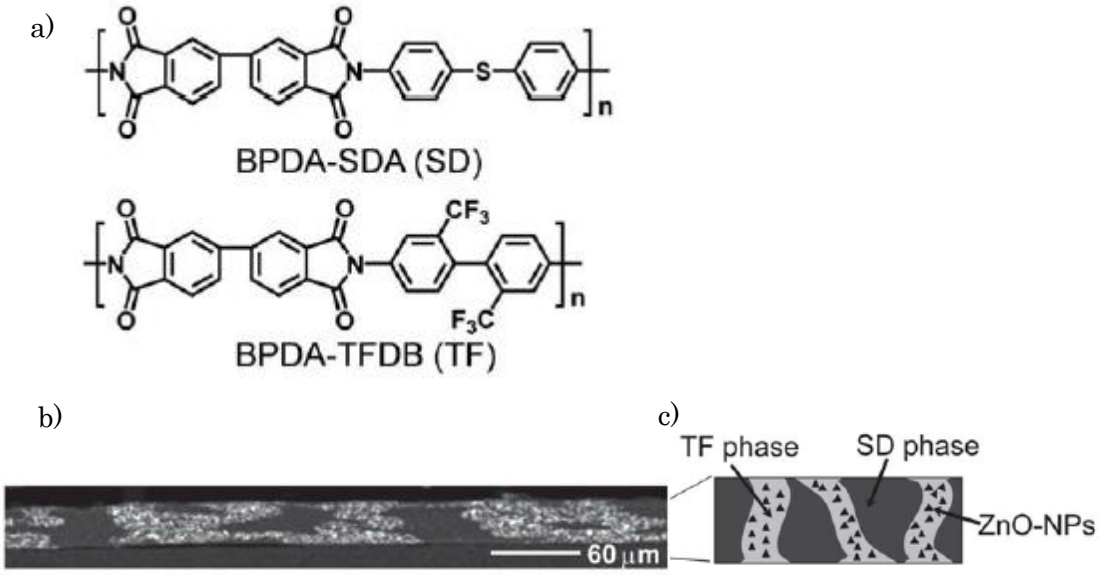

Figure 4. a) Polymer components for preparing PI blends: BPDA-SDA (SD) and BPDATFDB (TF). b) Cross-sectional SEM image observed by backscattering electron mode. c) Schematic representation of an ideal ‘‘vertical double percolation (VDP)’’ structure (reprinted from Ref. [11]).

3. Background for development of a thermally conductive polymer matrix

3-1. Bruggeman's theory

The equation of Bruggeman's theory[13] is given as

$$1-V=\frac{\lambda_c-\lambda_f}{\lambda_m-\lambda_f}\left(\frac{\lambda_m}{\lambda_c}\right)^{1/3} \quad (1)$$

where V is the volume fraction of the filler, λ_c, λ_f, and λ_m are the TCs (W m^{-1} K^{-1}) of the composite, filler, and polymer matrix, respectively. Figure 5 shows the relationship between the TC of the composite and the filler content at three different values of λ_m and λ_f: (λ_m, λ_f) = (0.2, 30); (0.2, 150); and (1, 30). To enhance the composite TC, Bruggeman's theory suggests that it is more effective to enhance the TC of polymer matrix than to enhance that of filler particles. In other word, the TC of polymer composites can be significantly increased when the polymer matrix serves as a good heat conductor between the filler particles. Such a thermally conductive matrix enables the production of polymer materials with (1) significantly high TC at a high filler loading or (2) higher TC than that of common thermoplastic composites at comparable loading levels.

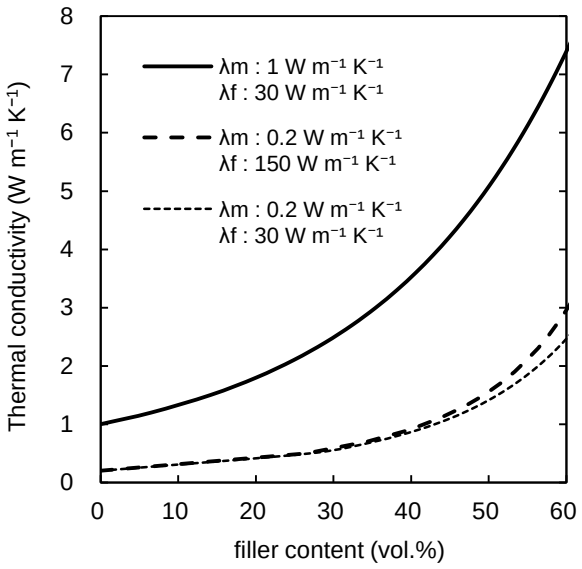

Figure 5. TC of polymer/filler composite calculated by Bruggeman's equation.

3-2. Low thermal conductivity of polymers

Heat conduction in insulating polymers is discussed in terms of the Debye equation:

$$\lambda = \frac{C_v u l}{3} \quad (2)$$

where λ is the thermal conductivity, C_v is the volumetric heat capacity, u is the sound velocity, and l is the mean free path of a phonon. For amorphous polymers, l is an extremely small constant (i.e. a few angstroms) due to phonon scattering from numerous defects, leading to a very low TC of polymers.

3-3. Influence of crystallinity on thermal conductivity

Polymer crystallinity strongly affects their TC, which roughly varies from 0.2 W m^{-1} K^{-1} for amorphous polymers such as polycarbonate (PC) or polystyrene (PS), to 0.5 W

m^{-1} K^{-1} for highly crystalline polymers as high-density polyethylene (HDPE). Previous papers revealed that the TC of HDPE increases with an increase in crystallinity.[3] Results suggest that thermal conduction occurs through the lattice vibrations (phonons) much more effectively in crystal phases than in amorphous regions, and it is also important to suppress phonon scattering caused by less ordered structures, various structural defects and interfaces between crystal and amorphous regions.

3-4. Literature survey

It is known that a polymer shows high TC along the molecular chain direction. Choy and co-workers reported that HDPE extended to 25 times the original length exhibited a TC of more than 10 W m^{-1} K^{-1} along the fiber axis and only 0.2 W m^{-1} K^{-1} in the vertical direction.[14] These results are due to the stronger covalent bonds within the molecular chain compared to the van der Waals forces between the chains. Recently, there are reports that a more extended HDPE nanofiber showed a TC of 104 W m^{-1} K^{-1} [15] and spider silk shows an anomalously high TC of 416 W m^{-1} K^{-1}, which is the same level as that of copper (Figure 6).[16] In addition, to get highly oriented polymers, some studies have focused on subjecting polymers in the molten state to a strong magnetic field.[17-20] Okamoto and co-workers reported that the TC of liquid crystalline polymers (LCP) themselves can be improved to more than 2.5 W m^{-1} K^{-1} (Figure 7).[20] These

findings indicate an important fact, that is, the TC mainly depends on the orientation order of molecule, not the molecular structure. Therefore, structual design for increasing TC of polymer should be for the ease of molecular orientation. In other words, the kind of covalent bond strength, weight of atoms and so on are not so important.

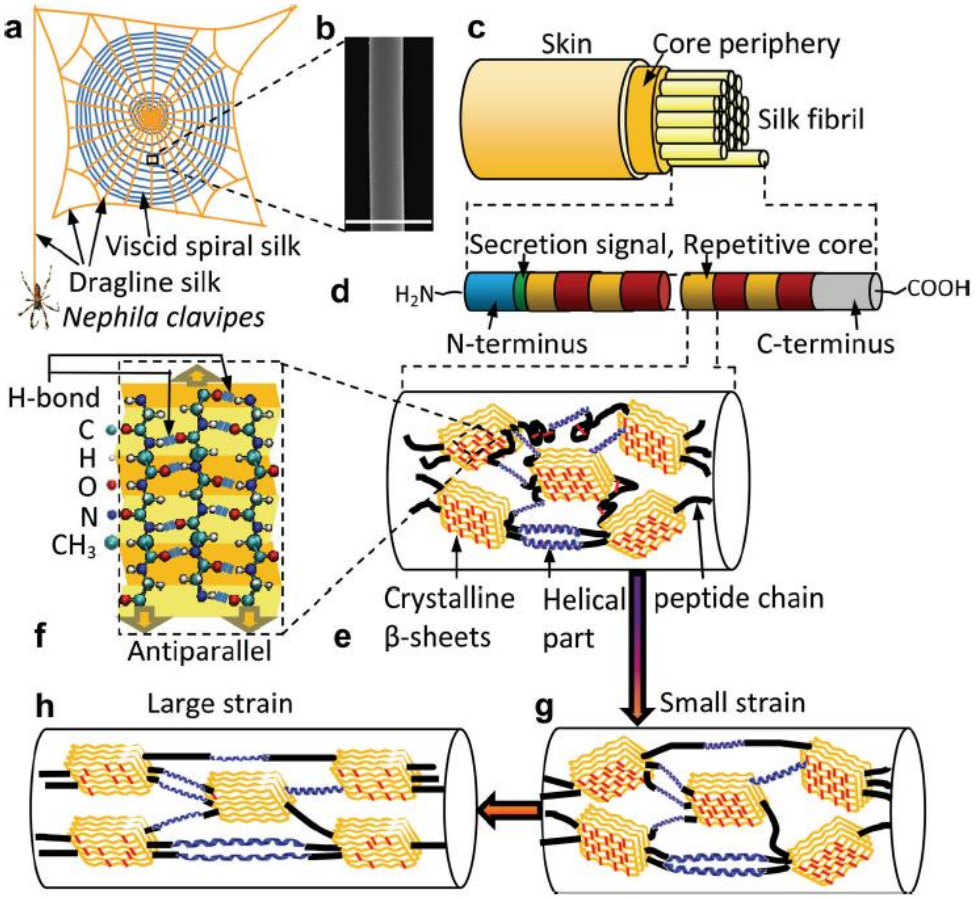

Figure 6. Spider silk, its unique hierarchical structure (reprented from Ref. [16]).

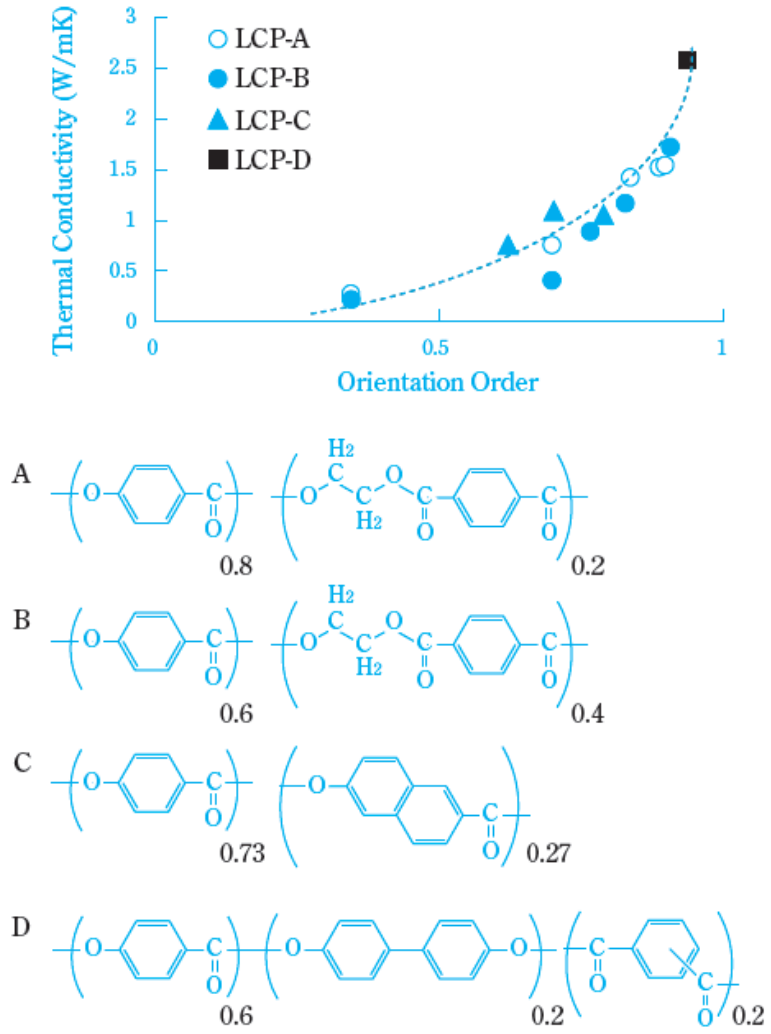

Figure 7. Relationship between orientation order of various LCP and thermal conductivity (reprinted from Ref. [20]).

Takezawa and co-worker reported that cured resins of phenyl benzoate twinmesogen-type bisepoxide compounds with 4,4-methylenedianiline show the highest TC values (0.85–0.96 W m^{-1} K^{-1}) among macroscopically isotropic polymeric materials, which depend on the central alkyl chain length (n = 4, 6 and 8) in the bisepoxides

(Figure 8).[21] These types of twin mesogen epoxy resins are known to preserve a smectic-like liquid crystalline (LC) structure at room temperature even after curing at the LC state.[22] The results suggest that the frozen LC-like ordered structures also function advantageously for effective thermal conduction.

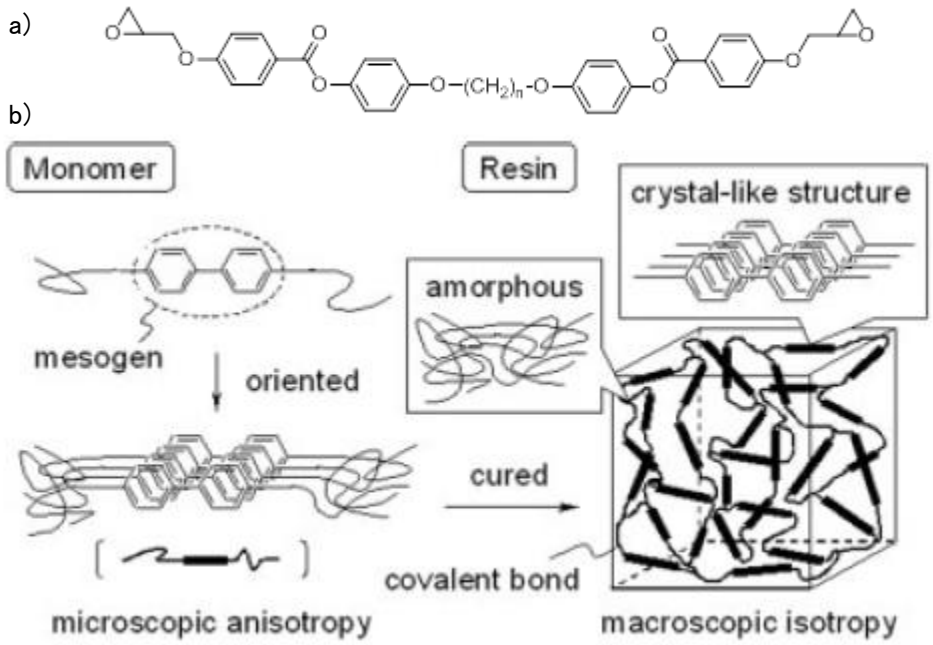

Figure 8. a) Chemical structure of epoxy resin. b) High-order structure of resin to afford isotropic high TC (reprinted from Ref.[21]).

4. Motivation

A polymer exhibits high TC along the molecular chain direction. However, the methods using drawing and subjecting the polymer to a magnetic field are impractical for molding various complex shapes. Plastics for manufacturing end-use products are

commonly formed by injection or compression molding, for example. Thus, the most suitable approach is to enhance the TC of polymers simultaneously with such a simple molding process.

As seen in Figure 7 and 8, main-chain liquid crystalline (LC) polymers will be good candidates for the thermally conductive matrices, since the "molecular chains" spontaneously align or the alignment can be controlled by external forces. That is one of the largest different points from side-chain LC polymers (Figure 9).

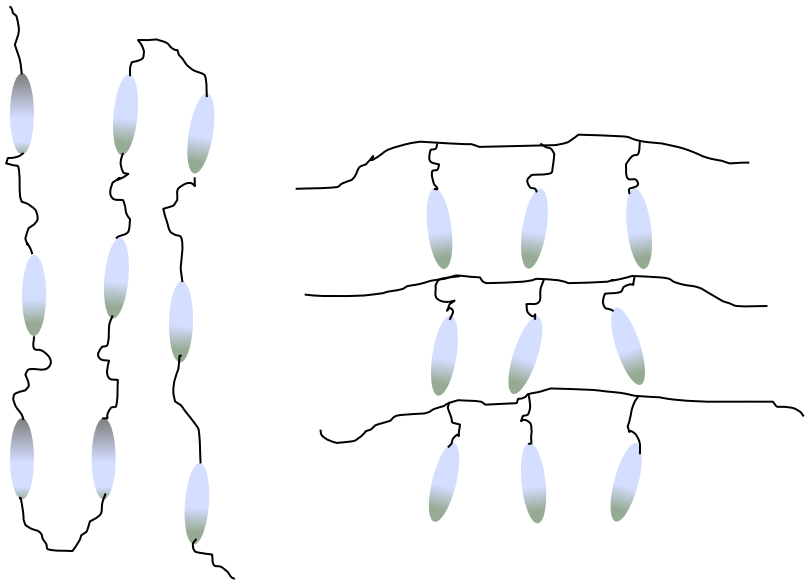

Main-Chain Liquid Crystalline Polymers

Side-Chain Liquid Crystalline Polymers

Figure 9. Schematics of main-chain and side-chain liquid crystalline polymers.

Hence, the following three points were development concepts.

(1) Molecular orientation of main-chain LC polymers is utilized to achieve high TC.

(2) Polymer composites can be molded by a simple molding process.

(3) Dramatic enhancement of TC is observed by incorporation of thermally conductive filler particles.

In this thesis, I report that a main-chain smectic LC PB-*n* polyester acts as an effective thermally conductive matrix in a composite with thermally conductive filler particles. PB-*n* polyesters, where *n* is the even number of methylene units in the spacer moiety, have been widely studied by our group (Figure 10). They form a highly ordered smectic LC phase and a lamellar structure in both smectic and crystalline phases.[23-25]

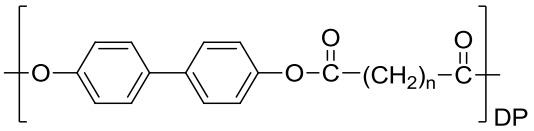

Figure 10. Chemical structure of PB-*n*.

Here, nematic and smectic liquid crystalline polymers are briefly explained as representative examples. One of the most common LC phases is the nematic phase, where molecules have no positional order but align themselves to achieve long-range directional order with their long axes roughly parallel. Thus, although the molecules are free to flow with their centers of mass randomly distributed as in a liquid, they still

maintain their long-range directional order (Figure 11a). The smectic phases form well-defined smectic layers (Figure 11b).

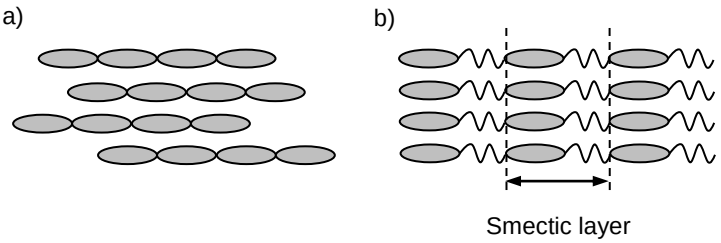

Figure 11. Liquid crystalline polymers. a) Nematic type. b) Smectic type.

To the best of my knowledge, all commercially available liquid crystalline thermoplastics are nematic liquid crystals. Since the polymer chains align parallel in the flow direction during injection molding, these materials have good fluidity. Almost all of a nematic polymer is a fully aromatic polyester with high heat resistance.

PB-*n* polyesters used in this thesis are a smectic type and the properties are much different from other nematic LC polyesters. Smectic polyesters consist of rigid mesogens connected by flexible spacer groups as shown in Figure 11b, leading to a low melting point. Therefore, smectic polymers tend to be inferior to fully aromatic LC polyesters regarding their heat resistance. Meanwhile, they form highly ordered structure and show different flow behavior from nematic LC polyesters. I utilized these characteristics and developed a thermally conductive polymer matrix.

5. Biomass-based polymer for commercial products

In this thesis, I mainly used PB-10 to clarify the enhancement mechanism of TC in smectic LC PB-*n* polyester. Meanwhile, I chose PB-8 to develop commercial products because the polyester comprises a sebacic acid, which is a biomass derived from a castor oil. In other words, PB-8 is a partially biomass-based polyester and can contribute to carbon neutral society.

Biomass plastics have attracted attentions from industries. In 20th century, a lot of useful plastics were developed and utilized in a lot of fields with the progress of petrochemistry. Plastics in 21st century are required to be based on “environmental considerations”, leading to attentions to biomass plastics.

Industries are required to reduce the consumption of fossil resources as much as possible in anticipation of future depletion of the resources. Therefore, the use of biomass resources becomes important and biomass plastics offer a sustainable alternative to petroplastics. Another advantage is relatively low greenhouse gas emissions during manufacture. Biomass polymers are considered to be synthesized from atmospheric carbon dioxide via photosynthesis of plants. Incineration of the biomass polymers, therefore, does not result in any additional load of carbon dioxide to the atmosphere.

In this thesis, I demonstrate that PB-8 polyester exhibits much higher TC than other fossil oil-based polymers. Consequently, customers using PB-8 for the heat dissipation ability can participate in the use of a biomass polymer, leading to contribution to sustainable environments. I think that such a material is ideal for the market growth of biomass polymers.

6. Organization of the thesis

This thesis consists of six chapters. Chapter 1 is the general introduction for thermally conductive polymers.

In Chapter 2, the type of mesophase formed by PB-10 is identified as smectic I using spinnable PB-10 polyester, which was obtained for the first time by solid state polymerization. Polymer chains are packed laterally in a 2D hexagonal lattice and lie along the *c*-axis and pass diagonally across the smectic layers. SAXS and SEM clarify lamellae stacking regularly along the fibre axis with a spacing of 41 nm, which is approximately 20 times the smectic layer thickness. The lamellar normal is thus parallel to the chain axis and tilted to the smectic layer normal.

In Chapter 3, TC enhancement of PB-*n* by lamellar crystal alignment is discussed. PB-*n* shows a parallel orientation of LC lamellae by shear flow during injection

molding, in which polymer chains are aligned in normal direction (ND) with respect to the molding surface, thus leading to high TC (1.2 W m^{-1} K^{-1}) in this direction. Furthermore, the composites containing plate-shaped hexagonal boron nitride (h-BN) particles exhibit a dramatic enhancement of TC in not only the ND but also the in-plane direction, indicating that polymer chains align in the ND served as effective heat paths between h-BN particles.

In Chapter 4, the effect of the molecular orientation direction of a polymer matrix on the in-plane thermal conductivity (TC) of injection-molded polymer/ h-BN composites is discussed. In this system, the h-BN platelets align in the in-plane direction owing to injection shear flow. Three molecular orientations (perpendicular, random, and parallel to the h-BN plane) are achieved using liquid crystalline polyesters and the in-plane TCs are compared. Although a parallel orientation of the polymer chains provides the highest TC of the matrix in the injection direction, the TC of the composites is the lowest of the three systems for this orientation. The highest in-plane TC is found in the perpendicularly oriented system, irrespective of the in-plane direction. These results reveal that perpendicularly oriented molecular chains serve as effective heat paths between h-BN platelets that are arranged one above the other, and consequently, a continuous thermal network is created in the in-plane direction.

In Chapter 5, the TC of an isotropic composite comprising of a main-chain smectic liquid crystalline PB-10 polyester and 50-μm-sized roughly spherical magnesium oxide (MgO) particles is discussed. The increase in the composite TC with higher MgO fractions is steeper than that expected by Bruggeman's theory for the TC of a polydomain PB-10 polyester (0.52 W m^{-1} K^{-1}). When the filler content is larger than 30 vol%, the composite TC approaches a value that can be explained only if the polyester functions as a thermally conductive matrix with 1.0 W m^{-1} K^{-1}, which is 5 times as high as those of isotropic common polymers (0.2 W m^{-1} K^{-1}). Such an unusually high TC for a polymer matrix is attributed to some polymer lamellae that lie parallel to the particle surface and are stacked toward neighboring particles, thus creating a continuous thermal network in a composite.

As an appendix, the TC of biomass based PB-8/MgO composites is measured, indicating that the PB-8 polyester also functions as thermally conductive polymer matrix like PB-10.

In Chapter 6, contents from chapter 2 to 5 are summarized, demonstrating that main-chain liquid crystalline polyesters will be commercially useful as the high TC matrices. Finally, the thesis concludes with future recommendations.

References

[1] Z. Han, A. Fina, *Prog. Polym. Sci.* **2011**, *36*, 914.

[2] C. L. Choy, E. L. Ong, F. C. Chen, *J. Appl. Polym. Sci.* **1981**, *26*, 2325.

[3] D. Hansen, G. A. Bernier, *Polym. Eng. Sci.* **1972**, *12*, 204.

[4] H. G. Chae, S. Kumar, *Science* **2008**, *319*, 908.

[5] L. M. Veca, M. J. Meziani, W. Wang, X. Wang, F. Lu, P. Zhang, Y. Lin, R. Fee, J. W. Connell, Y-P. Sun, *Adv. Mater.* **2009**, *21*, 2088.

[6] W-L. Song, P. Wang, L. Cao, A. Anderson, M. J. Meziani, A. J. Farr, Y-P. Sun, *Angew. Chem. Int. Ed.* **2012**, *51*, 6498.

[7] Y. Agari, *J. Adh. Socy. Japan.* **2007**, *43*, 325.

[8] M. Sumita, K. Sakata, Y. Hayakawa, S. Asai, K. Miyasaka, M. Tanemura, *Colloid Polym. Sci.* **1992**, *270*, 134.

[9] T. Matsumura, M. Ochi, K. Nagata, *J. Appl. Polym. Sci*, **2003**, *90*, 1980.

[10] W. Thongruang, R. J. Spontak, C. M. Balik, *Polymer* **2002**, *43*, 3717.

[11] D. Yorifuji, S. Ando, *J. Mater. Chem.* **2011**, *21*, 4402

[12] D. Yorifuji, *academic dissertation*, **2010**, Tokyo Institute of Technology.

[13] D. A. G. Bruggeman, *Ann. Phys.* **1935**, *24***,** 636.

[14] C. L. Choy, F. C. Chen, W. H. Luk, *J. Polym. Sci. Polym. Phys.* **1980**, *18*,

1187.

[15] S. Shen, A. Henry, J. Tong, R. Zheng, G. Chen, *Nat. Nanotechnol.* **2010**, *5*, 251.

[16] X. Huang , G. Liu , X. Wang, *Adv. Mater.* **2012**, *24*, 1482.

[17] M. Harada, M. Ochi, M. Tobita, T. Kimura, T. Ishigaki, W. Aoki, *J. Polym. Sci. Polym. Phys*. **2003**, *41*, 1739.

[18] M. Hasegawa, N. Suyama, N. Shimoyama, H. Aoki, T. Nunokawa, T. Kimura, *Polym. Int.* **2011**, *60*, 1240.

[19] T. Kimura, *J. Net. Polym. Jpn.* **2008**, *29*, 51.

[20] S. Okamoto, Y. Matsumi, S. Saito, R. Miyakoshi, T. Kondo, *R&D Report SUMITOMO KAGAKU*, **2011**, 2011-I.

[21] M. Akatsuka, Y. Takezawa, *J. Appl. Polym. Sci.* **2003**, *89*, 2464.

[22] A. Shiota, CK. Ober, *J. Polym. Sci. Part A* **1996**, *34*, 1291.

[23] J. Asrar, H. Toriumi, J. Watanabe, W. R. Krigbaum, A. Ciferri, *J. Polym. Sci. Polym. Phys.* **1983**, *21*, 1119.

[24] W. R. Krigbaum, J. Watanabe, T. Ishikawa, *Macromolecules* **1983**, *16*, 1271.

[25] M. Tokita, K. Osada, M. Yamada, J. Watanabe, *Macromolecules* **1998**, *31*, 8590.

Chapter 2

Identifying Smectic I Phase of Main-Chain PB-10 Polyester Consisting of 4,4′-Biphenol and 1,10-Dodecanoic acid by Fibre X-ray Diffraction

1. Abstract

Spinnable main-chain PB-10 liquid crystal (LC) polyester was obtained for the first time by solid state polymerization after conventional melt condensation of 4,4′-biphenol and 1,10-dodecanoic acid. The smectic LC phase oriented uniaxially in the fibre and exhibited an X-ray diffraction pattern attributable to a C-centred monoclinic unit cell with a = 0.64 nm, b = 0.90 nm, c = 2.31 nm and β = 126° with the c-axis parallel to the fibre axis. The type of mesophase can thus be identified as smectic I rather than smectic H, as speculated previously. Polymer chains are thus packed laterally into a hexagonal lattice and pass diagonally across the smectic layers. In the smaller angle region, the fibre exhibited a series of diffraction peaks attributed to lamellae stacking along the fibre direction with a spacing of 41 nm. The lamellae are thus perpendicular to the polymer chain axis and inclined to the smectic layer.

2. Introduction

Thermotropic main-chain polyesters have mesogens which are incorporated in the chain backbone and connected by flexible alkyl spacers. The mesogen is a rigid rod comprising a few benzene rings connected by appropriate linkages. Biphenyl is known to work as the mesogen when the moieties are connected with spacers at 4 and 4′ positions with ester linkages. Two series of main-chain liquid crystal (LC) polyesters with biphenyl mesogens have been widely investigated by our group[1-8] and other groups.[9–11] The first series of polyesters consisting of biphenyl dicarboxylic acid and α,ω-alkane diol forms smectic phases.[1-5,9-11] These polyesters are designated as BB-*n* where *n* is the number of methylene units in the spacer moiety. BB-*n* forms two types of smectic phase depending on the odd-even parity of *n*.[1] Whereas BB-*n* with an even *n*-number forms a smectic A phase, that with an odd *n*-number a smectic CA phase. These smectic phases can be identified by the well-oriented diffraction pattern of the fibre sample spun from the isotropic liquid. The oriented diffraction pattern thus provides powerful means to identify the type of LC phase formed by polymers.

The other polyester series consists of biphenol and α,ω-alkane dicarboxylic acid, and is designated as PB-*n*.[6–8] The type of LC phase formed by PB-*n* polyesters with an odd *n*-number has been identified as a nematic LC. On the other hand, PB-*n* with an even

n-number formed a highly ordered smectic phase, but no detailed structural assignment has been made because the isotropic melt of PB-*n* is not sufficiently sticky to be spun into fibres, even if it possesses inherent viscosity comparable with that of a spinnable BB-*n* polyester. Miscibility studies of binary mixtures with well-characterised low-molecular-weight mesogens, and the spacing data of powder X-ray diffraction pattern suggest that the smectic phase is smectic H. In this work, I succeeded in preparing higher molecular weight PB-10 polyester (Figure 1a), by the solid state polymerization method, which was spinnable in the isotropic phase (Figure 1b). Irradiating X-ray on the fibre at a LC temperature offered a well-oriented diffraction pattern which allowed us to identify the LC phase as smectic I. Small-angle diffraction and electron microscopy observations of the fibre sample confirmed the spontaneous formation of lamellae parallel to the fibre direction with spacing 20 times larger than the smectic layer spacing.

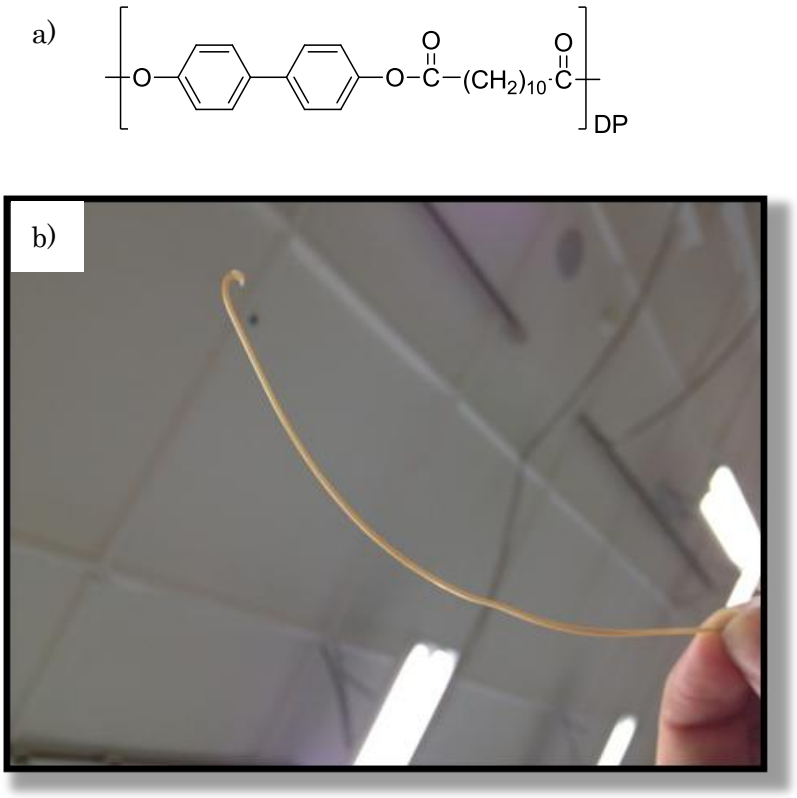

Figure 1. a) Chemical structure of PB-10. b) Photograph of a PB-10 fibre.

3. Experimental Section

The high-molecular-weight PB-10 polyester was prepared by melt condensation of 4,4′-biphenol (1.0 eq.), 1,10-dodecanoic acid (1.0 eq.) and acetic anhydride (2.0 eq.) followed by solid state polymerization (SSP). Sodium acetate (0.001 eq.) was used as a catalyst. The reactants were stirred and heated to 260 °C under a dry nitrogen atmosphere for 1 h, and then the pressure was reduced to 10 Torr for 3 h. After the melt condensation, the yielded polymer was allowed to cool to ambient temperature, then

powdered and subjected to SSP for 8 h at 230 °C under a reduced pressure of 10 Torr. The number- and weight-average molecular weights (M_n and M_w) of the polymers and polydispersity index (PDI) before and after SSP were estimated by gel permeation chromatography (GPC) using universal calibration. The melt viscosities of the polymers before and after SSP were measured at 320 °C (Shimazu Flow Tester CFT-500D), where the shear rate could not be made uniform because the melt viscosities of the polymers differed significantly from each other. The temperatures and enthalpies on the crystal-LC and LC-isotropic liquid transitions were determined by differential scanning calorimetry (DSC) thermogram (Perkin-Elmer DSC 7) measured at a heating rate of 10 °C min^{-1}. Before the measurement, the sample was cooled from the isotropic liquid phase to ambient temperature at a rate of 10 °C min^{-1} to erase any prior history. The molecular weight, melt viscosity and DSC data are listed in Table 1. A PB-10 fibre with a diameter of 0.5 mm was prepared by extruding the high-molecular-weight polymer into a fibre with a diameter of 1.5 mm, and elongating it on a hot plate at 280 °C using two tweezers.

Table 1. Characterisation of PB-10 Polyesters

	M_w	M_n	M_w/M_n	η /Pa s [a]	T_m /°C [b] ΔH_m /kJ mol^{-1} [d]	T_i /°C [c] ΔH_i /kJ mol^{-1} [e]
Before SSP	35,200	16,500	2.1	1.72	206 10.9	256 18.7
After SSP	111,000	19,000	5.9	1,820	203 9.1	254 18.8

[a] shear rates were 1,430 and 6.72 s^{-1} for the polymer before and after SSP, respectively.
[b] crystal–LC transition temperature. [c] LC– isotropic liquid transition temperature. [d] Enthalpy change on crystal–LC transition. [e] Enthalpy change on LC– isotropic liquid transition.

4. Results and Discussion

Figure 2 shows the wide-angle X-ray diffraction (WAXD) pattern of the PB-10 fibre at a LC temperature of 210 °C. The pattern was measured with a pin-hole collimated CuKα radiation (Rigaku UltraX18 X-ray generator) in the direction perpendicular to the fibre axis. It shows two equatorial reflections at 2θ = 19.8° (d-spacing of 0.45 nm) and 2θ = 34.5° (d-spacing of 0.26 nm). Another inner reflection is found in the quadrant at a low angle of 2θ = 4.72° (d-spacing of 1.87 nm) and is tilted 54° away from the

equatorial. Second- and third-order reflections with the spacings of 0.94 and 0.62 nm can also be seen at $2\theta = 9.38°$ and 13.8°, respectively. Such reflections can rationally be explained in the following way. The two equatorial reflections are the 10 and 11 reflections for a 2D hexagonal lattice that can be recognised by viewing the direction parallel to the fibre axis. The shape of the reflections are somewhat elongated in the fibre direction, suggesting that the hexagonal lattice has a restricted positional correlation within layers and weak interlayer correlation[12, 13]. A series of low-angle reflections are assigned to the (00*l*) smectic layer planes whose normal is tilted from the fibre axis by 36°. The diffraction pattern thus reveals that the mesogens lying parallel to the fibre axis are packed laterally in the 2D hexagonal lattice and compose layers with the normal tilted 36° away from the fibre axis, i.e. the long axes of the mesogens. Such a molecular packing can be connected with either smectic F (SmF) or smectic I (SmI) phases with C-centred monoclinic unit cells.[12–14]

SmF and SmI phases can be distinguished from each other by the tilting direction of the *c*-axis (Figure 3); the *c*-axis in SmF is tilted towards the longer side of the rectangular base of the monoclinic lattice, whereas that in SmI is tilted towards the shorter side.[12–14] However, this difference makes no distinction in the major WAXD reflections of the fibre with the *c*-axis parallel to the fibre axis.[14] A choice between

SmF and SmI is allowed by other two minor reflections which appear in the quadrant respectively at 2θ = 17.6° (d-spacing of 0.50 nm) and 2θ = 17.0° (d-spacing of 0.52 nm) and are tilted by 12° and 40°, respectively, from the equatorial. These reflections are attributed to the reflection planes $(\bar{1}11)$ and $(\bar{1}13)$ of the monoclinic unit cell with *a* = 0.64 nm, *b* = 0.90 nm, *c* = 2.31 nm and β = 126° with the *c*-axis parallel to the fibre axis as illustrated in Figure 2b. Thus, the *c*-axis (i.e. mesogens) is tilted along the shorter side of the rectangular base of the unit cell and I can assert that the type of smectic LC is SmI.

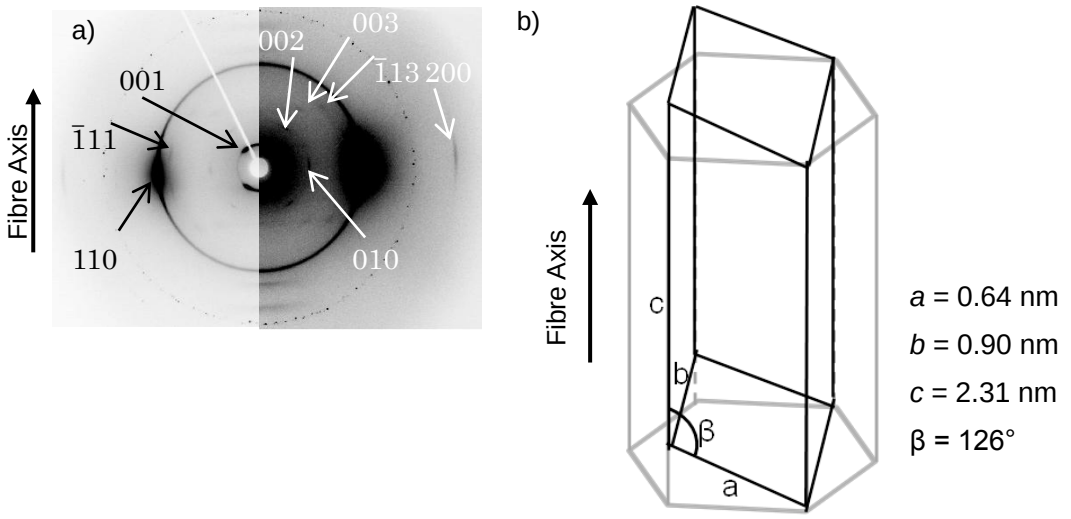

Figure 2. a) WAXD fibre pattern for PB-10 measured at 210 °C and b) the unit cell dimensions in the SmI phase.

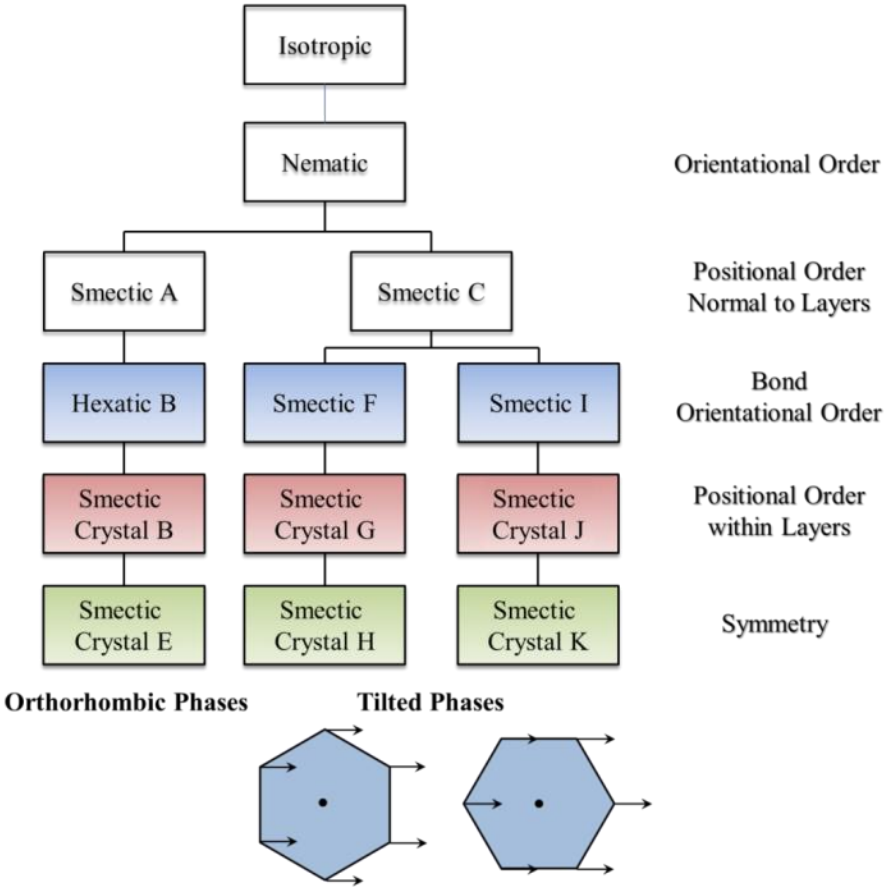

Figure 3. Classification of liquid-crystalline phases.

The observed and calculated d-spacings are compared in Table 2.[15] All the reflections observed are thus explained by this lattice except for one weak equatorial reflection at $2\theta = 9.78°$ (d-spacing of 0.90 nm). This reflection can be indexed as 010. However, its appearance is forbidden by the extinction rule in this lattice. I have not found any reason why this forbidden reflection appears.

Table 2. Comparison of observed and calculated d-spacings of PB-10 SmI LC

d_{obs} /nm	d_{calc} /nm	*hkl*
0.45	0.45	110
0.26	0.26	200
0.50	0.50	$\bar{1}11$
0.52	0.51	$\bar{1}13$
1.87	1.87	001
0.94	0.94	002
0.62	0.62	003

The question that arises is how polymer chains that include many mesogens in their backbone are accommodated in the SmI structure. When the repeat unit adopts an all-trans conformation as depicted in Figure 4a, the distance between the mesogens along the fibre axis is 2.25 nm which satisfies the *c*-axis length of 2.31 nm. However, in such a LC state, the spacer is not likely to adopt the all-trans conformation; the conformers are dynamic rather than static as revealed by solid-state ^{13}C-NMR spectra of the PB-18 polyester.[7] In the spectra, the NMR peak assigned to the internal carbons in the spacer moiety consists of a single component, showing that the trans and gauche conformers exchange rapidly with an average fraction of gauche conformer of 0.21. Thus, the spacers exchange conformers rapidly with connecting mesogens along the *c*-axis. One plausible snapshot of a repeat unit conformation is depicted in Figure 4b where the two mesogens nearly parallel to each other, at a spacing of 2.36 nm, are connected by a spacer with a $tttg^+tg^+tg^+t$ conformer which includes a helical

conformation ($tg^+tg^+tg^+$). Polymer chains packed laterally in a 2D hexagonal lattice thus lie along the *c*-axis and pass diagonally across the smectic layers.

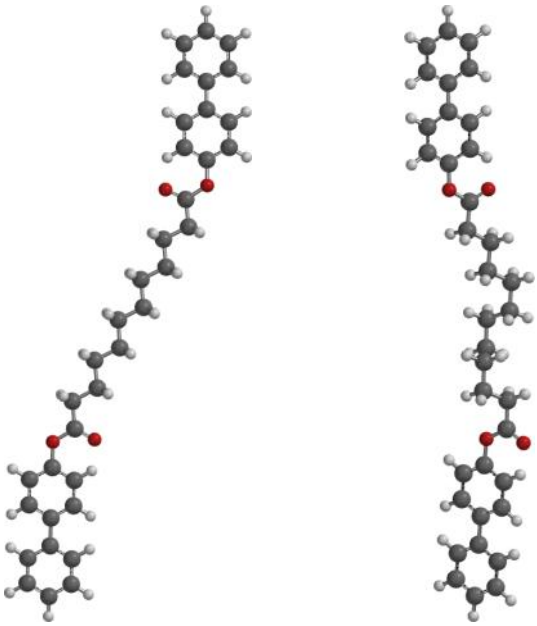

Figure 4. Two possible types of spacer conformation: a) all-trans and b) coexistence of trans and gauche conformers.

The structure characteristic to the PB-10 SmI LC is lamellae stacking along the polymer chain direction which produced other diffraction maxima at small angles along the fibre axis. Figure 5a shows the small-angle X-ray diffraction (SAXD) pattern of the fibre sample measured at 210 °C (Bruker AXS Nano STAR-U). It includes peaks on the

fibre axis at scattering vectors (q) with ratios of 1:2:3:4, indicating the existence of lamellae stacking along the polymer chain axis. The lamellae are thus not parallel to the smectic layers whose normal is tilted away from the fibre axis. The lamellar spacing is estimated to be 40.5 nm, which is 18 times the smectic layer thickness. The equivalent lamellae were observed by scanning electron microscopy (SEM) (JEOL JSM-7500F). As seen in Figure 5b, the lamellae stretch in the direction perpendicular to the fibre axis in the whole field of microscopy, indicating that the persistence length of the lamellae is extremely long. From these findings, higher order structure of PB-10 fibre can be depicted as seen in Figure 6.

SAXD maxima were also observed for both the pre- and post-SSP samples of PB-10 polyester cooled from the isotropic phase to ambient temperature at a rate of 10 °C min^{-1}. The lamellae spacing is estimated to be 47 nm for both polymers regardless of the difference in molecular weight. The lamellar spacing increased with annealing of the sample at SmI temperature. These trends of the lamellar spacing suggest that the lamella consists of folded polymer chains.[8]

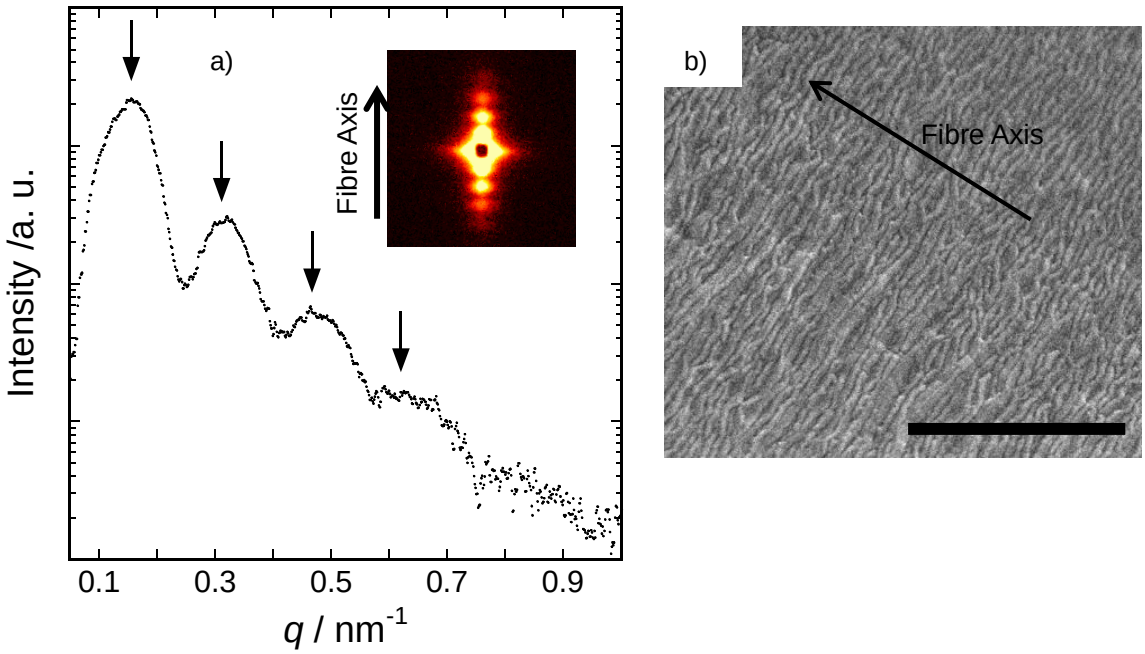

Figure 5. a) SAXD pattern and b) SEM measured for PB-10 fibre at ambient temperature. Before measurements, the as-spun fibrous sample was annealed at a LC temperature of 210 °C for 1h. The SAXD intensity profile was prepared from the two-dimensional pattern inserted in a) by averaging the intensities of peaks on the meridian over azimuthal sectors of 10° on each side of the each side of the fibre axis. The arrows indicate the SAXD peaks due to the lamella long spacing of 40.5 nm. The scale bar in the SEM pattern is 1 μm.

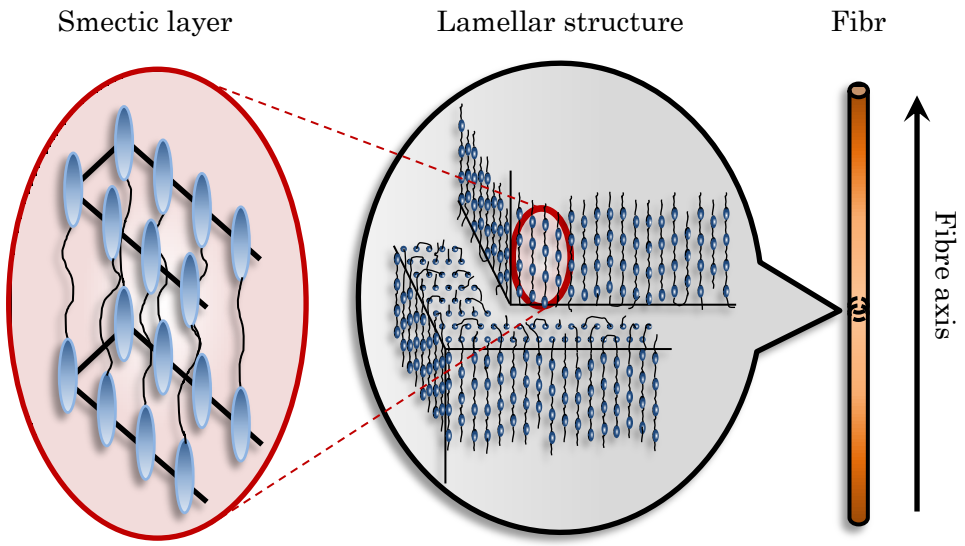

Figure 6. Schematic illustrations of higher order structures of PB-10 fibre.

5. Conclusion

SSP yielded a high-molecular-weight smectic LC PB-10 polyester with a high M_w of 111,000, which was spinnable in the isotropic liquid phase. The WAXD of the fibrous sample identified the type of smectic phase as SmI having a C-centred monoclinic unit cell with a = 0.64 nm, b = 0.90 nm, c = 2.31 nm and β = 126° where the c-axis was parallel to the fibre axis. Polymer chains are packed laterally in a 2D hexagonal lattice and lie along the c-axis and pass diagonally across the smectic layers. SAXD and SEM clarify lamellae stacking regularly along the fibre axis with a spacing of 41 nm, which is approximately 20 times the smectic layer thickness. The lamellar normal is thus parallel

to the chain axis and tilted to the smectic layer normal. Although the lamella seems to be formed by folded polymer chains, investigations into the detailed lamellar structure are planned for the future.

6. Appendix; Study on conditions of solid state polymerization.

The optimum condition of SSP was determined by changing the mean polymeric particle size, pressure, temperature, and time with an aim to fast increase of molecular weight. Table 3 summarizes the conditions and molecular weights of resultant PB-10 polyesters. Condition 1 provided the highest molecular weight. The condition is relatively small particle size, reduced pressure, and smectic phase temperature (230 °C). The small particle size and reduced pressure resulted in the ease of elimination of acetic acid generated by polycondensation. I found for the first time that PB-10 was able to be subjected to SSP at smectic temperature. Usually, SSP is conducted at solid temperature to avoid thermal fusion bonding of polymer particles, which results in a growth of particle size and, thus, slow polymerization rate. SmI phase of PB-10 is a highly ordered structure and solid-like (Figure 3). Thus, PB-10 didn’t show the thermal fusion bonding even under the smectic temperature. Condition 5 indicates that the molecular weight increased at solid temperature (180 °C). However, smectic temperature led to much

faster growth of molecular weight than solid one.

Table 3. Conditions of SSP

Condition No.	Before SSP	1	2	3	4	5
Mean particle size (mm)	-	0.2	4.0	0.2	0.2	0.2
Pressure (torr)	-	10	10	760[c]	10	10
Temperature (°C)	-	230[a]	230[a]	230[a]	180[b]	180[b]
Time (h)		8	8	8	8	16
M_n	16,500	19,000	18,700	17,000	16,300	17,900
M_w	35,200	111,000	46,500	70,500	35,400	44,400
PDI	2.1	5.9	2.5	4.1	2.2	2.5

[a]smectic phase temperature. [b]solid phase temperature. [c]under a dry nitrogen atmosphere.

References

[1] Tokita M., Watanabe, J. *Polym. J*. 2006; *38*: 611–638.

[2] Ishige R., Tokita M., Naito Y., Zhang C-Y, Watanabe J. *Macromolecules* 2008; *41*: 2671–2676.

[3] Ishige R., Naito Y., Kang S., Tokita M., Watanabe J. *Macromolecules* 2009; *42*:

2557–2562.

[4] Ishige R., Tokita M., Funaoka S., Kang S., Watanabe J. *Macromol*. *Chem*. *Phys*. 2011; *212*: 48–54.

[5] Ishige R., Ishii T., Tokita M., Koga M., Kang S., Watanabe J. *Macromolecules* 2011; *44*: 4586–4588.

[6] Krigbaum, W R, Watanabe J., Ishikawa T. *Macromolecules* 1983; *16*: 1271–1279.

[7] Tokita M., Sone M., Kurosu H., Ando I., Watanabe J. *J*. *Mol*. *Struct*. 1998; *446*: 215–221.

[8] Tokita M., Osada K., Yamada M., Watanabe J. *Macromolecules* 1998; *31*: 8590–8594.

[9] Pérez E., Riande E., Bello A., Benavente R., Pereña J. *Macromolecules* 1992; *25*: 605–610.

[10] Bello A., Riande E., Pérez E., Marugán M., Pereña J. *Macromolecules* 1993; *26*: 1072–1077.

[11] Fernández-Blázquez JP, Bello A., Pérez E. *Macromol*. *Chem*. *Phys*. 2007; *208*: 2611–2620.

[12] Gane P.A.C., Leadbetter A.J., Wrighton, P.G. *Mol*. *Cryst*. *Liq*. *Cryst*. 1981; *66*: 247–266.

[13] Gane P.A.C., Leadbetter A.J., Benattar J.J., Moussa F., Lambert M. *Phys*. *Rev*. *A* 1981; *24*: 2694–2700.

[14] Yoon Y., Ho R., Li F., Leland M.E., Park J., Cheng S.Z.D., Percec V., Chu P. Prog. *Polym*. *Sci*. 1997; *22*: 765–794.

[15] Cullity B.D., Stock S.R. Elements of X-ray Diffraction, 3rd ed. Upper Saddle River: Prentice Hall, 2001 (Appendix 3).

Chapter 3

Enhanced Thermal Conductivity of Thermoplastics by Lamellar Crystal Alignment of Polymer Matrices

1. Abstract

Thermal conductivity (TC) of injection-molded main-chain smectic liquid crystalline polyesters and the composites containing hexagonal boron nitride (h-BN) particles is investigated. Shear flow during injection molding induces alignment of lamellar crystals of polymer matrices, in which polymer chains are aligned in the normal direction (ND) with respect to the molding surface, thus leading to a high TC (1.2 W m^{-1} K^{-1}) in the ND. The composites exhibit a dramatic enhancement of TC in not only the ND but also the in-plane direction. The enhanced TC is much higher than that of common thermoplastic composites at comparable loading levels. These results indicate that the polymer matrices serve as effective heat conductors between h-BN particles.

2. Introduction

Here, I report a novel method for producing polymer materials that are lightweight and highly processable and achieve "unprecedentedly high TCs" afforded by the lamellar crystal alignment of polymer matrices using main-chain PB-*n* polyesters, as shown in Figure 1a. PB-*n*, where *n* is the even number of methylene units in the spacer moiety, forms a highly ordered smectic I phase as mentioned in chapter 2, and a lamellar structure in both smectic and crystalline phases.[1-3] I applied information acquired from previous studies showing that shear flow induces the lamellar alignment of main-chain smectic liquid crystalline (LC) polyesters.[4-8] Although two types of orientations, parallel and perpendicular (Figures 1b and 1c), are known and previous smectic polyesters usually show the perpendicular one (Figure 2), I found that shear flow in the LC state of PB-*n* during injection molding selectively induces the parallel orientation, in which polymer chains are aligned in the normal direction (ND) with respect to the molding surface, thus leading to a high TC in the ND. Furthermore, injection molded composites consisting of PB-10 and plate-shaped hexagonal boron nitride (h-BN) exhibit a dramatic enhancement of TC in not only the ND but also the in-plane direction. The enhanced TC is much higher than that of common thermoplastic composites at comparable loading levels.

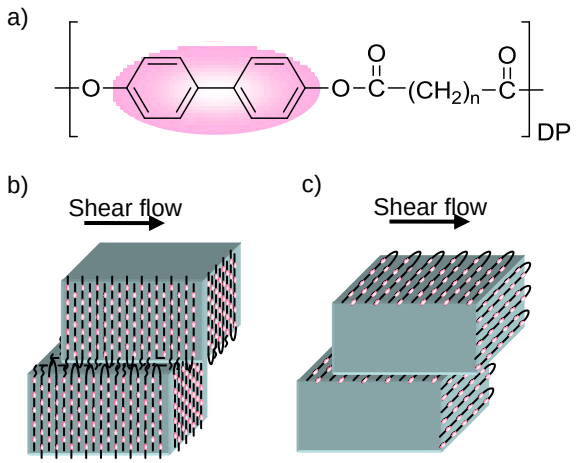

Figure 1. a) Chemical structure of PB-*n*. b) Parallel and c) perpendicular orientations of lamellae by shear flow.

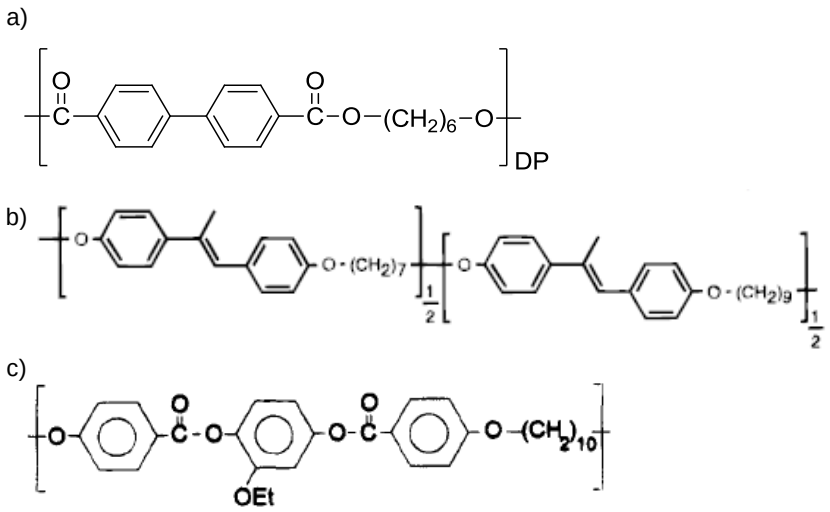

Figure 2. LC polyesters showing perpendicular orientation of lamellae. a) Ref. [4]. b) Ref. [5]. c) Ref. [7].

3. Experimental Section

3-1. Materials

4,4’-Diacetoxy biphenyl, dodecanedioic acid, and sodium acetate were purchased from Wako Pure Chemical Industries, Ltd.. Tetradecanedioic acid and eicosanedioic acid were purchased from Tokyo Chemical Industry Co., Ltd.. These materials were directly used as received. PB-10, PB-12, and PB-18 were synthesized according to a previous report.[1] A representative PB-*n* species, PB-10 was synthesized by the melt condensation of 4,4’-diacetoxy biphenyl and dodecanedioic acid with sodium acetate as a catalyst. After polycondensation, the molten polymer was discharged onto a stainless plate. The number average molecular weight (M_n) and polydispersity index (PDI) of the polymers were determined by gel permeation chromatography (GPC) (Viscotek HT-GPC with a refractive index detector) in a *p*-chlorophenol/toluene (3/8 volume ratio) solution using polystyrene as the standard. Differential scanning calorimetry (DSC) measurements were performed with a Perkin-Elmer Pyris 1 DSC calorimeter at a scanning rate of 10 °C min^{-1} under a flow of dry nitrogen. Powder X-ray diffraction (XRD) analysis is used to determine the crystallinity of the polymers at 25 °C with a Rigaku Ultima IV X-ray diffractometer using Cu Kα radiation. Shear viscosity measurements of polymer melts was conducted by capillary rheometer (Capillograph

1D, Toyo Seiki, Ltd.). Coefficient of thermal expansion (CTE) was measured with a thermo mechanical analyzer (TMA 4000, Bruker AXS). Polybutylene terephthalate (PBT; NOVADURAN 5008L) was supplied by Mitubishi Engineering-Plastics Co.. Hexagonal boron nitride (h-BN; PT110) with a mean particle size of 45 μm was purchased from Momentive Performance Materials Inc..

3-2. Morphology characterization

Two-dimensional small-angle X-ray scattering (2D-SAXS) patterns were recorded at 25 °C with a Bruker AXS Nano-STAR-U using Cu Kα radiation. The intensity profiles were plotted against the scattering vector q (= $4\pi \sin \theta/\lambda$). 2D-Wide-angle X-ray diffraction (2D-WAXD) patterns were recorded on an imaging plate at 25 °C using Cu Kα radiation, which was generated by a Rigaku-Denki UltraX18 X-ray generator equipped with a graphite crystal monochromator and a pinhole collimator. To observe lamellar crystals using a scanning electron microscope (SEM) (S-4800, Hitachi Ltd.), the specimens were first cut by a microtome to achieve a flat surface, exposed to RuO_4 vapor, and then, treated to platinum–palladium deposition. The lamellar crystals on the flat surface were observed.

3-3. Compounding and injection molding conditions

Polymers and h-BN were mixed using a twin-screw extruder (TECHNOVEL Corp.,

KZW15TW) (Figure 3). The screw rotation speed was 90 revolutions per minute. The temperature was set at 220 °C for PB-10 and 260 °C for PBT. The actual filler content of the composites was determined from their densities and residual content after a burn-out test at 450 °C. Polymers and composites were molded by a mini injection molder (DSM Xplore, Micro Injection Moulding Machine 5.5 ml, Figure 4) to plates with dimensions 10 × 40 × 1 mm^3. Cylinder and mold temperatures were 240 and 170 °C for PB-10 and the composites, 220 and 150 °C for PB-12, 180 and 130 °C for PB-18, and 260 and 170 °C for PBT and the composites, respectively; injection pressure was 0.7 MPa. The cylinder and mold temperatures for PB-*n* correspond to each smectic phase and crystal phase temperatures.

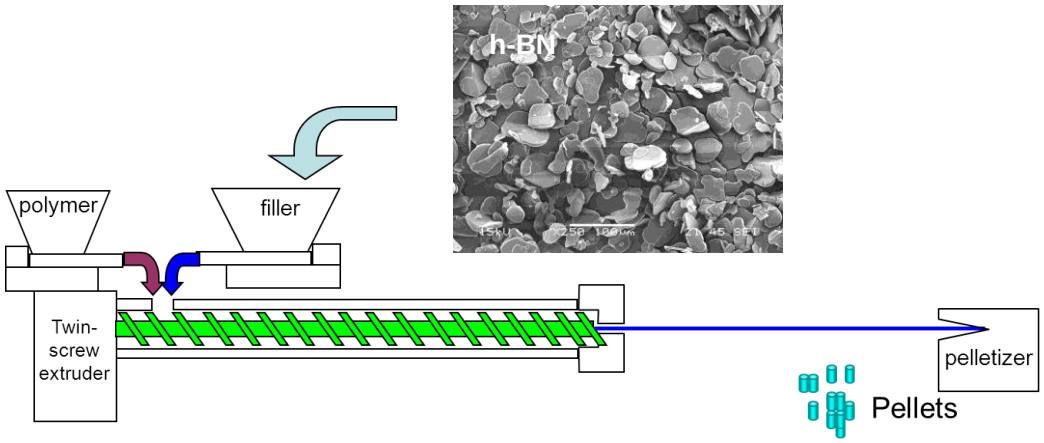

Figure 3. Twin-screw extruder for mixing polymers and filler particles.

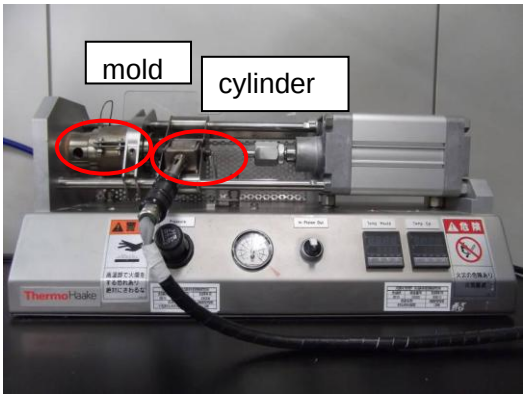

Figure 4. Mini injection molder (DSM Xplore, Micro Injection Moulding Machine 5.5 ml)

3-4. Thermal conductivity measurements

TC (λ) was evaluated from thermal diffusivity (α) according to Eq. (1):

$$\lambda = \alpha \rho c \quad (1)$$

where ρ and c are density and heat capacity, respectively. The thermal diffusivity of samples in the ND, machine (MD), and transverse directions (TD) was measured in triplicate for each direction at 25 °C in accordance with the American Society for Testing and Materials (ASTM) E-1461 by a Netzsch LFA 447 NanoFlash instrument with ±5% accuracy (Figure 5). Figure 6 shows sample preparation for thermal diffusivity measurements. In particular, for measurements in the MD and TD, 12 pieces ($10 \times 3 \times 1$ mm^3) were cut from molded plates, and the pieces were piled to obtain a sample size of $10 \times 3 \times 12$ mm^3. The samples were polished with sand paper and coated

with a carbon spray (Black Guard Spray FC153, Fine Chemical Japan Co., Ltd.). Density and heat capacity were determined by the Archimedian and DSC methods, respectively.

Figure 5. Netzsch LFA 447 NanoFlash instrument.

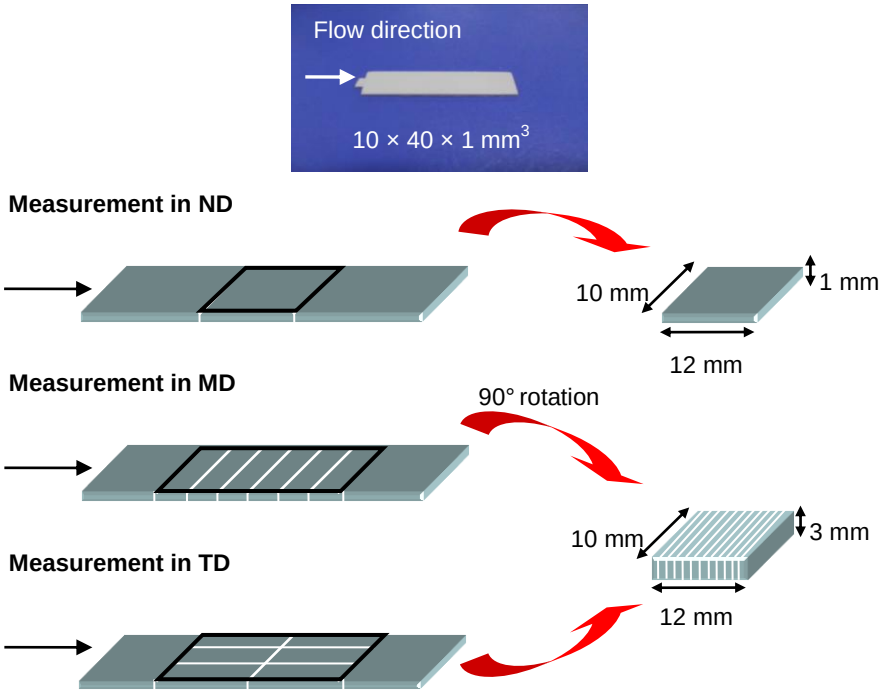

Figure 6. Preparation of samples for thermal diffusivity measurements

4. Results and Discussion

4-1. Characterization of PB-10, PB-12, and PB-18

PB-10, PB-12, and PB-18 used in this study exhibit the well-defined transition behavior, as found in the DSC thermogram of Figure 7. These polyesters show crystal-smectic transformations at T_{mh} on heating and T_{mc} on cooling and smectic-isotropic transformations at T_{ih} on heating and T_{ic} on cooling. The polystyrene-equivalent M_n, PDI and transition temperatures are listed in Table 1.

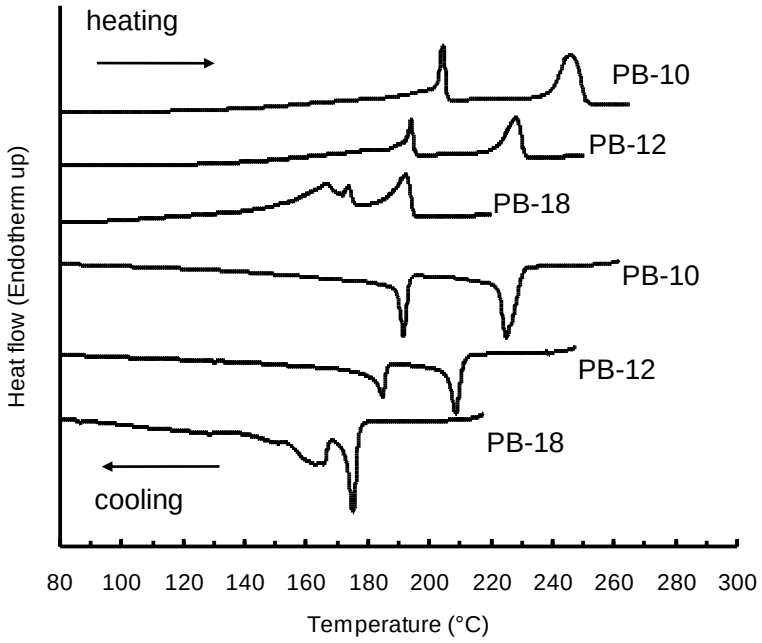

Figure 7. DSC thermograms of PB-10, PB-12, and PB-18 used in this study.

Table 1. Characterization of PB-*n* polymers

sample	M_n [kg mol^{-1}]	PDI	transition temperature			
			heating process		cooling process	
			T_{mh} [°C]	T_{ih} [°C]	T_{mc} [°C]	T_{ic} [°C]
PB-10	10.0	1.9	204	246	192	225
PB-12	10.5	2.2	194	228	185	208
PB-18	9.60	2.1	174	192	165	175

4-2. Morphology and TC of PB-10 before injection molding

At first, a PB-10 plate with dimensions 10 × 10 × 1 mm^3 before injection molding was prepared from as-discharged polymer for measuring TC. In this plate, the random orientation of lamellae was confirmed by 2D-SAXS (Figure 8) and SEM observations (Figure 9). The SAXS intensity profile indicates that lamellar thickness is 47 nm. TC (0.52 W m^{-1} K^{-1}) was determined by a flash method at 25 °C. The value represents the isotropic nature of PB-10.

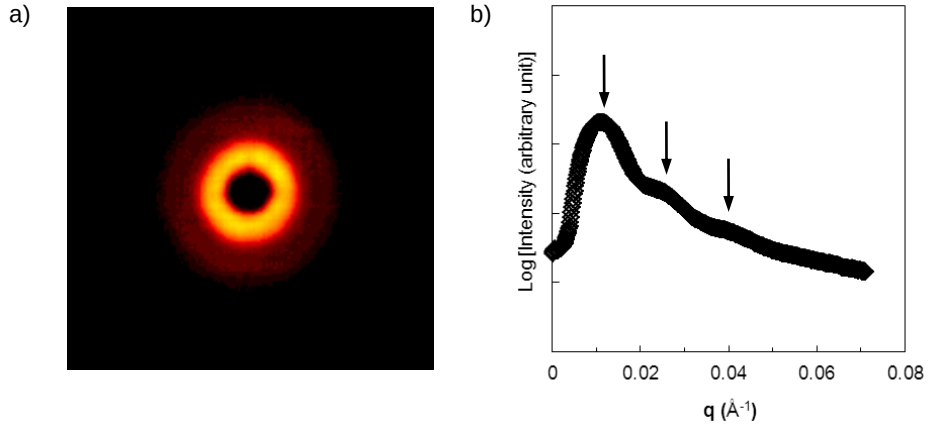

Figure 8. a) 2D-SAXS pattern and b) the intensity profile of PB-10 before injection molding, indicating a random orientation of the lamellae with 47-nm thickness.

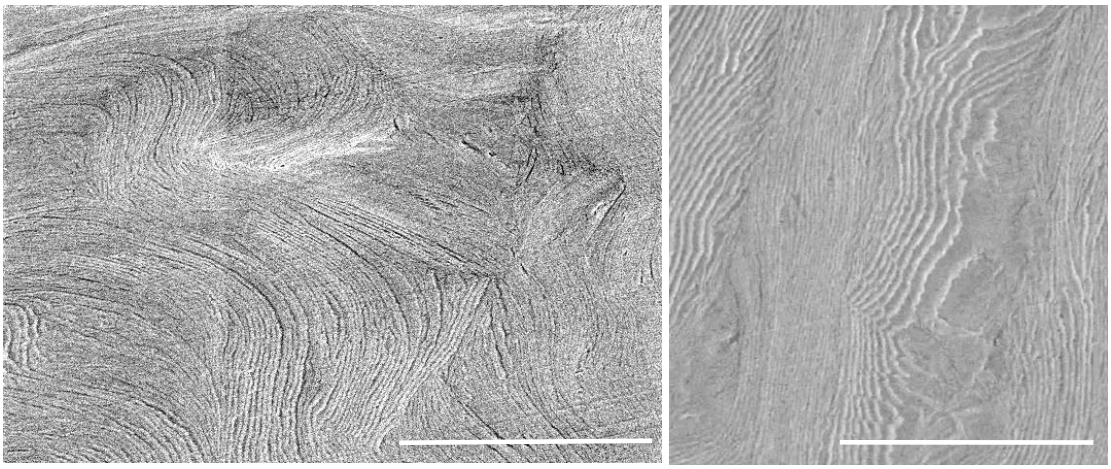

Figure 9. SEM images of the fracture surface of PB-10 before injection molding (left and right images taken from the region parallel and perpendicular to the lamellae, respectively). Scale bar, 5 μm.

4-3. Morphology and TC of PB-*n* after injection molding

Next, PB-10 plates with dimensions 10 × 40 × 1 mm^3 were injection molded. TC in the ND improved considerably to 1.2 W m^{-1} K^{-1}, which is 2–6 times higher than that of other isotropic polymers, compared to the modest level of 0.30 W m^{-1} K^{-1} in both MD and TD (Figure 10a). The TCs of PB-12 and PB-18 in the ND were also high, 1.1 and 0.82 W m^{-1} K^{-1}, respectively. Table 2 summarizes detailed results for TC, thermal diffusivity, density, and specific heat of injection-molded PB-10, PB-12, and PB-18.

Table 2. Physical properties of PB-*n* polymers in this work

sample	density	specific heat	thermal diffusivity [mm^2 s^{-1}]			thermal conductivity [W m^{-1} K^{-1}]		
	[g m^{-3}]	[J g^{-1} K^{-1}]	ND	MD	TD	ND	MD	TD
PB-10	1.20	1.38	0.71	0.18	0.18	1.2	0.30	0.30
PB-12	1.19	1.40	0.65	0.16	0.17	1.1	0.27	0.28
PB-18	1.13	1.50	0.49	0.16	0.15	0.83	0.27	0.25

To account for the observed high TC in the ND, the higher order structure was further characterized. The orientation of the lamellar crystals and polymer chains at the injection-molded PB-10 plate center was determined using 2D-SAXS and 2D-WAXD. Figure 10b shows the SAXS patterns. In both (ND, MD) and (ND, TD) patterns, the reflections attributable to the stack of lamellar crystals can be seen on the meridian. In

contrast, no corresponding reflection is observed in the (MD, TD) pattern. These results suggest that the lamellar crystals were aligned parallel to the (MD, TD) plane. The intensity profile from the (ND, MD) pattern indicates that the lamellar thickness was 47 nm even after shear flow (Figure 11). The 2D-WAXD pattern (Figure 10c) shows the outer (4.24 Å) and inner (21.0 Å) reflections. In both (ND, MD) and (ND, TD) patterns, outer peaks derived from the inter-mesogen reflections appear on the equator. No specific orientation is observed in the (MD, TD) pattern. These profiles indicate that polymer chains were well aligned perpendicular to the (MD, TD) plane (i.e., the lamellar plane). SEM observations of a cross-sectional surface of (ND, MD) near the molding surface (Figure 10d) confirmed the SAXS finding; that is, lamellar crystals were well aligned parallel to the (MD, TD) plane. CTE analysis also indicated the molecular orientation in the ND. Table 3 shows the CTE of PB-10. After injection molding, the CTE in the ND is much lower than those in the MD and TD. The crystallinity of injection-molded PB-10 was roughly estimated to be 70 to 80 % by powder XRD (Figure 12).

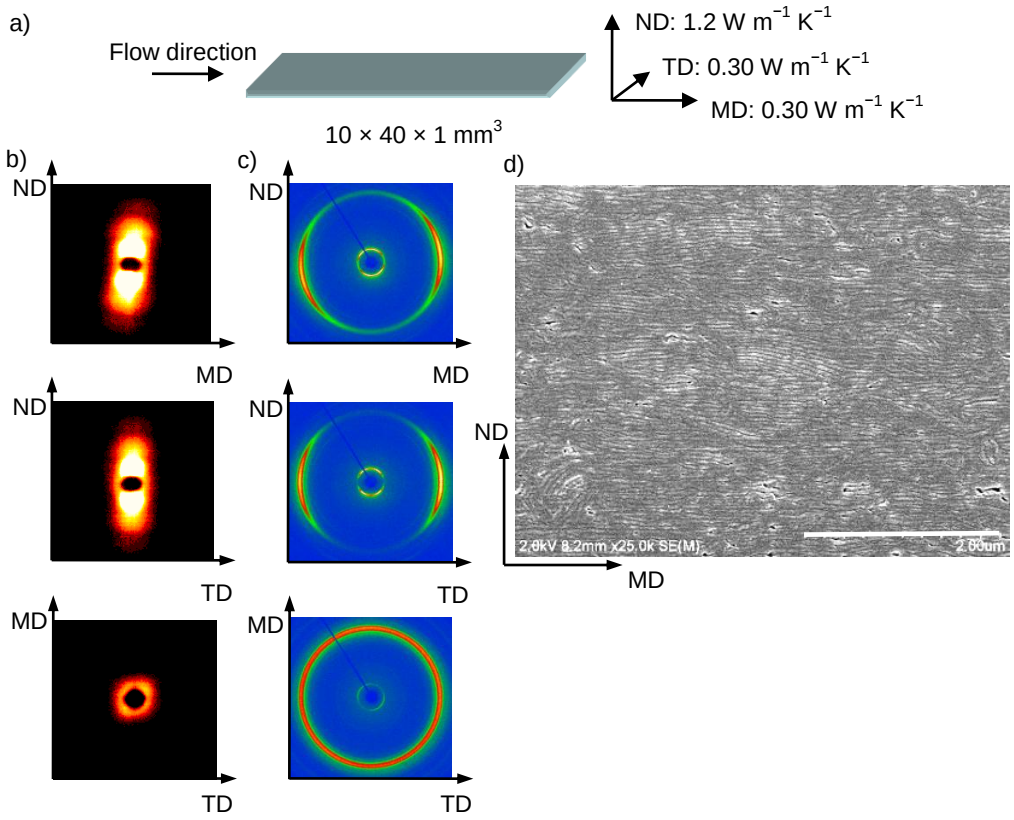

Figure 10. Characterization of injection-molded PB-10 plate. a) Shear geometry and thermal conductivity measured in three characteristic directions. b), c) 2D-SAXS and 2D-WAXS patterns along the MD, TD, and ND. d) SEM image observed on a cross-sectional surface of (ND, MD) near the molding surface. Scale bar, 2 μm.

Table 2. CTE of PB-10 before and after injection molding

sample	CTE ppm [K^{-1}]			
	before injection	after injection		
		ND	MD	TD
PB-10	91	29	163	169

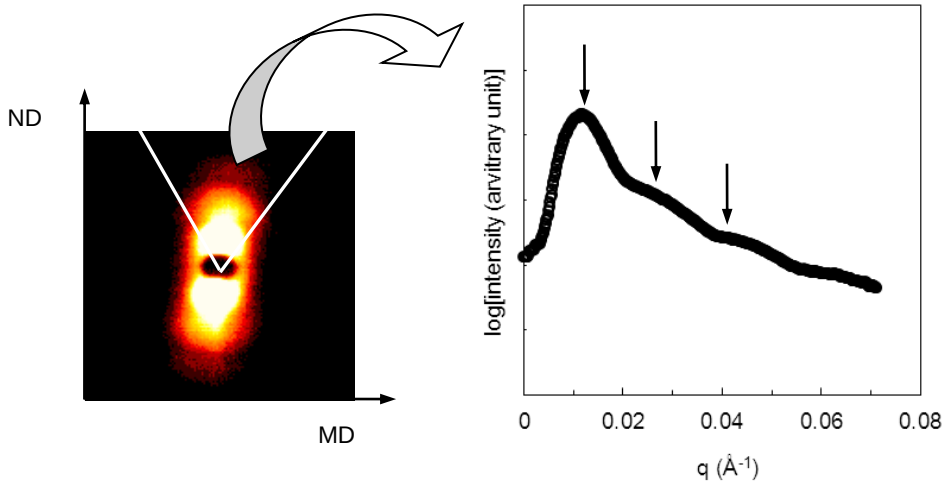

Figure 11. SAXS intensity profile of injection-molded PB-10 from the (ND, MD) pattern, indicating the lamellae with 47-nm thickness.

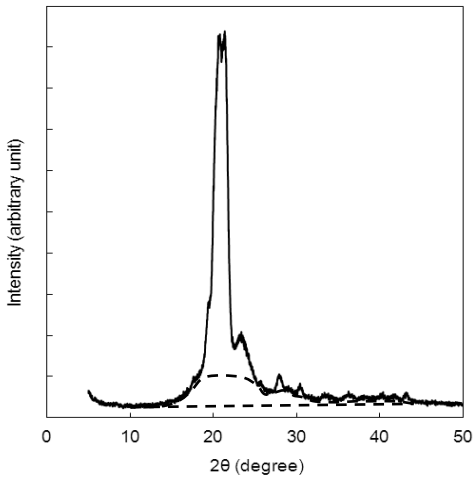

Figure 12. Powder XRD intensity profile of injection-molded PB-10, indicating the crystallinity of 70 to 80 %.

Other PB-*n* polyesters, PB-12 and PB-18 were also molded and measured by SAXS and WAXD; the results show the same orientation of lamellar crystal and polymer chain alignment (Figures 13 and 14). Figure 15 shows SEM image of a cross-sectional surface of injection-molded PB-18, indicating the parallel orientation of lamellae to the (MD, TD) plane.

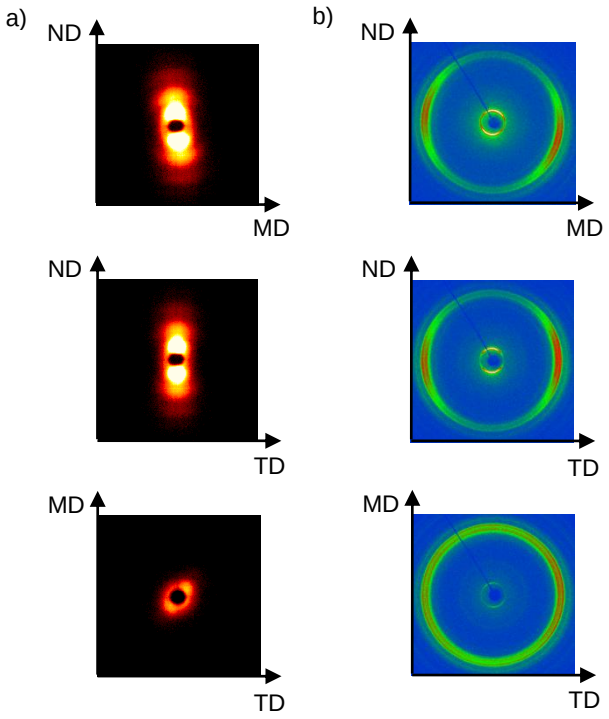

Figure 13. a), b) 2D-SAXS and 2D-WAXS patterns of injection-molded PB-12 along the MD, TD, and ND.

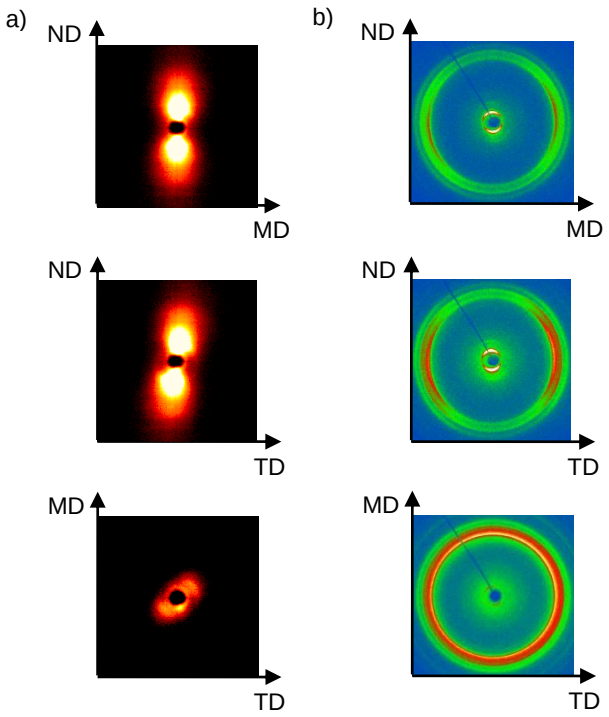

Figure 14. a), b) 2D-SAXS and 2D-WAXS patterns of injection-molded PB-18 along the MD, TD, and ND.

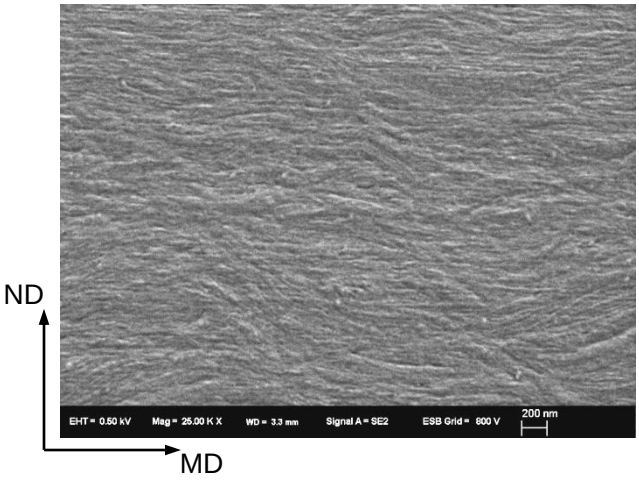

Figure 15. SEM image of PB-18 which is observed on a cross-sectional surface of (ND, MD) near the molding surface. Scale bar, 200 nm.

The SAXS intensity profiles indicate that the lamellar thicknesses were 41 nm for PB-12 and 29 nm for PB-18 (Figures 16 and 17). The crystallinities of injection-molded polyesters were 70 to 80 %, similar to that of PB-10 by powder XRD (Figures 18 and 19).

These findings suggest that the parallel orientation of the lamellar crystal of PB-*n* with high crystallinity is induced by a simple injection molding process, resulting in polymer chain alignment in the ND from a macroscopic viewpoint, and consequently a high TC in this direction.

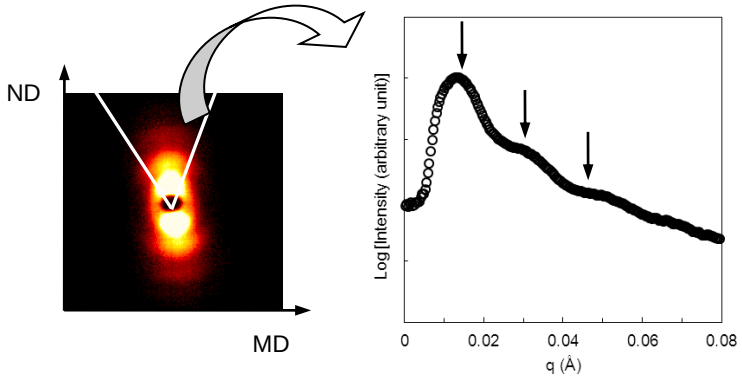

Figure 16. SAXS intensity profile of injection-molded PB-12 from the (ND, MD) pattern, indicating the lamellae with 41-nm thickness.

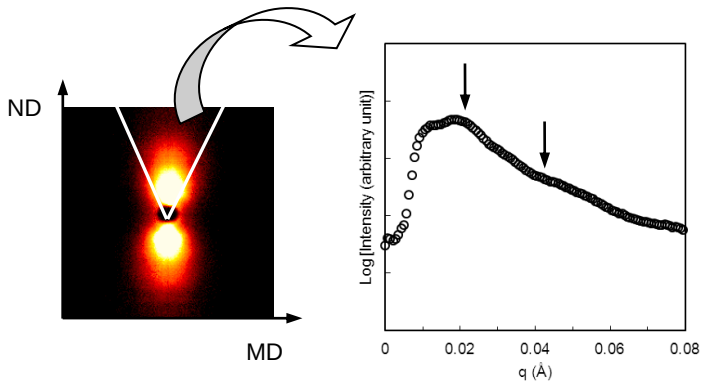

Figure 17. SAXS intensity profile of injection-molded PB-18 from the (ND, MD) pattern, indicating the lamellae with 29-nm thickness.

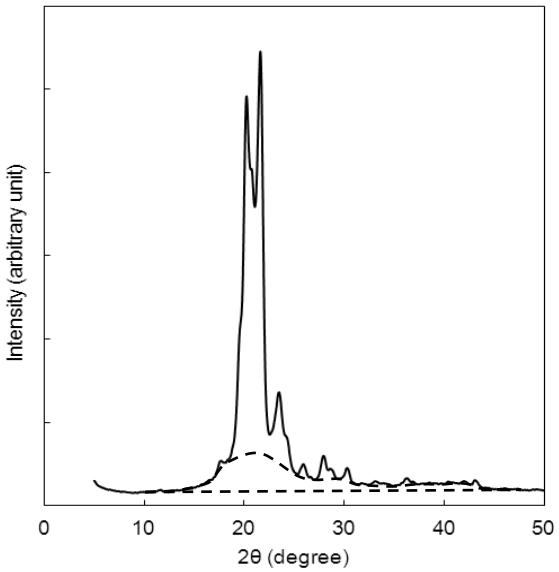

Figure 18. Powder XRD intensity profile of injection-molded PB-12, indicating the crystallinity of 70 to 80 %.

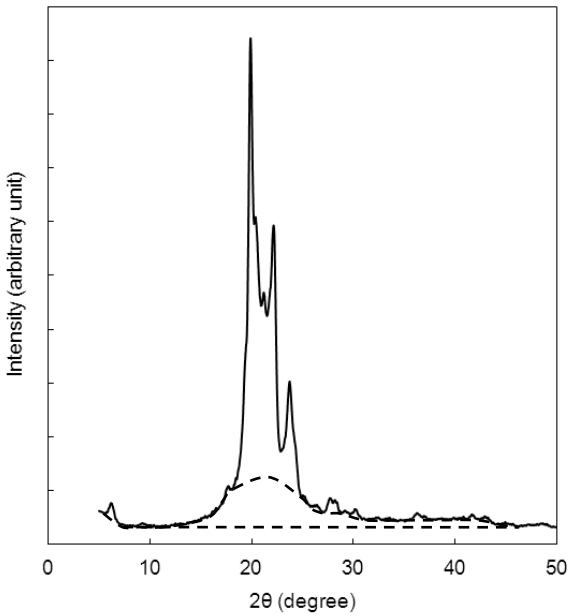

Figure 19. Powder XRD intensity profile of injection-molded PB-18, indicating the crystallinity of 70 to 80 %.

PB-*n* showed the parallel orientation of lamellae in Figure 1b and no perpendicular one in Figure 1c. Tokita and coworkers observed both parallel and perpendicular orientations of lamellae using a main-chain polyester showing smectic CA phase (Figure 20).[8] They reported that the parallel orientation can be appeared when the packing of mesogens in the smectic LC state is solidlike at low smectic temperatures. In contrast, perpendicular one can be observed when the packing is liquidlike at high temperatures because the orientation requires an internal flow of the mesogens. To

investigate the relationship between flow behavior of PB-*n* and molding conditions, TC in the ND after molding with several conditions (cylinder temperature, mold temperature, and injection pressure) was measured about PB-10 (Figure 21). Cylinder temperature at the range of 210−260 ºC resulted in high TC, whereas the TC drastically decreased at 270 ºC because PB-10 formed isotropic liquid at the temperature, leading to isotropic plate after injection molding. The TC increased with the cylinder and mold temperature increased, indicating that low viscosity of polymer melt and slow solidification contribute to the high orientation order of lamellae. In any case, the TC was higher than 0.8 W m^{-1} K^{-1}. These findings suggest that lamellar orientation of PB-10 is always parallel one when the cylinder temperature is within LC temperature. PB-*n*, where *n* is the even number, shows crystal-like (i.e., solid-like) packing of mesogens in the smectic I phase as mentioned in chapter 2. Therefore, the smectic lamella acts like a stiff plate. These facts strongly suggest that the shear flow in the smectic LC state of PB-*n* prefers the mutual slide of the lamellae whose boundary may possesses more fluidity to the internal flow with hard friction of mesogens.

a) 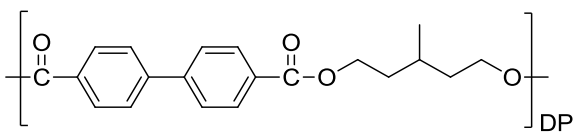

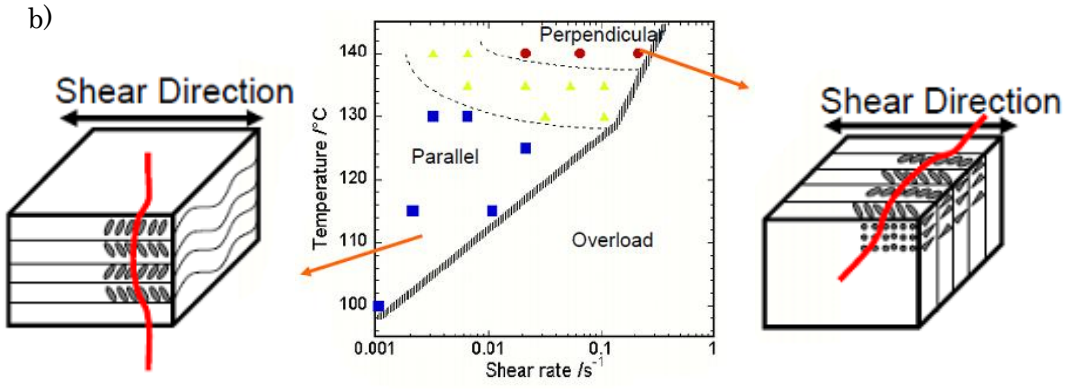

Figure 20. Smectic CA liquid crystalline polyester (BB5(3Me)). a) Chemical structure.

b) Shear behavior depending on temperature and shear rate (Ref. 8).

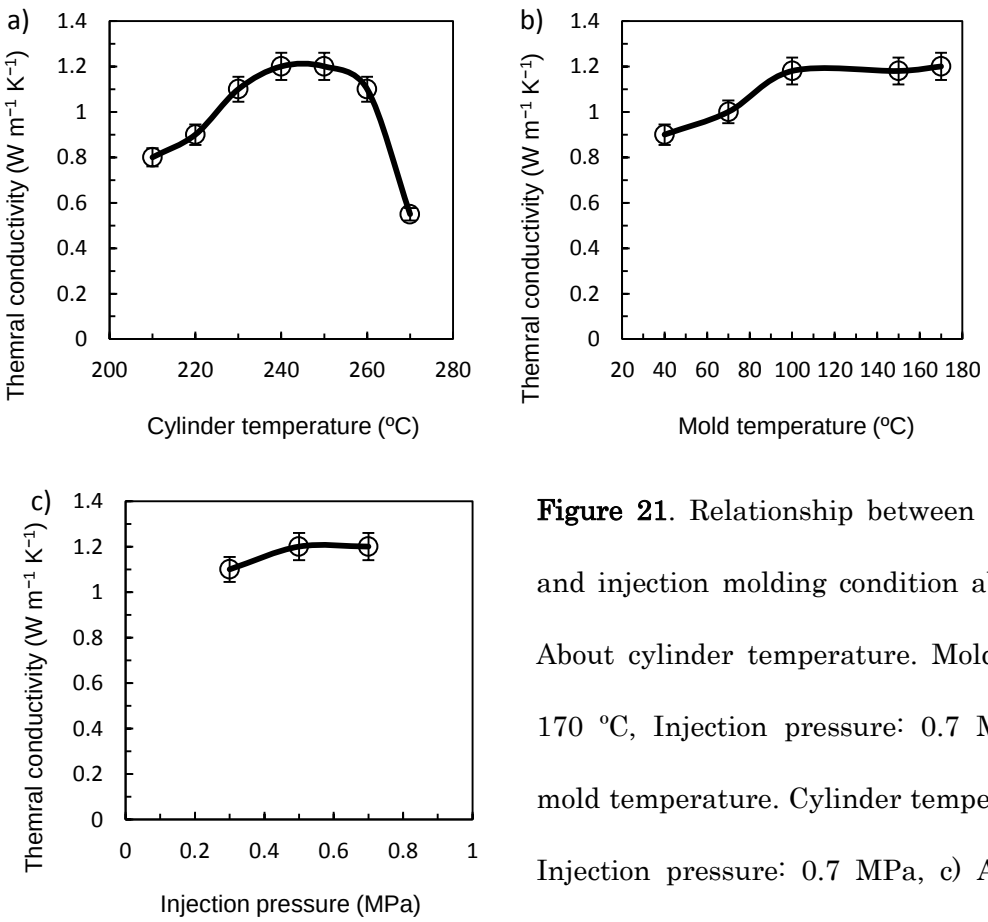

Figure 21. Relationship between TC in the ND and injection molding condition about PB-10. a) About cylinder temperature. Mold temperature: 170 ºC, Injection pressure: 0.7 MPa, b) About mold temperature. Cylinder temperature: 240 ºC, Injection pressure: 0.7 MPa, c) About injection

4-4. Influence of molecular weight of PB-10 on lamellar crystal alignment

PB-10 and PB-12 with different molecular weight were prepared by controlling the reaction period of melt condensation. Table 3 summarizes the TC in the ND of the molded polyesters. The polyesters with lower molecular weight than M_n: 16.0 kg mol^{-1} gave a similar type of lamellar crystal alignment and high TC in the ND. In contrast, the polyesters having higher molecular weight than M_n: 16.0 kg mol^{-1} showed a random orientation of lamellae even after injection molding. The TC value was about 0.5−0.6 W m^{-1} K^{-1}. Alt and coworkers investigated the alignment behavior of a main-chain polyester showing smectic phase depending on various shear conditions.[5] However, the parallel orientation of lamellae was not generally observed. About the reason for this, they reported that molecular entanglements or great interlayer connectivity might inhibit the sliding of lamellae, as is necessary in the parallel orientation. The viscosity of PB-10 with M_n: 10.0 kg mol^{-1} and PB-10-II with 24.0 kg mol^{-1} was measured with capillary rheometer. Figure 22 indicates that the viscosity of PB-10-II is 40 times as high as that of PB-10. The high viscosity is thought to be attributed to interlamellar connectivity. Therefore, the discussion of Alt is applicable to the reason for our results. I speculate that the random lamellar orientation for high M_n polymers results from the greater interconnectivity of the lamellae due to the higher molecular weight.

Table 3. Thermal conductivity in the ND depending on molecular weight

sample	M_n [kg mol^{-1}]	PDI	thermal conductivity ND [W m^{-1} K^{-1}]
PB10	5.60	2.1	1.1
	7.10	2.7	1.1
	8.00	1.9	1.2
	10.0	1.9	1.2
	14.6	2.2	0.72
	16.0	2.4	0.53
	19.6	2.8	0.55
	24.0	2.4	0.52
PB12	8.00	3.6	0.80
	10.5	2.5	1.1
	14.3	3.3	0.91
	18.8	2.7	0.60

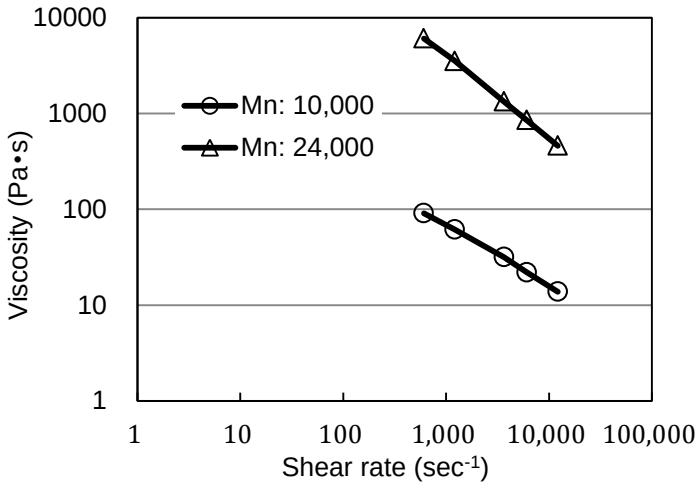

Figure 22. Viscosity of PB-10 polyesters.

4-5. Morphology and TC of injection-molded PB-10/h-BN composites

Finally, the TC of PB-10/h-BN composites was investigated. The plate-shaped particle h-BN has electrical insulation properties, density of 2.25 g cm^{-3}, and out-of-plane and in-plane TC values of 2 and 400 W m^{-1} K^{-1}, respectively.[9,10] Composites based on PBT, whose M_n and PDI were determined to be 16.9 kg mol^{-1} and 3.5, respectively, were also prepared for reference. The TCs of PBT were determined to be 0.25 W m^{-1} K^{-1} in the ND and 0.28 W m^{-1} K^{-1} in the MD and TD. Figures 23a and 23b show the TC of the composites having a different h-BN content in the ND and in-plane direction (average of the MD and TD), respectively. Table 4 summarizes detailed results for TC, thermal diffusivity, density, and specific heat of all the composites.

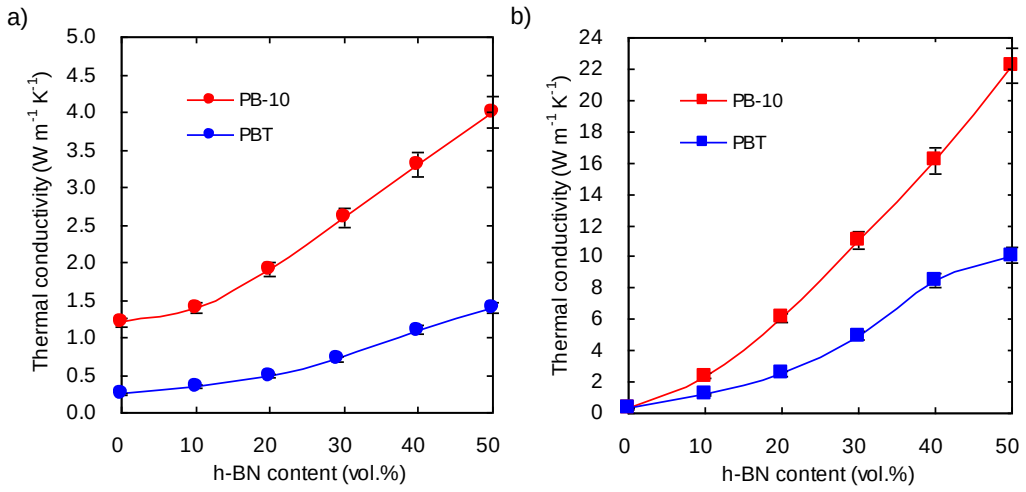

Figure 23. Effect of h-BN filler content on thermal conductivity of polymer composites in the a) ND and b) in-plane direction.

Table 4. Physical properties of h-BN and composites in this work

sample	h-BN content [vol.%]	density [g cm^{-3}]	specific heat [J g^{-1} K^{-1}]	thermal diffusivity [mm^2 s^{-1}]			thermal conductivity [W m^{-1} K^{-1}]		
				ND	MD	TD	ND	MD	TD
h-BN	100	2.25 [a]	0.81	-	-	-	2 [b]	400 [b]	400 [b]
PB-10/h-BN composites	10	1.30	1.28	0.83	1.5	1.4	1.4	2.5	2.3
	20	1.42	1.19	1.1	3.7	3.5	1.9	6.3	5.9
	30	1.51	1.13	1.5	6.5	6.6	2.6	11	11
	40	1.61	1.07	1.9	9.4	9.3	3.3	16	16
	50	1.73	1.00	2.3	13	12	4.0	23	21
PBT/h-BN composites	0	1.31	1.25	0.15	0.17	0.17	0.25	0.28	0.28
	10	1.41	1.18	0.21	0.66	0.78	0.35	1.1	1.3
	20	1.51	1.11	0.29	1.6	1.4	0.49	2.7	2.3
	30	1.59	1.07	0.42	3.0	2.8	0.71	5.1	4.8
	40	1.69	1.01	0.70	4.9	5.0	1.2	8.4	8.5
	50	1.79	0.965	0.80	5.7	6.0	1.4	9.8	10

[a] W. S. Lee, J. Yu, *Diam. Relat. Mater.* **2005**, *14*, 1647. [b] M. T. Hung, H. Ishida, *J. Polym. Sci. Part B: Polym. Phys.* **1999**, *37*, 2360.

In the ND, the TC of PB-10 composites is 3–4 times higher than that of PBT composites. The difference in the TCs of the composites is a direct reflection of the difference in the TCs of the respective polymer matrices. Surprisingly, a significant enhancement of TC in the in-plane direction was also observed with the PB-10 matrix, although PB-10 is a poor conductor in this direction similar to PBT. When the filler

content was 50 vol%, TC reached 22 W m^{-1} K^{-1}, which to the best of our knowledge is a new record for the TC of thermoplastics with electrical insulation properties.

The 2D-WAXD pattern of the PB-10 composite (40 vol%) (Figure 24a) shows (002) reflections (3.33 Å) derived from h-BN (Figure 24b) in addition to reflection patterns from PB-10 that are the same as those shown in Figure 10c. In both (ND, MD) and (ND, TD) patterns, (002) reflections were observed at the meridian and the (MD, TD) pattern showed no (002) reflection. These profiles indicate a parallel orientation of h-BN and a substantially perpendicular orientation of polymer chains to the (MD, TD) plane. On the basis of these results, I propose a heat conductive model in which polymer chains aligned in the ND serve as effective heat paths between h-BN filler particles, which conduct heat mainly in the in-plane direction (Figure 25). This orientation of polymer chains perpendicular to the h-BN plane was accomplished for the first time using the current technique. I found that the arrangement is highly effective toward increasing TC in both ND and in-plane direction.

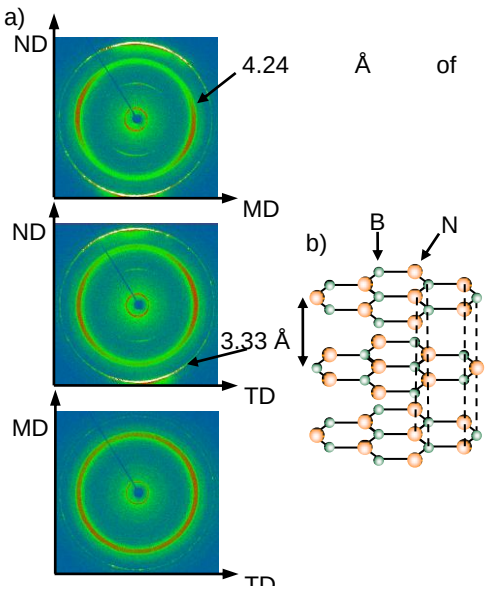

Figure 24. a) 2D-WAXS patterns of injection-molded PB-10/h-BN composites at 40 vol.% h-BN loading. b) Crystal structure of h-BN.

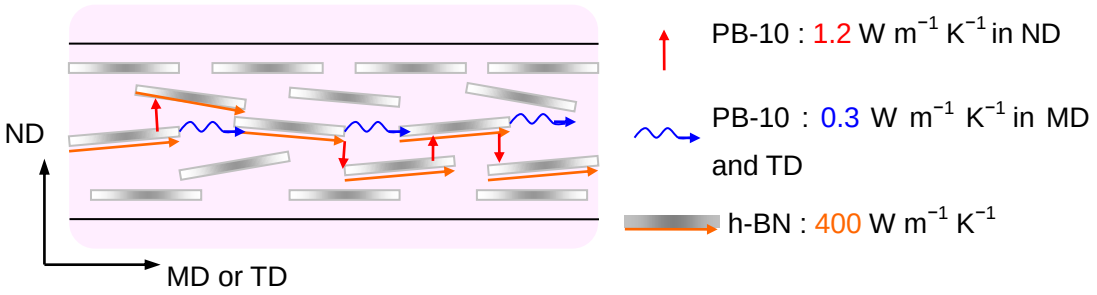

Figure 25. Heat conductive model in the in-plane direction for injection-molded PB-10/h-BN composites.

This technique enables producing polymer materials with unprecedentedly high TCs that can replace metal or ceramic parts in cases where heat dissipation is necessary.[11]

Moreover, to attain a TC of 10 W m^{-1} K^{-1}, for example, PB-10 requires a 20 vol% lower amount of h-BN than other common polymers. This leads to more lightweight composites with good processability.

5. Conclusion

Thermal conductivities of injection-molded PB-*n* and PB-10/h-BN composites were investigated. Shear flow in the LC state of PB-*n* during injection molding induces the parallel orientation of lamellae, in which polymer chains are aligned in the ND with respect to the molding surface, thus leading to a high TC in this direction. This flow behavior results from the mutual slide of smectic lamellae. However, if the molecular weight was too high, any orientation of lamellae was not observed due to the inter-lamella connectivity. The composites exhibited a dramatic enhancement of TC in not only the ND but also the in-plane direction. Polymer chains aligned in the ND served as effective heat paths between h-BN filler particles, which conduct heat mainly in the in-plane direction. To achieve high TC, PB-10 requires a lower amount of h-BN than other common polymers. This leads to more lightweight composites with good processability. For this approach, no special equipment is required, and an injection

molding process is suitable. Therefore, this approach can be readily scaled up for various applications.

6. Appendix; Heat dissipation performance of in-plane thermally conductive composites.

To confirm the heat dissipation performances of thermally conductive composites, samples having in-plane TCs of 5–14 W m^{-1} K^{-1} were prepared and molded into heat sink components by injection molding (Figure 26). The TC of base plate and fin part in a heat sink made of composite A (14 W m^{-1} K^{-1}) was measuared. Both parts exhibit in-plane TC of 14 W m^{-1} K^{-1} (Figure 27), indicating that current technique is available to mold complex shapes.

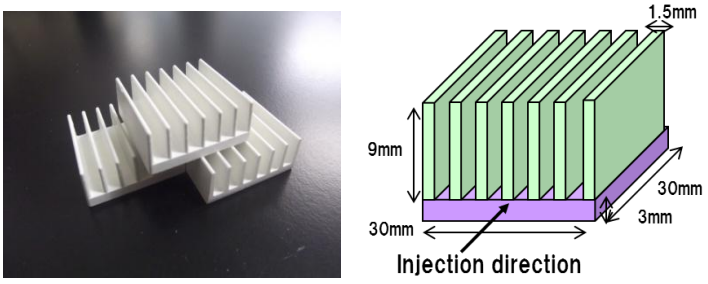

Figure 26. Heat sink used for evaluation of heat dissipation ability of some composites.

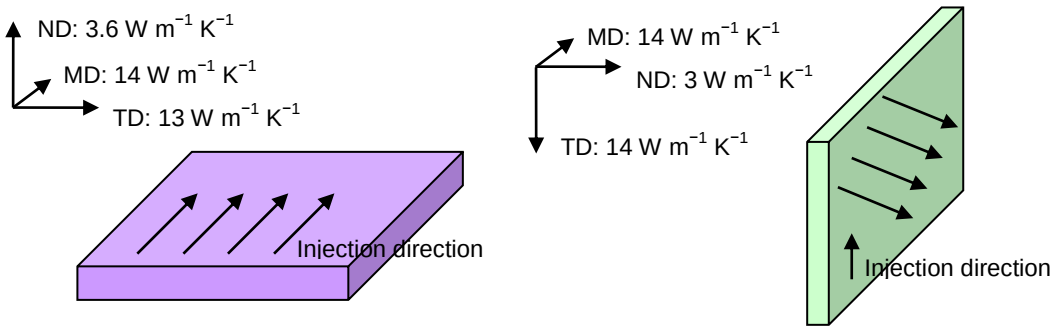

Figure 27. TC of base plate and fin part in a heat sink made of a composite A (14 W m^{-1} K^{-1}).

As a comparison, the performance of an aluminum die-cast component with the same shape and a TC of 180 W m^{-1} K^{-1} was also evaluatd, where the thermal emissivity was adjusted to 0.85 of resin by an alumite treatment. The contact between the heat sink and heater was made using adhesive tape, and the temperature of the heater with a power of 1.2 W was measured with a thermocouple under room conditions. Figure 28 shows the relationship between the TC of the heat sink materials and the heater temperature under equilibrium. The temperature was 210 °C without a heat sink. Using a heat sink, the temperature decreased as the TC of the heat sink material increased. When a coposite A (14 W m^{-1} K^{-1}) was used, the temperature was reduced to 65 °C. On the other hand, the aluminum die-casting heat sink decreased the temperature to 60 °C, indicating that the composite A has a comparable heat dissipation performance to the die-cast aluminum. This result was attributed to the small size of the heat sink used in this study. When the

TC of the material increased to some extent, the heat transfer to the end of the fin is saturated and heat radiation to the air becomes rate-limiting. From these findings, composite A is expected to be an alternative material to metals such as aluminum for the purpose of reducing the weight of small electronic devices.

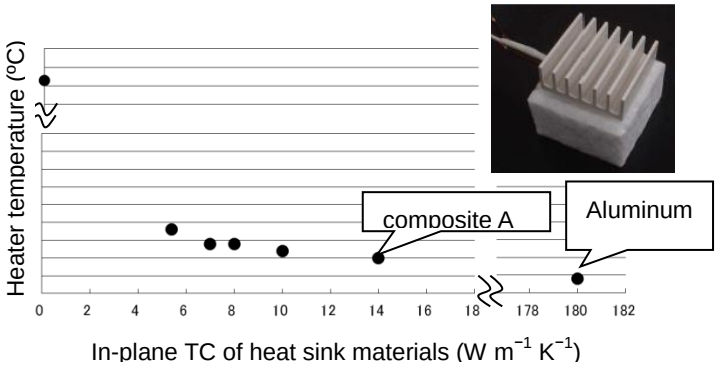

Figure 28. The relationship between a TC of heat sink materials and heater temperature.

References

[1] J. Asrar, H. Toriumi, J. Watanabe, W. R. Krigbaum, A. Ciferri, *J. Polym. Sci. Polym. Phys.* **1983**, *21*, 1119.

[2] W. R. Krigbaum, J. Watanabe, T. Ishikawa, *Macromolecules* **1983**, *16*, 1271.

[3] M. Tokita, K. Osada, M. Yamada, J. Watanabe, *Macromolecules* **1998**, *31*, 8590.

[4] W. R. Krigbaum, J. Watanabe. *Polymer* **1983**, *24*, 1299.

[5] D. J. Alt, S. D. Hudson, R. O. Garay, K. Fujishiro, *Macromolecules* **1995**, *28*, 1575.

[6] M. Tokita, T. Takahashi, M. Hayashi, K. Inomata, J. Watanabe, *Macromolecules* **1996**, *29*, 1345.

[7] W.-J. Zhou, J. A. Kornfield, V. M. Ugaz, W. R. Burghardt, D. R. Link, N. A. Clark, *Macromolecules* **1999**, *32*, 5581.

[8] M. Tokita, K. Tokunaga, S. Funaoka, K. Osada, J. Watanabe, *Macromolecules* **2004**, *37*, 2527.

[9] W. S. Lee, J. Yu, *Diam. Relat. Mater.* **2005**, *14*, 1647.

[10] M. T. Huang, H. Ishida, *J. Polym. Sci. Part B:Polym. Phys*. **1999**, *37*, 2360.

[11] Ir. R. H. C. Janssen, Ir. L. Douren, H. K. Van Dijk, *LED professional Review* **2010**, *Jan/Feb*, 38.

Chapter 4

Influence of Molecular Orientation Direction on the In-plane Thermal Conductivity of Polymer/Hexagonal Boron Nitride Composites

1. Abstract

The effect of the molecular orientation direction of a polymer matrix on the in-plane thermal conductivity (TC) of injection-molded polymer/hexagonal boron nitride (h-BN) composites is investigated. In this system, the h-BN platelets align in the in-plane direction owing to injection shear flow. Three molecular orientations (perpendicular, random, and parallel to the h-BN plane) are achieved using liquid crystalline polyesters and the in-plane TCs are compared. Although a parallel orientation of the polymer chains provides the highest TC of the matrix in the injection direction, the TC of the composites is the lowest of the three systems for this orientation. The highest in-plane TC is found in the perpendicularly oriented system, irrespective of the in-plane direction. These results reveal that perpendicularly oriented molecular chains serve as effective heat paths between h-BN platelets that are arranged one above the other, and consequently, a continuous thermal network is created in the in-plane direction.

2. Introduction

In chapter 3, I found that a main-chain smectic liquid crystalline PB-10 polyester acts as an effective thermally conductive matrix in a composite with hexagonal boron nitride (h-BN). PB-10 polyester forms a smectic I liquid crystalline (LC) phase with 47-nm-thick lamellae stacked regularly along the polymer chain direction as seen in chapter 2 and Ref. 1-3. Shear flow during injection molding induces lamellar crystal alignment, in which the polymer chains are aligned in the normal direction (ND) with respect to the molding surface (Figure 1a), thus leading to a high TC (1.2 W m^{-1} K^{-1}) in the ND (Figure 1b). In contrast, the TCs in both the machine direction (MD) and the transverse direction (TD) are only modest at 0.30 W m^{-1} K^{-1}. However, the composites with h-BN exhibit a dramatic enhancement of the TC in not only the ND but also the MD and TD. Thus, I proposed a heat conductive model involving polymer chains aligned in the ND that serve as effective heat paths between the h-BN plates, which mainly conduct heat at a high TC of 400 W m^{-1} K^{-1} in the in-plane direction.[4]

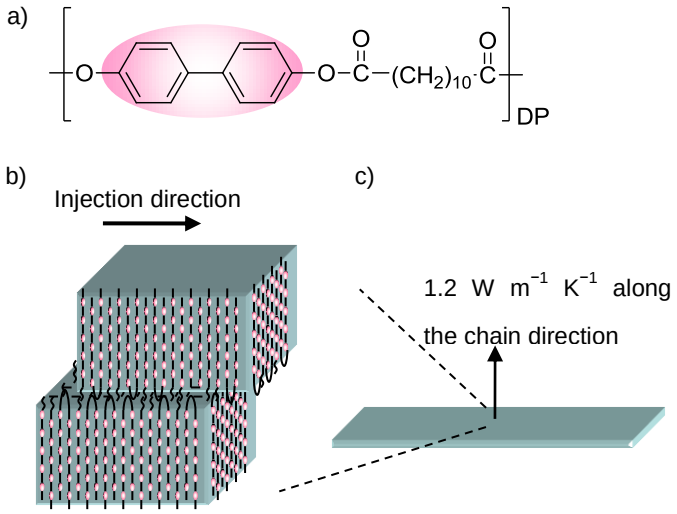

Figure 1. Characteristics of PB-10-I. a) Chemical structure of PB-10. b) Alignment of the LC lamellae induced by injection shear flow. c) High TC of molded PB-10-I in the ND.

The anisotropic TC property observed in polymer/h-BN composites exhibits strong correlation with the orientation and the size of h-BN platelets. S. Ando and co-worker reported that polyimide (PI)/h-BN films filled with large plate-shaped particles exhibited a large anisotropy in TC due to the strong in-plane orientation of h-BN platelets, while smaller anisotropy was observed in films filled with aggregates and small flakes which are less likely to orient in the in-plane direction during film processing.[5] When the in-plane TC of a polymer/h-BN composite must be increased, thus, in-plane orientation of heat-conducting basal plane of h-BN should be utilized. For

the same purpose, in addition, a polymer matrix with a high in-plane TC is also thought to be more effective. Actually, S. Ando and co-worker also showed that PI matrix with higher in-plane TC effectively enhanced the in-plane TC of PI/h-BN composites using two PI specimens, which exhibit the TC value of 1.22 and 0.526 W m^{-1} K^{-1} in the in-plane direction, respectively, whereas the out-of-plane TCs are similar (0.248 and 0.277 W m^{-1} K^{-1}).[5] From the point of view, then, aligned PB-10 polyesters are not efficient but isotropic PB-10 polyesters should be better because the TC of isotropic PB-10 polyesters is 0.52 W m^{-1} K^{-1} in all directions (Chapter 3). Moreover, it is well known that conventional fully aromatic thermotropic LC polyesters (LCP) can readily provide molecular orientation in the MD under injection shear. C. L. Choy and co-worker reported that the highly oriented structure of the resultant materials results in a high TC of more than 1 W m^{-1} K^{-1} in the MD.[6] Therefore, LCPs might be the optimum matrix to achieve a higher in-plane TC in h-BN composites.

Herein, I report that a polymer matrix with high TC in the ND enhances the in-plane TC of the polymer/h-BN composites more effectively than a matrix with high in-plane TC. In this study, three LC polyesters were used: PB-10-I and PB-10-II with different molecular weights and a commercially available LCP (Ueno LCP A-8000). Since 45-μm-sized h-BN platelets were used, the injection shear flow induced in-plane

orientation of h-BN. PB-10-II is always isotropic even after injection molding owing to its high molecular weight (Chapter 3). The LCP exhibited the highest TC in the MD. However, the order of the composite TC in the MD was PB-10-I > PB-10-II > LCP. These findings revealed that molecular chains oriented in the ND serve as the most effective heat paths between h-BN platelets stacked closely, leading to the formation of a continuous thermal network.

3. Experimental Section

3-1. Materials

PB-10 polyesters (Figure 1a) were synthesized by melt condensation of 4,4′-diacetoxy biphenyl and 1,10-dodecanedioic acid with sodium acetate as the catalyst. These chemicals were purchased from Wako Pure Chemical Industries, Ltd. and were used as received. The PB-10 polyesters showed crystal-smectic transformations at T_m and smectic-isotropic transformations at T_i, which were measured by differential scanning calorimetry (DSC) at a heating rate of 10 °C min^{-1} (PerkinElmer Pyris 1 DSC). Two specimens with different molecular weights, PB-10-I (M_n: 10,000, M_w: 19,000, T_m: 204 °C, T_i: 246 °C) and PB-10-II (M_n: 24,000, M_w: 58,000, T_m: 206 °C, T_i: 256 °C) were prepared by controlling the reaction period of the melt condensation. After polycondensation, the molten polymer was discharged onto a stainless plate. An LCP

sample (Ueno LCP A-8000) was provided by Ueno Fine Chemicals Industry. It showed a solid-LC transition temperature (T_m) at 220 °C. Kimura and co-worker reported the chemical structure (Figure 2b) and the molecular weight (M_n: 10,000, M_w: 31,000).[7] Plate-shaped h-BN (PT110) with a mean particle size of 45 μm in diameter and 2 μm in thickness was purchased from Momentive Performance Materials Inc. (Figure 2c). The h-BN platelets have electrical insulation properties, density of 2.25 g cm and out-of-plane and in-plane TC values of 2 and 400 W m^{-1} K^{-1}, respectively.[4,8]

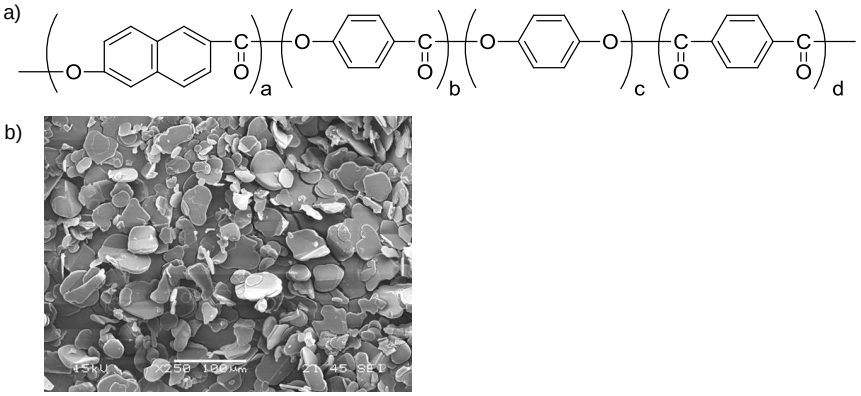

Figure 2. Components of the polymer composites. a) Chemical structures of Ueno LCP A-8100. b) SEM image of the hexagonal boron nitride platelets (h-BN). Scale bar, 100 μm.

3-2. Gel Permeation Chromatography (GPC)

The number average molecular weight (M_n) and weight-average molecular weight (M_w)

of the PB-10 polyesters were determined by gel permeation chromatography (GPC) in a *p*-chlorophenol/toluene (3/8 volume ratio) solution (Viscotek Ht-GPC with a RI detector). The molecular weight was calibrated as a relative value to a polystyrene standard.

3-3. Morphology Characterization

Two-dimensional wide-angle X-ray diffraction (2D-WAXD) patterns were recorded on an imaging plate at 25 °C using Cu Kα radiation, which was generated by a Rigaku-Denki UltraX18 X-ray generator equipped with a graphite crystal monochromator and a pinhole collimator. The 2D-WAXD patterns for the PB-10-II/h-BN composite were recorded at 25 °C with a Bruker AXS D8 Discover using Cu Kα radiation. Scanning electron microscopy (SEM) was performed using a Hitachi S-4800 SEM microscope. To observe the dispersion of h-BN in composites, each specimen with the surface smoothed using a microtome was subjected to platinum–palladium deposition. To observe the crystalline lamellae of PB-10, the specimen with the surface smoothed using a microtome was exposed to RuO_4 vapor before platinum–palladium deposition. To observe the LCP fibrils, the specimen was first fractured and then subjected to platinum–palladium deposition.

3-4. Compounding and Injection Molding Conditions

The polymers and h-BN were mixed using a twin-screw extruder (TECHNOVEL Corp., KZW15TW). The screw rotation speed was 90 revolutions per minute. The temperature was set at 220 °C for PB-10-I, 230 °C for PB-10-II, and 250 °C for LCP. The actual filler content of the composites was determined from their densities and residual content after a burn-out test at 450 °C. The polymers and composites were molded by a mini injection molder (DSM Xplore, Micro Injection Moulding Machine 5.5 ml) to plates with dimensions of 10 × 40 × 1 mm^3. The cylinder and mold temperatures were 240 °C and 170 °C for the PB-10s and their composites and 250 and 170 °C for the LCP and its composites, respectively. The injection pressure was 0.7 MPa.

3-5. Thermal Conductivity Measurements

TC (λ) was evaluated using thermal diffusivity (α) data according to Eq. (1):

$$\lambda = \alpha\rho c, \quad (1)$$

where ρ and c are the density and heat capacity, respectively. The thermal diffusivities of the samples in the ND, MD, and TD were measured in triplicate for each direction at 25 °C in accordance with the American Society for Testing and Materials (ASTM) E-1461 using a Netzsch LFA 447 NanoFlash instrument with ±5% accuracy. The density and heat capacity were determined by the Archimedean and DSC methods,

respectively.

4. Results and discussion

4-1. Morphology and TC of the Neat Polymers after Injection Molding

The orientation direction of the polymer chains at each injection-molded polymer plate center was determined using 2D-WAXD (Figure 3a). In Chapter 3, the 2D-WAXD patterns for PB-10-I were shown, indicating that the polymer chains are well aligned perpendicular to the (MD, TD) plane. Figure 3b shows the patterns for PB-10-II and indicates a random chain orientation. We speculate that this flow behavior results from the inhibition of lamellar sliding derived from the inter-lamellar connectivity by the higher M_n polymer. Figure 3c shows the patterns for the LCP, in which the peaks from the inter-mesogen reflections (5.34 Å) are observed. In both the (ND, MD) and (TD, MD) patterns, the peaks strongly appear on the meridian. These profiles indicate a polymer chain orientation in the MD. In the (ND, TD) pattern, the inter-mesogen reflection is somewhat concentrated on the meridian, indicating that the molecules also lie slightly in the TD.

The TCs of the three specimens are shown in Figure 4. The LCP exhibited a high TC of 1.2 W m^{-1} K^{-1} in the MD, but a very low TC of 0.17 W m^{-1} K^{-1} in the ND. The TC in the TD (0.40 W m^{-1} K^{-1}) is attributed to the moderate molecular orientation in this

direction. The TC value in the MD was as large as that of PB-10-I in the ND. PB-10-II exhibited a TC of 0.52 W m^{-1} K^{-1} in all directions, which is greater than that of PB-10-I in the in-plane direction.

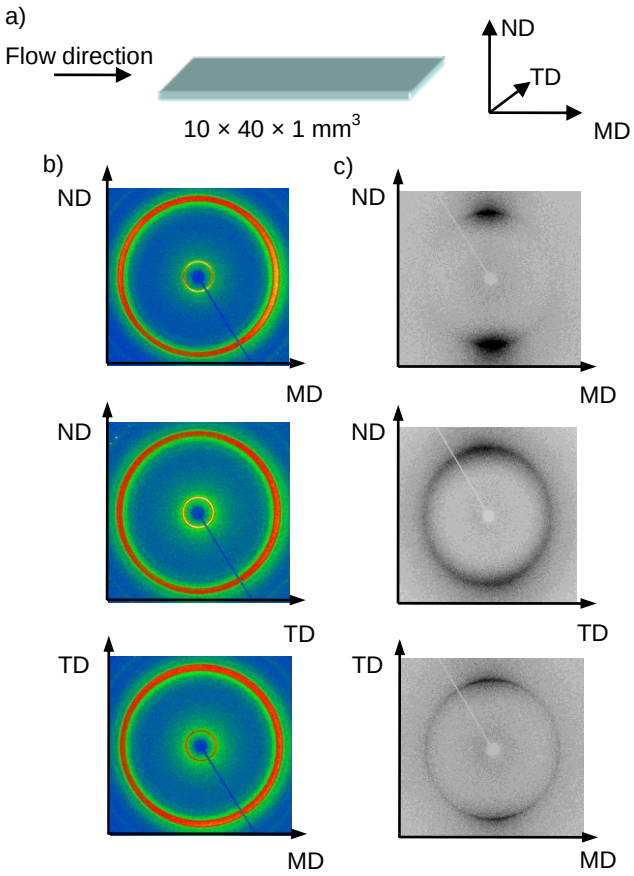

Figure 3. Characterization of injection-molded polymer plates. a) Shear geometry. b) and c) 2D-WAXS patterns along the MD, TD, and ND for PB-10-II and the LCP, respectively.

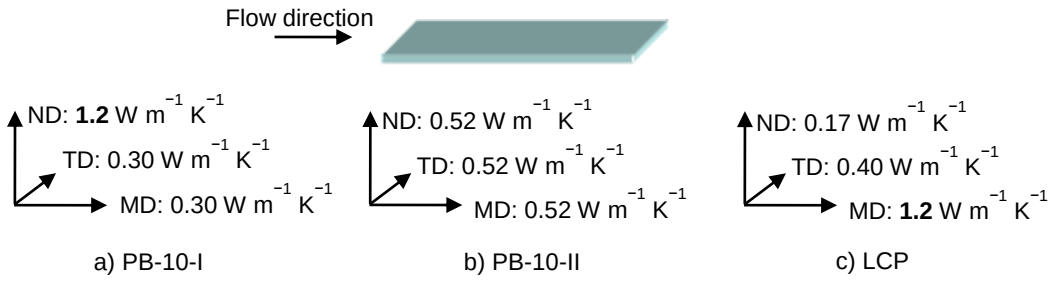

Figure 4. Thermal conductivity measured in three characteristic directions for each polymer plate.

4-2. Morphology and TC of the Injection-Molded Polymer/h-BN Composites

Next, the orientation directions of the polymer chains and h-BN platelets in each composite (40 vol%) were investigated using 2D-WAXD. There are two dimensions in the h-BN, which are the graphite-like structure with strong bonding within the planar, fused, six-membered rings (*a*-axis) and the van der Waals bonding in-between layers (*c*-axis) (Figure 5a). Figures 5b and 5c show the (002) reflections (3.33 Å) derived from the h-BN in addition to the same reflection patterns from each polymer (PB-10-II and LCP) as seen in Figures 3b and 3c. In both the (ND, MD) and (ND, TD) patterns, the (002) reflections are observed on the meridian, and the (MD, TD) pattern shows a weak (002) reflection. These profiles indicate that the h-BN platelets tend to align in the in-plane direction, and the preferred orientation for each polymer is achieved even after incorporation of h-BN. The 2D-WAXD patterns for PB-10-I composite (40 vol%) were shown in chapter 3, indicating the similar orientation of h-BN platelets and molecular

orientation in the ND.

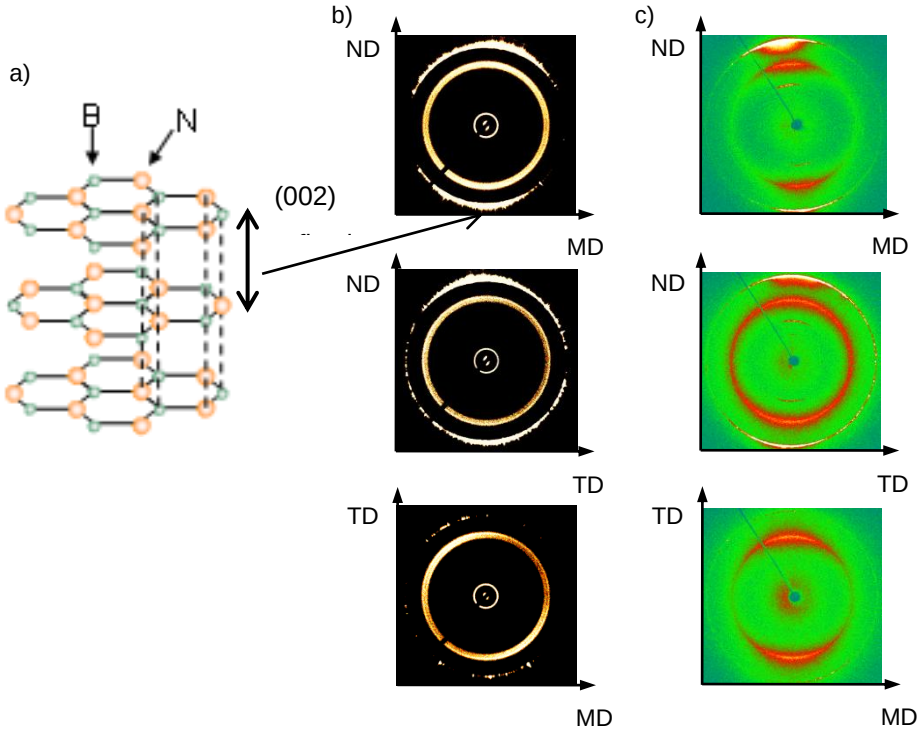

Figure 5. Characterization of injection-molded composite plates (40 vol%). a) Crystal structure of h-BN. b) and c) 2D-WAXS patterns along the MD, TD, and ND for PB-10-II and the LCP, respectively.

Figure 6 shows the SEM images observed on a cross-sectional surface of (ND, MD) plane about PB-10-I and LCP composites at 30 and 29 vol%, respectively, indicating that h-BN platelets are comparatively oriented in the in-plane direction. Moreover, the interface between polymer matrix and h-BN platelets appears to be continuous without

voids and the dispersion of platelets are similar between PB-10-I and LCP composites.

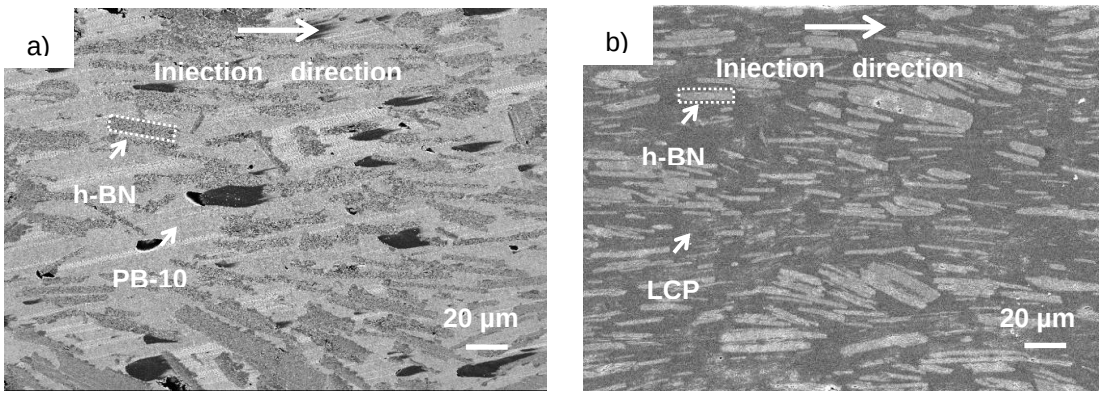

Figure 6. SEM images of the cross-sectional surface (ND, MD) for the a) molded PB-10-I composite (30 vol%) and b) molded LCP composite (29 vol%). Scale bar, 20 μm.

Figures 7a and 7b show the TC of composites with different levels of h-BN content in the ND and in the MD, respectively. Table 1 lists detailed results for the TC, thermal diffusivity, density, and specific heat of all of the composites. In the ND, the TC of the PB-10-I composites is the highest of the three systems. This result is a direct reflection of the difference in the TCs of the respective polymer matrices. The TC of PB-10-I composite at 50 vol% was 4.0 W m^{-1} K^{-1}, which is more than out-of-plane TC (2 W m^{-1} K^{-1}) of h-BN platelets. This is thought to be due not only to the existence of the *a*-axis of h-BN along the thickness direction of the molded plates but also to the molecular orientation in the same direction. Surprisingly, the highest TC in the MD was also

observed with the PB-10-I matrix, although PB-10-I is a poor conductor in this direction. Unexpectedly, the TC of the LCP composites in this direction was the lowest. At a 50 vol% loading, the TC value was 10 W m^{-1} K^{-1}, which is the same level as that of a conventional polymer composite at a comparable loading level (see the data based on polybutylene terephthalate (0.25 W m^{-1} K^{-1}) in chapter 3).

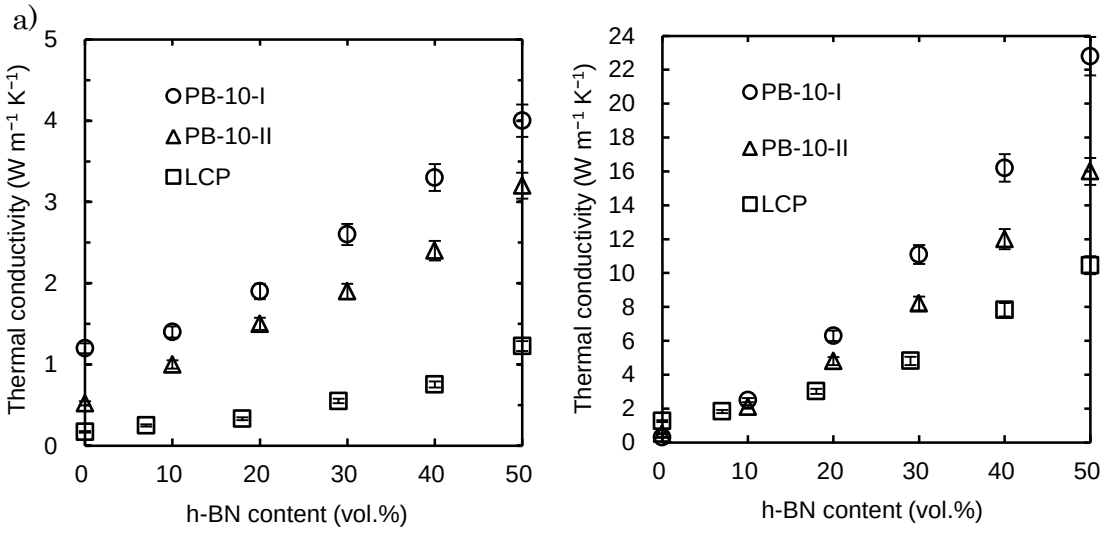

Figure 6. Effect of h-BN filler content on the thermal conductivity of polymer composites in the a) ND and b) MD.

Table 1. Physical properties of h-BN and composites in this work

sample	h-BN content	density[a)]	specific heat[b)]	thermal diffusivity [$mm^2 s^{-1}$]			thermal conductivity [$W m^{-1} K^{-1}$]		
	[vol.%]	[$g cm^{-3}$]	[$J g^{-1} K^{-1}$]	ND	MD	TD	ND	MD	TD
h-BN	100	2.25[c)]	0.81	-	-	-	2[d)]	400[d)]	400[d)]
PB-10-I composites	0	1.20	1.38	0.71	0.18	0.18	1.2	0.30	0.30
	10	1.30	1.28	0.83	1.5	1.4	1.4	2.5	2.3
	20	1.42	1.19	1.1	3.7	3.5	1.9	6.3	5.9
	30	1.51	1.13	1.5	6.5	6.6	2.6	11	11
	40	1.61	1.07	1.9	9.4	9.3	3.3	16	16
	50	1.73	1.00	2.3	13	12	4.0	23	21
PB-10-II composites	0	1.20	1.38	0.31	0.31	0.31	0.52	0.52	0.52
	10	1.30	1.28	0.6	1.3	1.4	1.0	2.1	2.3
	20	1.42	1.19	0.89	2.8	2.8	1.5	4.8	4.7
	30	1.51	1.13	1.1	4.8	4.7	1.9	8.2	8.0
	40	1.61	1.07	1.4	7.0	6.8	2.4	12	12
	50	1.73	1.00	1.8	9.2	8.5	3.2	16	15
LCP composites	0	1.40	1.05	0.12	0.84	0.28	0.17	1.2	0.40
	7	1.46	1.02	0.17	1.2	0.54	0.25	1.8	0.81
	18	1.56	0.98	0.22	2.0	0.96	0.33	3.0	1.5
	29	1.65	0.95	0.35	3.0	1.7	0.55	4.7	2.6
	40	1.75	0.92	0.47	4.9	2.9	0.76	7.8	4.7
	50	1.84	0.90	0.76	6.5	5.2	1.2	10	8.4

[a)] The density was measured by the Archimedean method.

[b)] The heat capacity was measured by the differential scanning calorimetry (DSC) method.

[c)] Lee, W. S.; Yu, J. *Diam. Relat. Mater.* **2005**, *14*, 1647-1653.

[d)] Hung, M. T.; Ishida, H. *J. Polym. Sci. Part B: Polym. Phys*. **1999**, *37*, 2360-2372.

Such a difference between in-plane TCs of the composites can be attributed to the difference of the heat conductive functions of the matrices between the h-BN platelets closely stacked. The in-plane-oriented h-BN platelets are arranged “one above the other”

or “adjacent to each other” (Figure 8). However, in composites containing plate-shaped particles, it is known that the main thermal or electrical path is the way through the contact of the platelets arranged “one above the other” because of the large contact area of the platelets.[9-11] Therefore, the effective heat path of the matrix between such arranged platelets (Figure 8a) is expected to significantly increase the in-plane TC values of the composites.

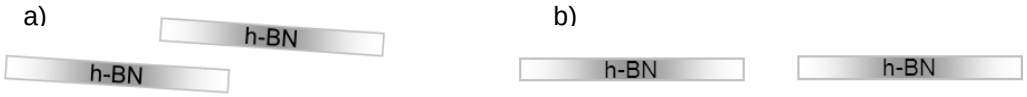

Figure 8. In-plane-oriented h-BN platelets, which is arranged a) one above the other, and b) adjacent to each other.

The SEM images in Figure 9 show the morphology between h-BN platelets closely stacked one above the other in composites. In the PB-10-I composite (30 vol%), the crystalline lamellae aligned along the h-BN surfaces (Figure 9a). This arrangement is ideal for the lamellae to behave as effective heat paths between the h-BN platelets. In the LCP composite (29 vol%), the LCP fibrils align well parallel to the MD, and this orientation is responsible for the high TC of the matrix in this direction (Figure 9b). However, the fibrils do not seem to serve as heat paths between the h-BN platelets. The

fibrils lie along the h-BN surface, thus causing high thermal resistance. As a result, the TC value along the heat paths is thought to be 0.17 W m^{-1} K^{-1} (Figure 4c).

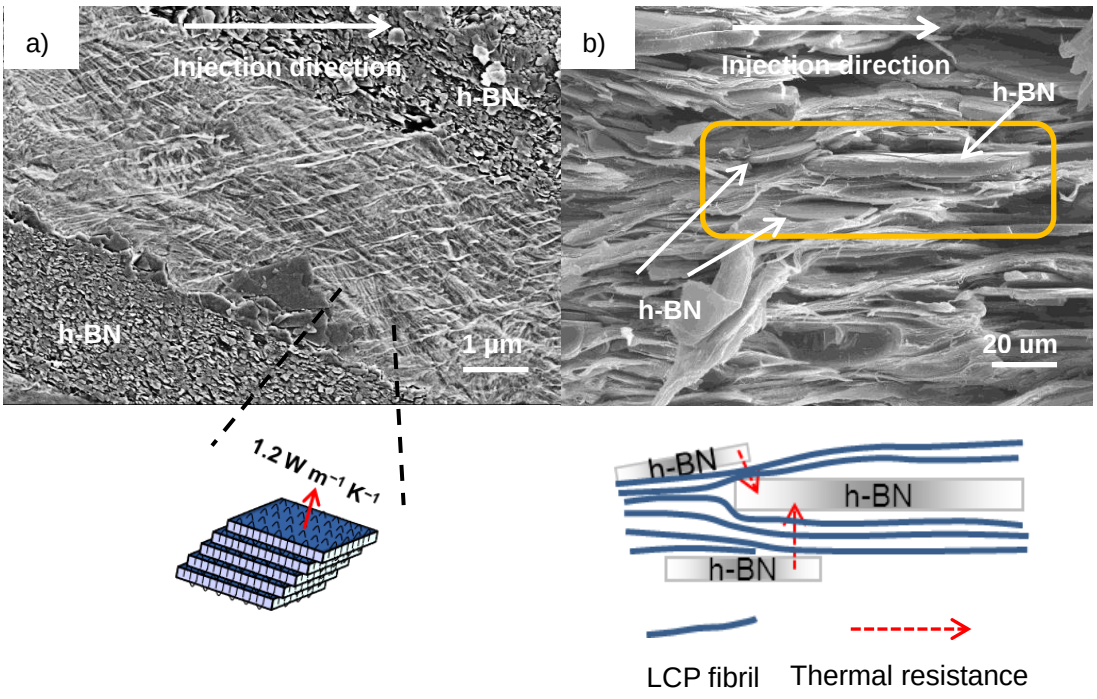

Figure 9. SEM images and schematic illustrations of the polymeric morphology between the h-BN platelets arranged one above the other. a) Molded PB-10-I composite (30 vol%). Scale bar, 1 μm. b) Molded LCP composite (29 vol%). Scale bar, 20 μm.

On the other hand, the fibrils could serve as effective heat paths between h-BN platelets arranged adjacent to each other. In fact, the TC in the MD of the composites is larger than that in the TD (Table 1). However, the comparison between composite TCs of PB-10-I and LCP in Figure 7 indicates that the high thermal resistance of LCP in

Figure 9b has a more powerful effect on the in-plane TC of the composites because of the large contact area of the platelets.

About the difference between the TCs of the PB-10-I and PB-10-II composites, the same discussion is applicable. Figure 7 shows the TC of the PB-10-I composite is higher in both the ND and the MD than those of the PB-10-II composite. In this case, the TC of each matrix must directly contribute to the TC of each composite because the same PB-10-type matrices were used. Based on these findings, it is concluded that the high TC of the matrix in the ND leads to effective heat pathways between h-BN platelets arranged one above the other, resulting in the formation of a continuous thermal linkage in the in-plane direction.

To increase the TC of polymer composites, increasing the TC of polymer itself is important. However, even if such a polymer is successfully developed, whether the polymer functions as an effective heat path between filler particles is another matter. This function is an essential factor for increasing the TC of the composite. In a composite system with in-plane-oriented h-BN platelets, a perpendicular relationship between the polymer and h-BN orientations results in dramatic enhancement of the in-plane TC.

5. Conclusion

In a polymer/h-BN composite system, three types of polymer chain orientations relative to the h-BN plane were investigated to determine if controlling the orientation could lead to enhancement of the in-plane TC. Although the polymer orientation in the in-plane direction was initially thought to be the best condition, polymer chains oriented in the ND led to composites with the highest TCs. Since the main thermal path of the composites is the way that heat transfers through the linkage between h-BN platelets arranged one above the other, the matrix serving as an effective heat pass between such arranged platelets can provide composites with high in-plane TC. For this purpose, the molecular chains oriented in the ND were found to be the most ideal.

References

[1] Asrar, J.; Toriumi, H.; Watanabe, J.; Krigbaum, W. R.; Ciferri, A. *J. Polym. Sci. Polym. Phys.* **1983**, *21*, 1119-1131.

[2] Krigbaum, W. R.; Watanabe, J.; Ishikawa, T. *Macromolecules* **1983**, *16*, 1271-1279.

[3] Tokita, M.; Osada, K.; Yamada, M.; Watanabe, J. *Macromolecules* **1998**, *31*, 8590-8594.

[4] Hung, M. T.; Ishida, H. *J. Polym. Sci. Part B: Polym. Phys.* **1999**, *37*, 2360-2372.

[5] Tanimoto, M.; Yamagata, T.; Miyata, K.; Ando, S. ACS. *Appl. Mater. Interfaces.*

2013, 5, 4374-4382.

[6] Choy, C. L.; Leung, W. P.; Kwok, K. W. *Polym. Commun.* **1991**, *32*, 285-288.

[7] Yang, Q.; Hirata, M.; Lu, D.; Nakajima, H.; Kimura, Y. *Biomacromol*. **2011**, *12*, 354-358.

[8] Lee, W. S.; Yu, J. *Diam. Relat. Mater.* **2005**, *14*, 1647-1653.

[9] Zhou, S.; Xu, J.; Yang, Q-H.; Chiang, S.; Li, B.; Du, H.; Xu, C.; Kang, F. *Carbon* **2013**, *57*, 452-459.

[10] Zou, H.; Zhang, L.; Tian, M.; Wu, S.; Zhao, S. *J. Appl. Polym. Sci.* **2010**, *115*, 2710-2717.

[11] Ye, L.; Lai, Z.; Liu, J.; Tholen, A. *IEEE Trans. Electron. Packag. Manuf.* **1999**, *22*, 299-302.

Chapter 5

Main-Chain Smectic Liquid Crystalline Polymer Exhibiting Unusually High Thermal Conductivity in an Isotropic Composite

1. Abstract

The thermal conductivity (TC) of an isotropic composite comprising of a main-chain smectic liquid crystalline PB-10 polyester and 50-μm-sized roughly spherical magnesium oxide (MgO) particles is investigated. The increase in the composite TC with higher MgO fractions is steeper than that expected by Bruggeman's theory for the TC of a polydomain PB-10 polyester (0.52 W m^{-1} K^{-1}). When the filler content is larger than 30 vol%, the composite TC approaches a value that can be explained only if the polyester functions as a matrix with 1.0 W m^{-1} K^{-1}, which is 5 times as high as those of isotropic common polymers (0.2 W m^{-1} K^{-1}). Such an unusually high TC for a polymer matrix is attributed to some polymer lamellae that lie parallel to the particle surface and are stacked toward neighboring particles, thus creating effective heat paths between the particles and a continuous thermal network in a composite.

2. Introduction

High density polyethylene (HDPE) exhibits the highest TC value (ca 0.5 W m^{-1} K^{-1}) of common thermoplastics.[1] To the best of our knowledge, cured resins of phenyl benzoate twin mesogen-type bisepoxide compounds with 4,4′-methylenedianiline exhibit the highest TC (0.85–0.96 W m^{-1} K^{-1}) of all isotropic polymer materials.[2] Therefore, other thermally conductive polymer matrices are being investigated with the immediate aim of increasing the TC to more than 1 W m^{-1} K^{-1}.

In chapter 3, I found that a main-chain smectic liquid crystalline (LC) PB-10 polyester acted as a thermally conductive matrix in composites. The PB-10 polyester, consisting of 1,10-dodecanedioic acid and 4,4′-biphenol (Figure 1a), forms a smectic I LC phase in which 2-nm-length polymer repeat units are accommodated in monoclinic lattices with a very extended conformation (Chapter 2). At a larger length scale, 47-nm-thick lamellae with large lateral dimensions regularly stack along the polymer chain direction (Figure 1b), as seen in Chapter 2−4 and Ref. 3−5. Injection molding of the PB-10 polyester in the LC state aligned the lamella normal in the normal direction (ND) with respect to the molding surface, thus leading to a high TC (1.2 W m^{-1} K^{-1}) in the direction. Such a lamellar orientation was also observed in injection-molded PB-10 composites with plate-shaped hexagonal boron nitride (h-BN), where both the h-BN

plates and the polymer lamellae aligned with their normal in the ND. Increasing the h-BN content significantly enhanced the TC in the in-plane direction (ID) as well as in the ND, indicating that the polymer lamellae served as effective heat paths between the h-BN platelets (Chapter 3 and 4).

Herein, I examined the TC of PB-10 composites with magnesium oxide (MgO) roughly spherical particles with a mean size of 50 μm (Figure 1c). The compression-molded composites at more than 30 vol% exhibited much larger TC than that expected by Bruggeman's theory for the TC of the polydomain PB-10 matrix. Moreover, these results indicated that the polydomain PB-10 polyester with only 0.52 W m^{-1} K^{-1} functioned as an isotropic matrix with 1 W m^{-1} K^{-1}. Such an unexpectedly high TC value is attributed to the polymer lamellae that lie parallel to the particle surface and are stacked between the particles, thus serving as heat paths between the MgO particles.

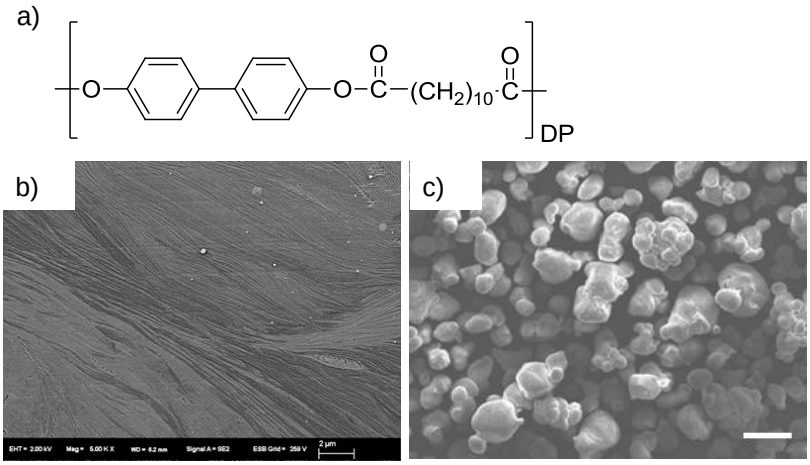

Figure 1. Components of the polymer composite: a) Chemical structure of PB-10. b) SEM image of the lamellae of PB-10. Scale bar, 2 μm. c) SEM image of the magnesium oxide (MgO) spherical particles. Scale bar, 50 μm.

3. Experimental Section

3-1. Materials

PB-10 polyester (Figure 1a) was synthesized by melt condensation of 4,4′-diacetoxy biphenyl and 1,10-dodecanedioic acid with sodium acetate as the catalyst. The number average molecular weight (M_n) and polydispersity index (PDI) of the polymer were determined by gel permeation chromatography (GPC) in a *p*-chlorophenol/toluene (3/8 volume ratio) solution using polystyrene standards (Viscotek Ht-GPC with an RI detector) to be 2.4×10^4 and 2.4, respectively. The crystal-smectic and smectic-isotropic phase transition temperatures of the polymer were T_m = 206 °C and T_i = 256 °C,

respectively, as determined by differential scanning calorimetry (DSC) at a heating rate of 10 °C min^{-1} (Perkin Elmer Pyris 1 DSC, Figure 2).

The composites were prepared by mixing PB-10 with MgO particles with a mean particle size of 50 μm (Ube Materials RF-50-SC, treated the surfaces by vinylmethylsiloxane homopolymer) at 220 °C using a TECHNOVEL KZW15TW twin-screw extruder at a screw rotation speed of 90 rpm. The MgO content was determined by the composite density and residual content after a burn-out test at 450 °C. The polymer and composites were molded via compression molding at 270 °C for 3 min (Toyoseiki mini test press-10) to shape them into plates that were 25.4 mm in diameter and 1 mm in thickness. The plates were then cooled to 25 °C at 50 °C min^{-1}.

As references, HDPE and PC were supplied by Prime Polymer Co. Ltd. (HI-ZEX 1608J) and Idemitsu Kosan Co., Ltd. (TARFLON A2200), respectively. The composites were prepared by mixing the polymers with MgO using a TECHNOVEL KZW15TW twin-screw extruder at a screw rotation speed of 90 rpm. The temperature was set at 160 °C for HDPE and 280 °C for PC. The polymers and composites were molded via compression molding for 3 min (Toyoseiki mini test press-10) to shape them into plates that were 25.4 mm in diameter and 1 mm in thickness. Compression temperature was 180 °C for HDPE and 280 °C for PC, respectively. The plates were then cooled to 25 °C

at 50 °C min^{-1}.

3-2. Measurements

The TC (λ) of the samples was calculated using Equation (1) and the results of density (ρ), heat capacity (C_P), and thermal diffusivity (α) measurements:

$$\lambda = \alpha \rho C_P. \quad (1)$$

The α was measured in triplicate at 25 °C in accordance with the American Society for Testing and Materials E-1461 using a Netzsch LFA 447 NanoFlash with an accuracy of ±5 % (Figure 3). The ρ and C_P were determined using the Archimedes and DSC methods, respectively.

Scanning electron microscope (SEM) observations were conducted using a Hitachi S-4800 SEM. To observe the dispersion of MgO particles in composites, each specimen with the surface polished with sand paper was subjected to platinum–palladium deposition. To observe the crystalline lamellae of PB-10, the specimen with the surface smoothed using a microtome was exposed to RuO_4 vapor before platinum–palladium deposition. Polarizing optical microscopy (POM) was performed using an Olympus B-50 microscopy with an inserted 530-nm sensitive tint plate.

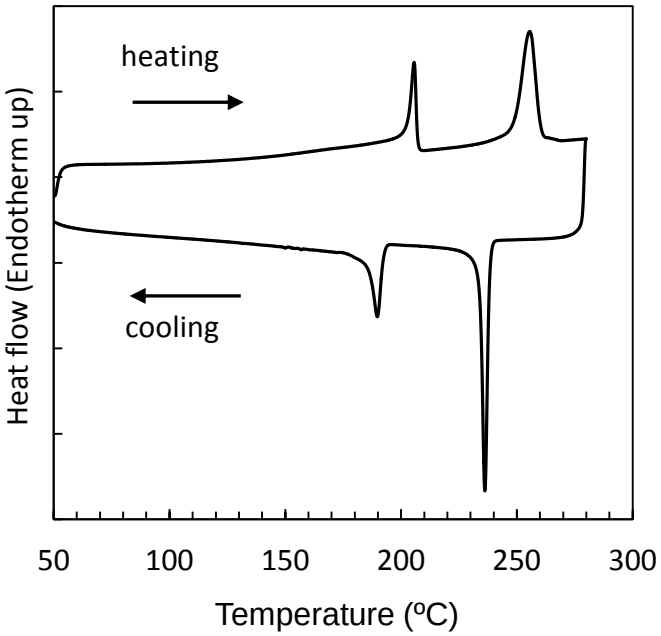

Figure 2. DSC thermogram of PB-10.

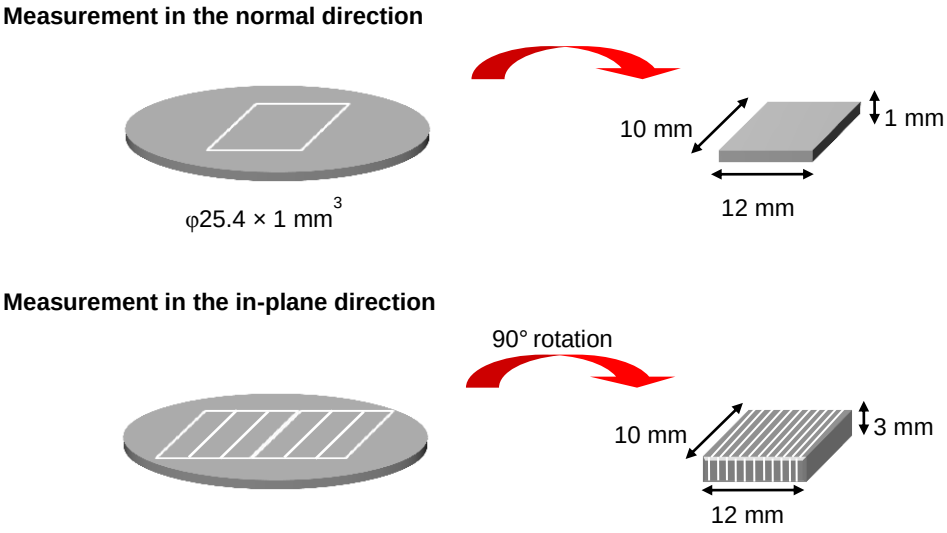

Figure 3. Preparation of samples for thermal diffusivity measurements.

4. Results and Discussion

PB-10 composites with MgO fractions ranging from 0 to 37 vol% were prepared. Figure

4a and 4b show the SEM images observed on a polished surface of the composites at 9 and 29 vol%, respectively, indicating that MgO particles are randomly distributed and the interface between polymer matrix and particles appears to be continuous without voids.

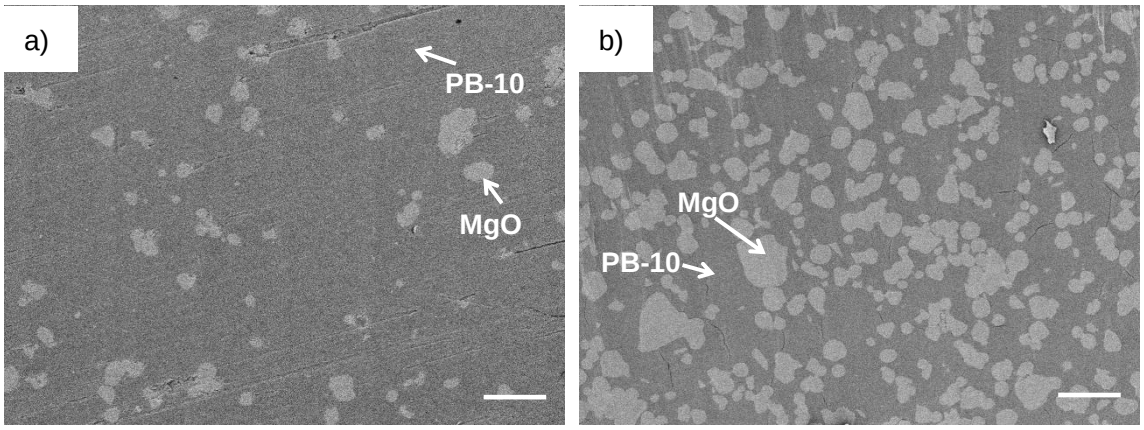

Figure 4. SEM images of the polished surface for PB-10 composites. a) 9 vol% and b) 29 vol%. Scale bar, 100 μm.

The detailed values of the λ, α, ρ, and C_P for all polymers and composites in this study are summarized in Table 1. Figure 5 shows the TC of the composites in the ND and ID as a function of the volume fraction of MgO (v) compared with the theoretical curves calculated using Bruggeman's equation:[6]

$$1 - v = \frac{\lambda_1 - \lambda_3}{\lambda_2 - \lambda_3}\left(\frac{\lambda_2}{\lambda_1}\right)^{1/3}, \quad (2)$$

where λ_1, λ_2, and λ_3 are the TCs of the composite, PB-10, and MgO (42 W m^{-1} K^{-1}),[7] respectively. Bruggeman model was based on spherical particles homogenously suspended in a matrix, similar in these composites. Generally, it is known that experimental values are in agreement with those predicted by this equation at low filler content (< 40 vol%).[8-10] Therefore, composites at up to 40 vol% loading are discussed here. The solid and broken lines in Figure 5 represent the calculated λ_1 values with λ_2 = 0.52 W m^{-1} K^{-1} and 1 W m^{-1} K^{-1}, respectively. The value of 0.52 W m^{-1} K^{-1} is equal to the experimental TC value of the pure polydomain PB-10. The TCs in the ND and ID are similar, indicating that the composites are isotropic. It is interesting to note that the increase in the TC of the composites is steeper than that of the solid line curve in Figure 5. In contrast, the TC of HDPE/MgO and polycarbonate/MgO composites with the same MgO fraction range are well explained by the same equation (Figure 6). Thus, such an anomalous increase in the TC cannot be ascribed to the percolation effects that are remarkable at v > 50 vol%.[11,12] In addition, the crystallinity of the polymer matrix in each composite was estimated from the transition enthalpy (ΔH) value per unit weight of polymer at T_m and T_i in an attempt to account for the steep TC enhancement. However, the enthalpy changes were nearly constant, irrespective of the MgO content

(Table 2). Thus, such an increase in the TC of the PB-10 composite is entirely unexpected.

Table 1. Detailed properties of MgO, PB-10, HDPE, PC and the composites

sample	MgO content [vol.%]	density[a] [g cm^{-3}]	specific heat[b] [J g^{-1} K^{-1}]	thermal diffusivity [mm^2 s^{-1}]		thermal conductivity [W m^{-1} K^{-1}]	
				ND	ID	ND	ID
MgO	100	3.65[c]	0.88	-	-	42 [d]	42 [d]
Compression-molded PB-10/MgO composites	0	1.20	1.38	0.31	0.32	0.52	0.53
	9	1.42	1.26	0.50	0.45	0.89	0.81
	19	1.66	1.17	0.73	0.66	1.4	1.3
	29	1.91	1.10	1.1	1.0	2.4	2.2
	37	2.10	1.06	1.6	1.7	3.5	3.7
Compression-molded HDPE/MgO composites	0	0.955	2.31	0.24		0.52	
	10	1.23	1.88	0.32		0.75	
	25	1.63	1.51	0.53		1.3	
	34	1.87	1.36	0.67		1.7	
	43	2.11	1.25	0.99		2.6	
Compression-molded PC/MgO composites	0	1.20	1.26	0.17		0.25	
	10	1.45	1.16	0.21		0.35	
	20	1.69	1.10	0.27		0.51	
	30	1.94	1.04	0.39		0.78	
	40	2.18	1.01	0.55		1.2	

[a] The density was measured by the Archimedean method.

[b] The heat capacity was measured by the differential scanning calorimetry (DSC) method.

[c] Lee, J. H.; Eun, J. H.; Park, S. Y.; Kim, S. G.; Kim, H. J. *Thin Solid Films* **2003,** *435*, 95-101.

[d] Jeong, I.; Kim, J.; Lee, J.; Hong, J. *Trans.Electr.Electron.Mater.* **2010,** *11*, 261-265.

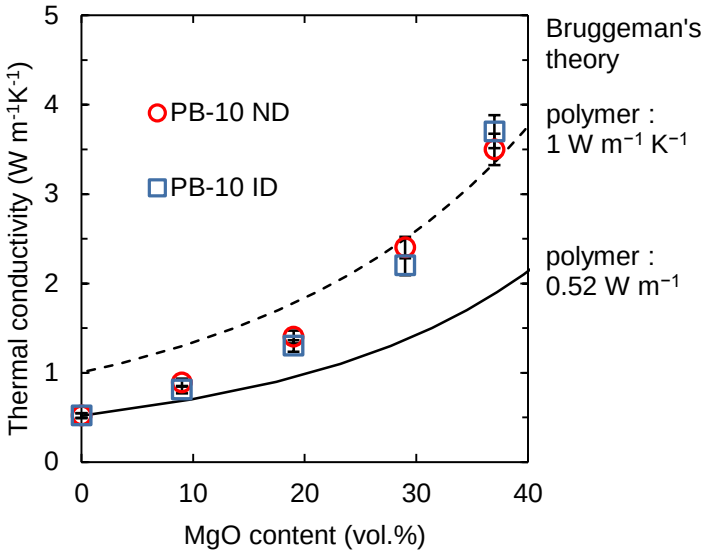

Figure 5. Effect of MgO filler content on the thermal conductivity of compression-molded PB-10 composites compared with the theoretical curves calculated using Bruggeman's equation. The solid and broken lines represent the calculated λ_1 values with (λ_2, λ_3) = (0.52, 42) and (1, 42), respectively.

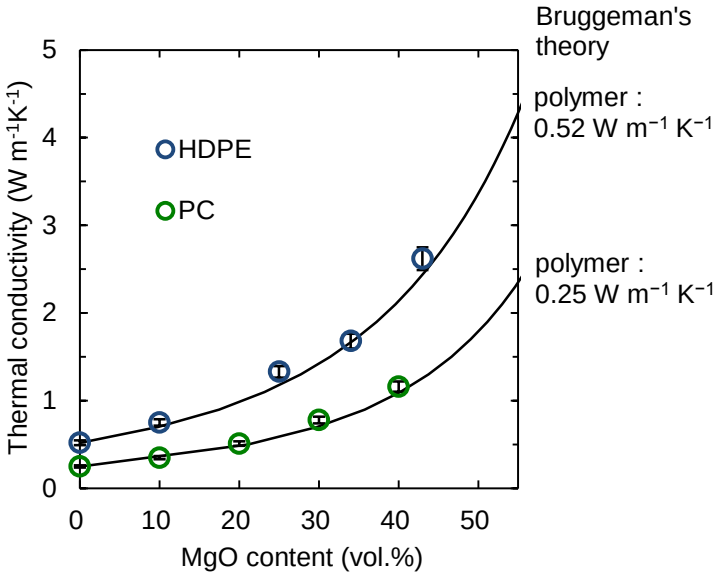

Figure 6. Effect of MgO filler content on the thermal conductivity of compression-molded HDPE and PC composites in the normal direction compared with Bruggeman's theory curves.

The experimental values for HDPE and PC are well plotted on the theoretical curve with $(\lambda_2, \lambda_3) = (42, 0.52)$ and $(42, 0.25)$, respectively.

Table 2. Transition enthalpy of the matrix in molded PB-10/MgO composites

MgO content [vol.%]	transition enthalpy[a)] [J/g]	
	ΔH_m	ΔH_i
0	26.8	60.8
9	31.5	61.5
19	26.7	48.3
29	26.1	52.9
37	27.0	51.0

[a)] Transition enthalpy per unit weight of polymer based on first heating DSC data.

Such a high TC can, however, be ascribed to polymer lamellae stacking between the MgO particles. Figure 7 shows SEM images of the composite at an MgO fraction of 9 vol%. Between the MgO particles at a greater distance, the lamellae stack in various directions (Figure 7a). On the other hand, between the filler particles at a shorter distance (~5 μm), some lamellae lie parallel to the surfaces of the MgO particles and are regularly stacked toward the surface of the neighboring MgO sphere (Figure 7b). These lamellae can serve as heat paths between the MgO particles; the TC is estimated to be greater than 1 W m^{-1} K^{-1}, because the injection-molded PB-10 exhibits a TC of 1.2 W m^{-1} K^{-1} along the lamellar stacking direction (Chapter 3). In fact, the TC of the PB-10 composites asymptotically approaches the broken line curve with λ_2 = 1 W m^{-1} K^{-1} in Figure 5, suggesting that the matrix TC gradually increases from 0.52 W m^{-1} K^{-1} to 1 W m^{-1} K^{-1} with the increase in MgO fractions.

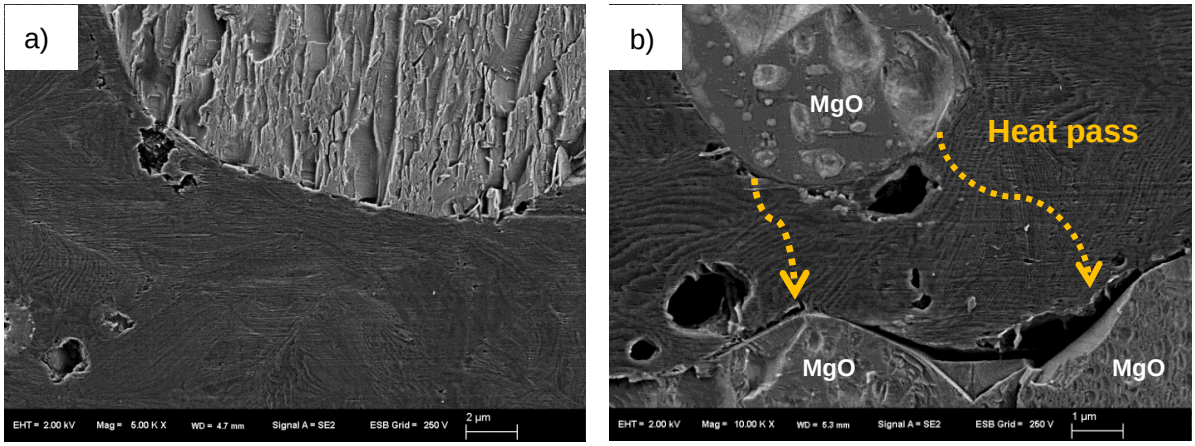

Figure 7. SEM images of a compression-molded PB-10/MgO composite at 9 vol% loading. a) A large gap between the MgO particles. Scale bar, 2 μm. b) A small gap between the MgO particles. Scale bar, 1 μm.

Such regular polymer lamellar stacking is thought to be achieved when the dimensions of the gap between the MgO particles decreases and becomes comparable to the coherence length of the polymer lamellar stacking. The coherence length of PB-10 lamellar stacking can be as large as 20 μm. Figure 8 shows a POM image of a PB-10 thin film microtomed from a bulk polymer (thickness: 500 nm). The blue domains are due to an increase in the retardation of the uniaxially oriented domain and the sensitive tint plate (530 nm) resulting from the alignment of the chain axis direction with the Z′ direction. Therefore, the lamellae are stacked along the polymer chain direction in length from a few micrometers to about 20 μm. In addition, the anisotropic domain is

expected to have high TC of 1 W m^{-1} K^{-1} along the lamellar stacking direction and only modest at 0.30 W m^{-1} K^{-1} in the perpendicular direction. The disorderly oriented domains and the domain boundaries cause phonon scattering, leading to the polydomain TC value of 0.52 W m^{-1} K^{-1}. On the other hand, the distance between the filler particles decreases with the increase in filler fractions as seen in Figure 4a and 4b. The mean distance can be calculated as 47.5 μm at 10 vol% and decreases to 17.6 μm at 30 vol%, assuming a face-centered cubic lattice model (Figure 9). Thus, the amount of disordered domains and domain boundaries in the inter-particle gap decreases. This is thought to result in the gradual increase of matrix TC as the MgO content increases. The matrix TC values (λ_2) at 9 vol% and 19 vol% can be calculated from the composite TC values in Figure 5 using Bruggeman's equation (2) to be 0.65 W m^{-1} K^{-1} and 0.75 W m^{-1} K^{-1}, respectively. At around 30 vol%, all particles are arranged near to each other (Figure 4b). Figure 10 shows a POM image of the composite film (29 vol%) prepared using sandpaper (thickness: about 2 μm). The image indicates that the inter-particle gaps within 20 μm are filled by one or a few domains with lamellar normal connecting the filler surfaces. Such domains can serve as effective heat paths between the MgO particles as depicted schematically in Figure 11, and create a continuous thermal network in composites. Consequently, the TC of the PB-10 matrix (λ_2) becomes 1 W

$m^{-1} K^{-1}$.

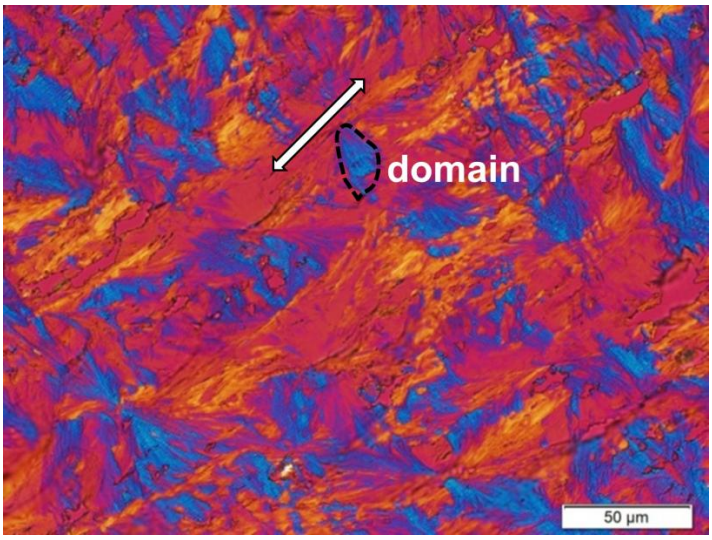

Figure 8. POM image of a PB-10 thin film (500 nm). The double-headed arrow shows the Z′ direction of the 530-nm sensitive tint plate. Scale bar, 50 µm.

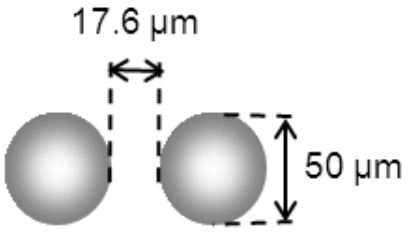

Figure 9. Theoretical distance between 50-µm MgO particles at 30 vol% loading.

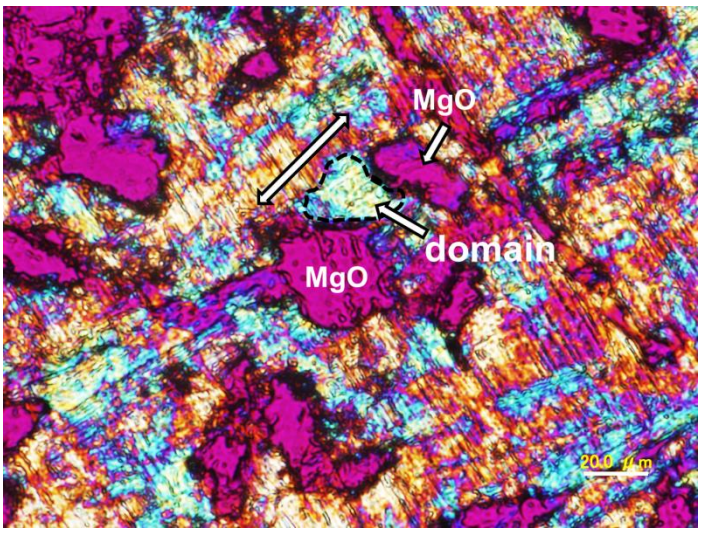

Figure 10. POM image of a PB-10/MgO composite thin film (about 2 μm) at 29 vol% loading. The double-headed arrow shows the Z′ direction of the 530-nm sensitive tint plate. Scale bar, 20 μm.

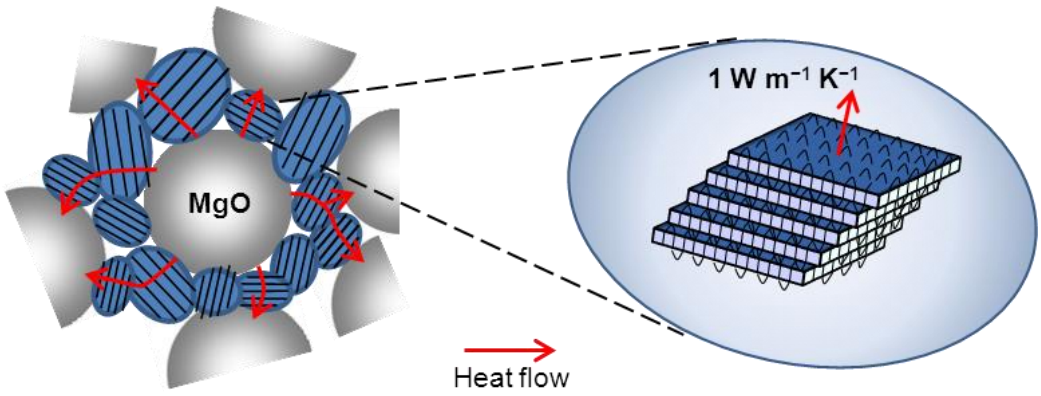

Figure 11. Schematic illustration of the structural model for TC enhancement of PB-10/MgO composites at high MgO particle loadings. a) Heat conduction between the MgO particles via the crystal domain of PB-10. b) Laterally large and well-stacked lamellar crystals with more than 1 W m^{-1} K^{-1} heat conduction along the chain direction.

Above filler concentration of 30 vol%, the polydomain PB-10 polyester can be utilized as a matrix with a TC of 1.0 W m^{-1} K^{-1}, which is 5 times as high as those of isotropic common polymers; without fillers, it has a TC as high as 0.52 W m^{-1} K^{-1}. To attain a composite TC of 2 W m^{-1} K^{-1}, which is 10 times higher than those of common polymers, PB-10 requires an amount of MgO that is 20 vol% lower than that required for other common polymers with TC values of 0.25 W m^{-1} K^{-1} (Figure 5 and 6). As a result, lighter weight composites with good processability can be prepared using PB-10.

It is still difficult to enhance the TC of an isotropic polymer itself to the level of 1 W m^{-1} K^{-1}. However, a polymer matrix with a TC of 1 W m^{-1} K^{-1} is obtainable using the current technique.

5. Conclusion

Polydomain LC PB-10 polyester serves as a heat path with a TC of 1.0 W m^{-1} K^{-1} in composites at 50-μm-sized MgO content of more than 30 vol%, although the TC of the polydomain is 0.52 W m^{-1} K^{-1}. Such a high TC value of the polymer matrix is ascribed to the fact that the polymer lamellae are stacked at a coherence length of micron order and exhibit a TC of 1.0 W m^{-1} K^{-1} in the normal direction. When the MgO content is more than 30 vol%, some polymer lamellae lying parallel to the MgO particles can

stack toward neighboring MgO spheres and a continuous thermal network is created in composites. Thus, a polymer with a TC of only 0.52 W m^{-1} K^{-1} functions as a thermally conductive matrix with a TC as large as 1 W m^{-1} K^{-1}.

6. Appendix

6-1. Influence of lamellar crystal alignment of PB-10 on TC of composites with MgO particles.

In addition, a composite comprising of lower molecular weight PB-10-II (M_n: 10,000, PDI: 1.9) and MgO (11 vol%) was prepared to investigate the polymer chain orientation by injection molding and the resulting TC value. The composite was moled by injection molding (DSM Xplore, Micro Injection Moulding Machine 5.5 ml) to plates that were 25.4 mm in diameter and 1 mm in thickness. The orientation of the polymer chains at the center of the plate was observed using 2D-WAXD (Figure 12a). The 2D-WAXD pattern in Figure 12b shows the outer (4.24 Å) and inner (21.0 Å) reflections. In both (ND, x) and (ND, y) patterns, outer peaks derived from the inter-mesogen reflections appear on the equator. No specific orientation is observed in the (x, y) pattern. These patterns are similar as those observed in the pure injection-molded resin as seen in chapter 3, indicating that the polymer chains were aligned perpendicular to the (x, y)

plane even under incorporation of MgO particles.

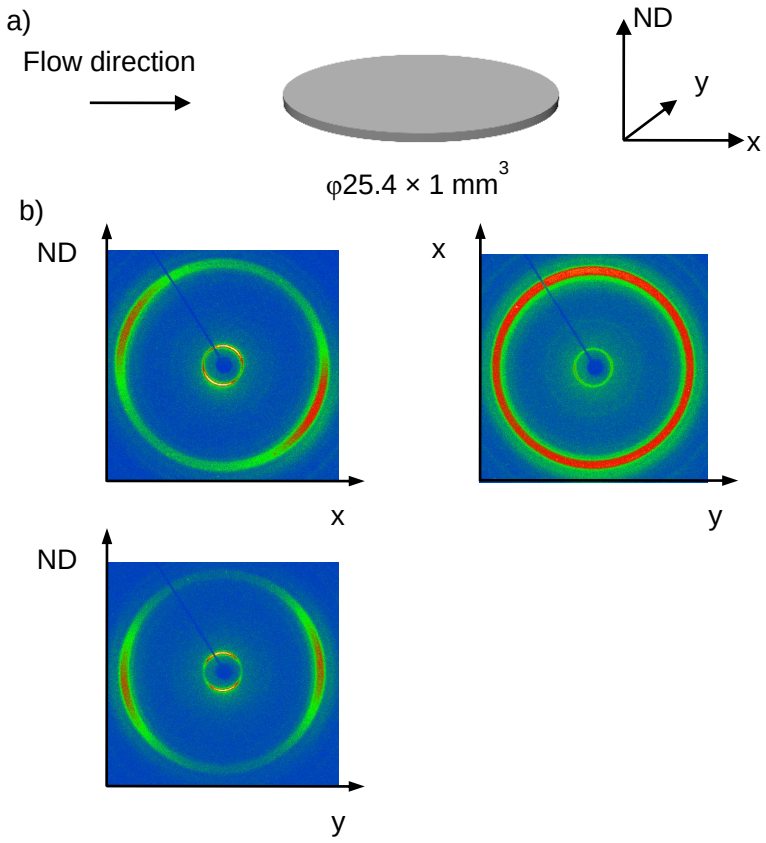

Figure 12. Characterization of injection-molded PB-10-II/MgO composites. a) Shear geometry in three characteristic directions. b) 2D-WAXS patterns along the x, y, and ND axes measured for the composites at 11 vol% loading.

Therefore, the PB-10 composite exhibited dramatic TC enhancement in the ND. Figure 13 shows the TC value in the ND of 1.6 W m^{-1} K^{-1}, which is 4–5 times higher than 0.35 W m^{-1} K^{-1} of PC composite at 10 vol% loading. To achieve the TC value of 1.6 W m^{-1} K^{-1}, the PC composite requires a MgO fraction of about 50 vol% according to

Bruggeman's theory as seen in Figure 6. These findings indicate that aligned PB-10 has a great advantage over other common polymers in the use of not only plate-shaped filler particles such as h-BN but also spherical particles such as MgO.

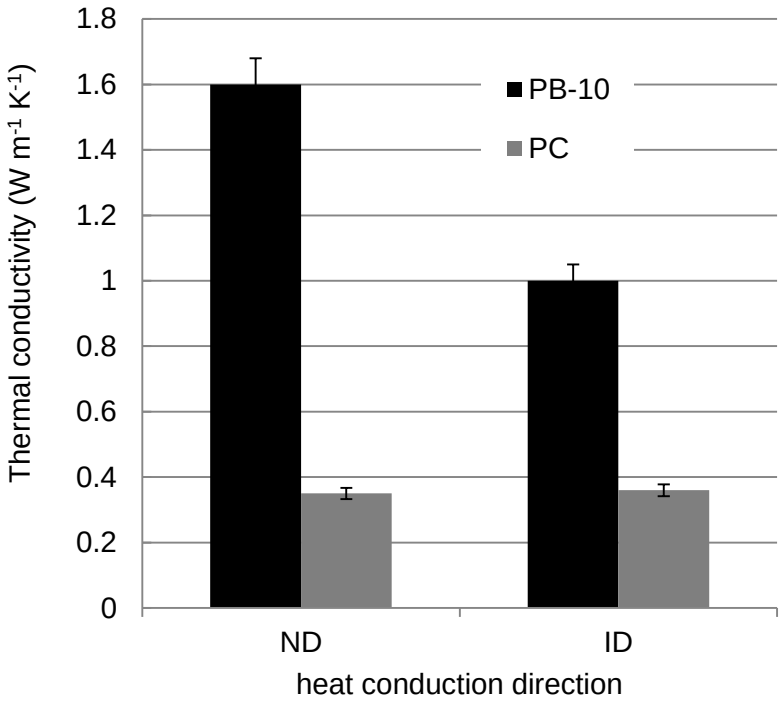

Figure 13. TC of composites for PB-10 and PC with MgO fraction of 11 and 10 vol%, respectively.

When the filler content was more than 30 vol%, the lamellar orientation could not be observed. This is attributed to the large sized MgO particles which physically

suppressed the lamellar alignment. The TC was, thus, isotropic as seen in Figure 14, and similar to that of compression-molded PB-10 in Figure 5.

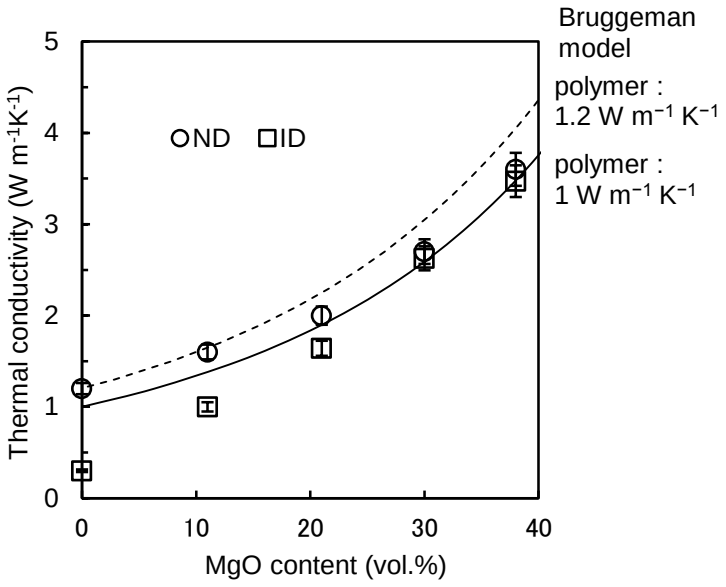

Figure 14. Effect of MgO filler content on the thermal conductivity of injection-molded PB-10-II composites compared with Bruggeman's theory curves with (λ_2, λ_3) = (42, 1) and (42, 1.2).

6-2. Use of partially biomass-based PB-8 polyester for commercial products

It is known that PB-*n*, where *n* is an even number of methylene spacer unit, also forms smectic LC state and similar higher order structure to PB-10.[3,4] Herein, I decide PB-8 should be adopted to develop commercial products. One of the reasons is the polyester comprises a sebacic acid, which is a biomass derived from a castor oil. In other words, PB-8 is a partially biomass-based polyester and can contribute to carbon neutral society

(Figure 15).

Biomass plastics have attracted attentions from industries. In 20th century, a lot of useful plastics were developed and utilized in a lot of fields with the progress of petrochemistry. Plastics in 21st century are required to be based on “environmental considerations”, leading to attentions to biomass plastics.

Industries are required to reduce the consumption of fossil resources as much as possible in anticipation of future depletion of the resources. Therefore, the use of biomass resources becomes important and biomass plastics offer a sustainable alternative to petroplastics. Biomass polymers are also considered to be synthesized from atmospheric carbon dioxide via photosynthesis of plants. Incineration of the biomass polymers, therefore, does not result in any additional load of carbon dioxide to the atmosphere.

In this section, first, the other advantages of partially biomass-based PB-8 against other PB-*n* polyesters are demonstrated. Next, the TC of PB-8 based composites is measured and it is shown that the PB-8 polyester also functions as thermally conductive polymer matrix like PB-10.

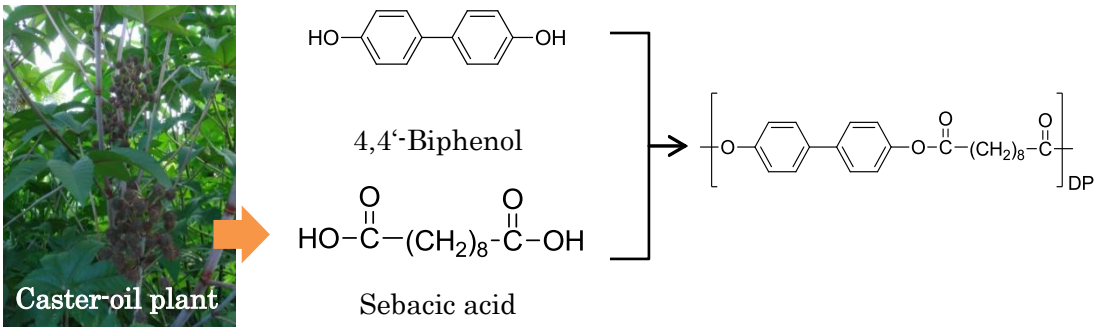

Figure 15. PB-8 polyester made of a sebasic acid derived from biomass caster oil. The bio-content is 48 wt%.

Figure 16 shows DSC thermograms of PB-*n* (*n* = 8−18) and the phase diagram at heating process. It is known that PB-*n* polyesters exhibit the well-defined transition behavior and show crystal-smectic LC transformation at T_m and smectic LC-isotropic transformation at T_i.[1] The phase diagram indicates that the T_m and T_i increase as the number of *n* decreases. These results are attributed to increase of main-chain rigidity with the number of *n* decreases. In terms of an application for electronic devices, high T_m is so important because the value directly influences the heat resistance of the materials. Since the PB-8 polyester exhibits the highest T_m value (210 ºC), the polyester is a good candidate for commercial products.

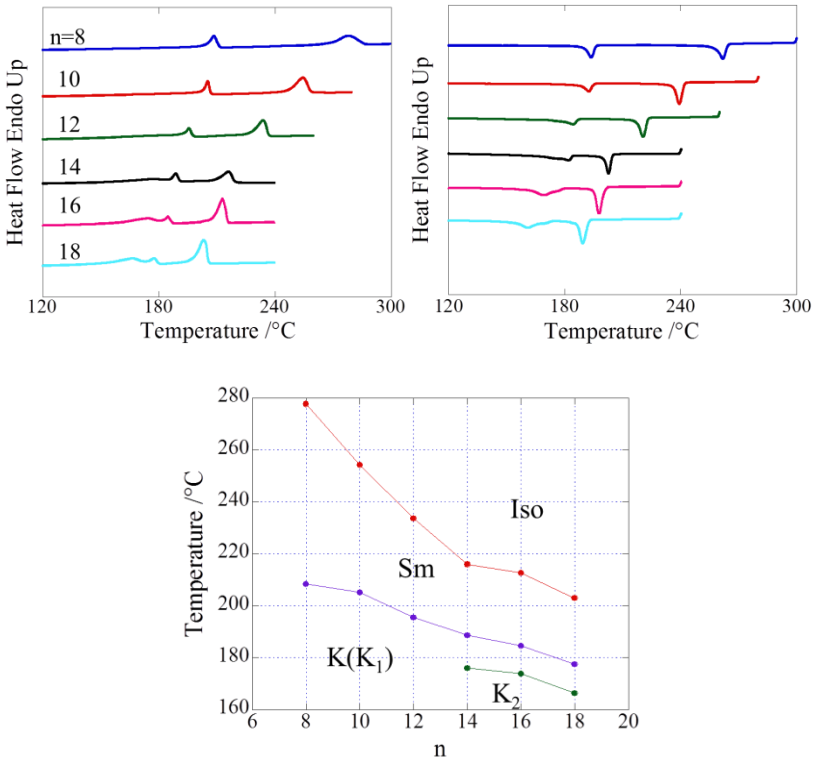

Figure 16. DSC thermogram of PB-*n* (*n* = 8−18) a) Heating process. b) Cooling process. c) Phase diagram at heating process. Iso means isotropic phase. Sm means smectic LC phase. K means crystal phase.

Lamellar structure of PB-*n* (*n* = 8−18) was observed by SAXS intensity profile. Figure 17 shows that PB-8 polyester (Mn: 1.6 kg mol^{-1}, PDI: 2.1) forms the largest lamellae (60 nm), indicating that the shortest spacer leads to main-chain rigidity and difficulty of molecular chain folding. Since the lamellar structure is one of the largest factors for high TC, PB-8 is also expected to function as thermally conductive matrix.

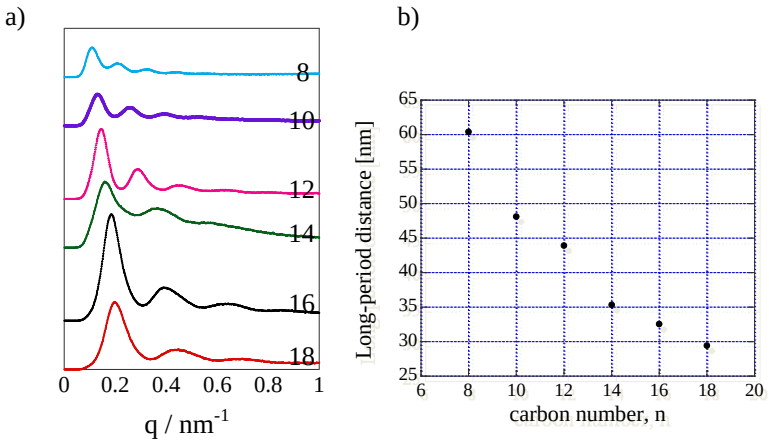

Figure 17. Results of SAXS measurements of PB-*n*. a) SAXS intensity profiles. c) Lamellar long-periodic spacings.

PB-8 composites with MgO fractions of 30 and 40 vol% were prepared. Figure 18 shows the TC, which is as high as those of PB-10. The broken line represent the calculated λ_1 values with λ_2 = 1 W m^{-1} K^{-1}, indicating that PB-8 also serves as a heat path with a TC of 1 W m^{-1} K^{-1} between MgO particles.

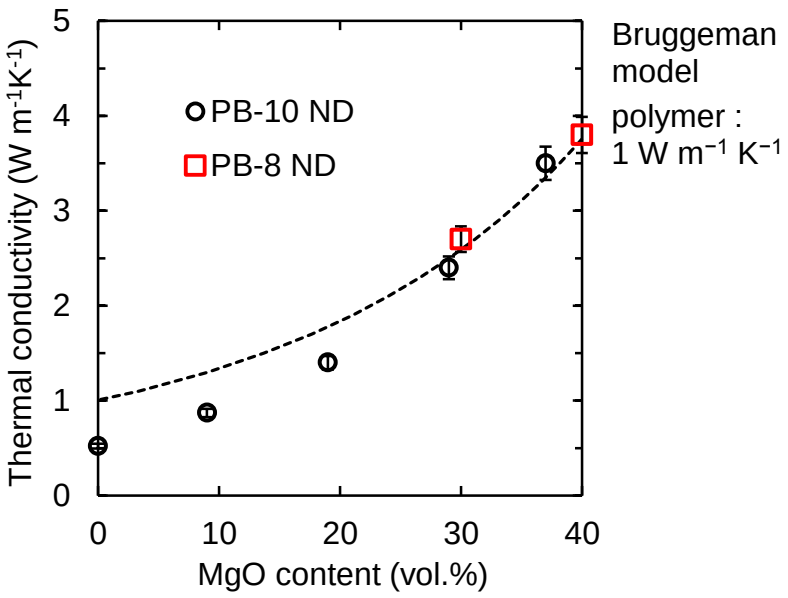

Figure 18. Thermal conductivity of PB-8/MgO composites.

Therefore, PB-8 polyester exhibits much higher TC than other fossil oil-based polymers. Consequently, PB-8 has several advantages, which are (1) partially biomass polymer, (2) highest T_m of PB-n (n =8-18) species, (3) higher TC than that of other fossil oil-based polymers. Customers using PB-8 for the heat dissipation ability can participate in the use of a biomass polymer, leading to contribution to sustainable environments. I think that such business is ideal for the market growth of biomass polymers.

References

[1] D. Hansen, G. A. Bernier, *Polym. Eng. Sci.* **1972**, *12*, 204.

[2] M. Akatsuka, Y. Takezawa, *J. Appl. Polym. Sci.* **2003**, *89*, 2464.

[3] J. Asrar, H. Toriumi, J. Watanabe, W. R. Krigbaum, A. Ciferri, *J. Polym. Sci. Polym. Phys.* **1983**, *21*, 1119.

[4] W. R. Krigbaum, J. Watanabe, T. Ishikawa, *Macromolecules* **1983**, *16*, 1271.

[5] M. Tokita, K. Osada, M. Yamada, J. Watanabe, *Macromolecules* **1998**, *31*, 8590.

[6] D. A. G. Bruggeman, *Ann. Phys*. **1935**, *24***,** 636.

[7] I. Jeong, J. Kim, J. Lee, J. Hong, *Trans. Electr. Electron. Mater.* **2010**, *11*, 261.

[8] C-C. Teng, C-C M. Ma, K-C. Chiou, T-M. Lee, *Compos: Part B* **2012**, *43*, 265.

[9] C. P. Wong, R. S. Bollampally, *J. Appl. Polym. Sci.* **1999**, *74*, 3396.

[10] D. Yorifuji, S. Ando, *J. Mater. Chem.* **2011**, *21*, 4402.

[11] K. Monden, *Adv. Sci. Technol.* **2006**, *45*, 2664.

[12] D. M. Bigg, *Adv*. *Polym*. *Sci*. **1995**, *119*, 1.

Chapter 6

General Conclusion

1. Summary

There has been long-standing interest in multifunctional polymer materials, which are both thermally conductive and electrically insulating. Although being good electrical insulators, polymers are, in general, poor thermal conductors. One solution to this problem is to design and fabricate polymer composites that have improved TC. Other advantages of polymer materials are good processability, light weight, and chemical stability, which are all desired properties. Even though many articles have been published on the improvement of TCs of polymers by fillers, little has been done on enhancement of TCs of polymer matrices. It was, therefore, the purpose of this thesis to create a thermally conductive polymer matrix and clarify the enhancement mechanism of the high TC. In this chapter, contents from chapter 2 to 5 are summarized, and they will show you enhancement mechanism of thermal conductivity in main chain liquid crystalline PB-*n* polyesters and their composites.

Chapter 2

The type of mesophase is identified as smectic I using spinnable PB-10 polyester, which was obtained for the first time by solid state polymerization after conventional melt condensation of 4,4′-biphenol and 1,10-dodecanoic acid. Polymer chains are packed laterally in a 2D hexagonal lattice and lie along the *c*-axis and pass diagonally across the smectic layers. SAXD and SEM clarify lamellae stacking regularly along the fibre axis with a spacing of 41 nm, which is approximately 20 times the smectic layer thickness. The lamellar normal is thus parallel to the chain axis and tilted to the smectic layer normal.

Chapter 3

TC enhancement of PB-*n* by lamellar crystal alignment is shown. PB-*n* represents a parallel orientation of chain-folding lamellae by shear flow during injection molding, in which polymer chains are aligned in normal direction (ND) with respect to the molding surface, thus leading to high TC (1.2 W m^{-1} K^{-1}) in this direction. Furthermore, the composites containing plate-shaped hexagonal boron nitride (h-BN) particles exhibit a dramatic enhancement of TC in not only the ND but also the in-plane direction. This technique enables producing polymer materials with high TCs without a high filler

content. This leads to more lightweight composites with good processability. For this strategy, no special equipment is required, and an injection molding process is suitable. Therefore, this approach can be readily scaled up for various applications.

Chapter 4

In a polymer/h-BN composite system, three types of polymer chain orientations relative to the h-BN plane were investigated to determine if controlling the orientation could lead to enhancement of the in-plane TC. Although the polymer orientation in the in-plane direction was initially thought to be the best condition, polymer chains oriented in the ND led to composites with the highest TCs. Since the main thermal path of the composites is the way that heat transfers through the linkage between h-BN platelets arranged one above the other, the matrix serving as an effective heat pass between such arranged platelets can provide composites with high in-plane TC. For this purpose, the molecular chains oriented in the ND were found to be the most ideal.

Chapter 5

Polydomain LC PB-10 polyester serves as a heat path with a TC of 1.0 W m^{-1} K^{-1} in composites at 50-μm-sized MgO content of more than 30 vol%, although the TC of the

polydomain is 0.52 W m^{-1} K^{-1}. Such a high TC value of the polymer matrix is ascribed to the fact that the polymer lamellae are stacked at a coherence length of micron order and exhibit a TC of 1.0 W m^{-1} K^{-1} in the normal direction. When the MgO content is more than 30 vol%, some polymer lamellae lying parallel to the MgO particles can stack toward neighboring MgO spheres and a continuous thermal network is created in composites. Thus, a polymer with a TC of only 0.52 W m^{-1} K^{-1} functions as a thermally conductive matrix with a TC as large as 1 W m^{-1} K^{-1}.

As appendix, I demonstrate that PB-8 has several advantages, which are (1) partially biomass polymer, (2) highest T_m of PB-n (n =8-18) species, (3) higher TC than that of other fossil oil-based polymers. Such a material can contribute to sustainable environments.

The current technique enables producing polymer materials with significantly high TCs at low filler loadings. This leads to more lightweight composites with good processability. For this approach, no special equipment is required, and a simple molding process such as injection and compression molding is suitable. Therefore, this approach can be readily scaled up for various applications such as automobile parts, heat dissipation circuit boards, and lighting apparatuses (Figure 1 and 2). In addition,

PB-8 is a partially biomass-based polyester, in which the bio-content is about 48 wt%. Such the polyester can contribute to both sustainable environments and market growth of energy saving electronic devices such as LED lighting and electric vehicle.

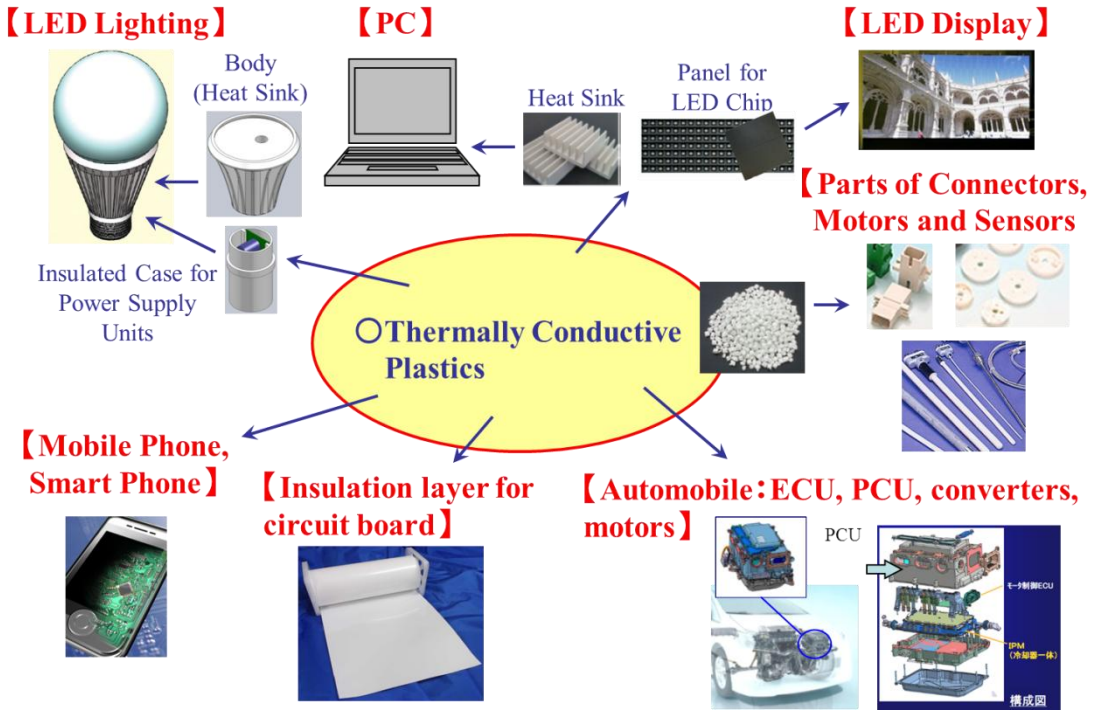

Figure 1. Possible applications of thermally conductive plastics.

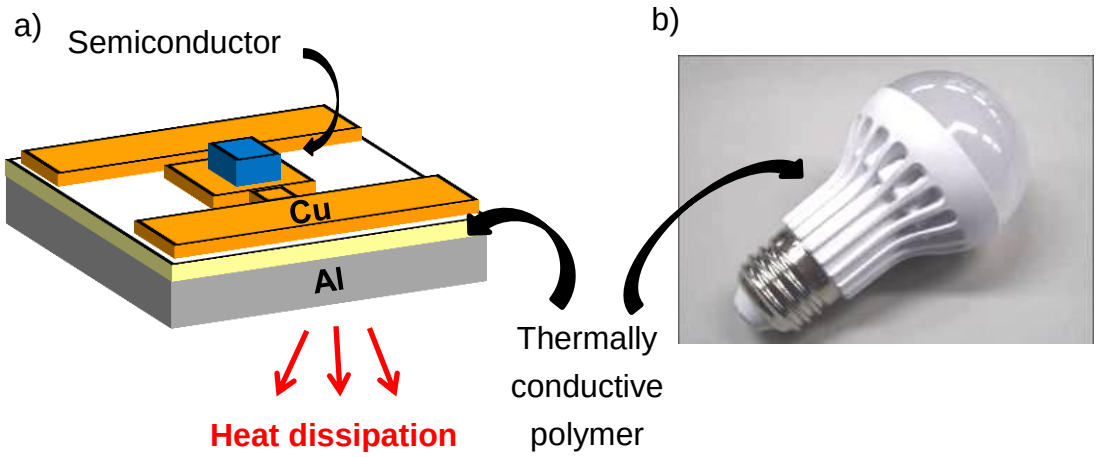

Figure 2. a) Metal Core print circuit board (MCPCB). MCPCBs are the boards which incorporate a base metal material as heat spreader as an integral part of the circuit board. Furthermore, MCPCB has a dielectric polymer layer with high "out-of-plane" TC for lower thermal resistance. Thus, the technique found in chapter 5 is possibly available in this application. b) LED light. Thermally conductive polymers with high "in-plane" TC are utilized to spread heat generated from LED chips. Therefore, polymer materials represented in chapter 3 can be good candidates in this application.

The current technique discussed in this thesis provides a starting point to fabricate polymer materials for practical applications in industries. The materials are in a state of continual development that will provide greater benefits; hence, some recommendations for future work are summarized in the next section.

2. Recommendations

Relationship between lamellar thickness of PB-*n* polyesters and the TC of the matrix have to be investigated. The amount of amorphous regions decreases as the lamellae thickness increases, which might lead to further enhancement of polymer matrix.

Molecular weight of PB-*n* was limited to induce lamellar crystal alignment by injection molding, leading to sacrifice of mechanical strength, chemical stability, and so on. Materials for end-use-products are required to have high mechanical strength such as toughness, impact strength, and tensile strength. In this thesis, such the strengths of PB-*n* materials has not been discussed, however, the materials look brittle. First, the reason for the brittleness should be clarified by investigation of the viscoelasticity, the fracture behavior and so on. Technique using higher molecular weight polymer might improve the strength. Another possible reason for the issue is the high crystallinity, that is, less molecular entanglement. Therefore, other techniques such as further molecular design, copolymer, and polymer alloy are necessary.

Usually, materials for recent electronic devices have to possess high heat resistance, especially resistance against reflow soldering in lead-free conditions. The reflow

temperature is more than 260 ºC although the time is usually less than 1 minute. Since all PB-*n* (*n* = 8−18) polyesters transform LC or isotropic state at the temperature, the polyesters cannot be used here. Possible solutions to this issue could include further molecular design to increase crystal−smectic LC transition point or cross-linking the PB-*n* molecule with maintenance of the higher order structure.

Electrical insulation property should be evaluated for PB-*n* composites. The property is so important for applications in electronic devices. Since dielectric breakdown strength dramatically decreases as filler content increase, PB-*n* could have great advantage over the other polymers in the compatibility between high TC and dielectric breakdown strength.

Finally, the TC of composites is affected by the presence of the interfacial thermal resistance between the matrix and filler particles. An effective method of reducing phonon scattering is needed to improve the heat dissipation ability of composites. A possible solution to this issue could include an optimum surface treatment of the filler particles, allowing improved bonding of the particles to the matrix. Studies on filler surface treatment could lead to further TC enhancement of composites.

List of Publications

I. Original Papers

Chapter 2

- M. Tokita, S. Okuda, S. Yoshihara, C. Takahashi, S. Kang, K. Sakajiri, J. Watanabe, "Identifying smectic I phase of main-chain PB-10 polyester consisting of 4,4′-biphenol and 1,10-dodecanoic acid by fibre X-ray diffraction", *Polymer* **2012**, *53*, 5596.

Chapter 3

- S. Yoshihara, T. Ezaki, M. Nakamura, J. Watanabe, K. Matsumoto, "Enhanced thermal conductivity of thermoplastics by lamellar crystal alignment of polymer matrices", *Macromol. Chem. Phys.* **2012**, *213*, 2213.

Chapter 4

- S. Yoshihara, M. Sakaguchi, K. Matsumoto, M. Tokita, J. Watanabe, "Influence of molecular orientation direction on in-plane thermal conductivity of

polymer/hexagonal boron nitride composites", *J. Appl. Poym. Sci.*, published online, DOI: 10.1002/APP.39768.

Chapter 5

- S. Yoshihara, M. Tokita, T. Ezaki, M. Nakamura, M. Sakaguchi, K. Matsumoto, J. Watanabe, "Main-Chain Smectic Liquid Crystalline Polymer Exhibiting Unusually High Thermal Conductivity in an Isotropic Composite", *J. Appl. Poym. Sci.*, submitted.

Publications not included in this thesis

- K. Tatsuta, S. Yoshihara, N. Hattori, S. Yoshida, S. Hosokawa, "The first total synthesis of nidulalin A, a dihydroxanthone possessing multiple bioactivities", *J. Antibiot.* **2009**, *62*, 469.
- S. Okuda, S. Yoshihara, S. Kang, M. Tokita, J. Watanabe, "Formation of regularly spaced wetting ridges at 1 μm intervals on the surface of a liquid-crystalline polymer", *Langmuir* **2012**, *28*, 14518.

Review Article

- S. Yoshihara, “New thermally conductive liquide crystalline polyester and its composites”, *Nova publication, “*New Developments in Polymer Composites Research”, accepted.

Review Article (Japanese)

- 吉原秀輔, 「高熱伝導性樹脂の開発と応用展開」, Polyfile（大成社）, **2012**, *49*, 26.
- 吉原秀輔, 「ベース樹脂高熱伝導化技術の開発とその展開」, プラスチックス・エージ, **2012**, *58*, 92.
- 吉原秀輔,「ベース樹脂の高熱伝導化による熱可塑性高熱伝導性樹脂の開発」, S&T 出版, 「導電・絶縁材料の電気および熱伝導特性制御」, 2013, 第 3 章第 1 節（３）.

II. Patents

Total 24 unexamined patent applications

- WO2010/050202「高熱伝導性熱可塑性樹脂および組成物および放熱・伝熱用樹脂材料」

- 特開 2011-233608「高熱伝導性熱可塑性樹脂製ヒートシンク」
- WO2011/132390「高熱伝導性熱可塑性樹脂」
- WO2011/132389「高熱伝導性熱可塑性樹脂」
- 特開 2012-172018「スメクチック液晶ポリマーの製造方法」
- WO2012/108412「高熱伝導性熱可塑性樹脂及び組成物」

Others

特開 2010-150377, WO2011/033815, 特開 2011-231157, 特開 2011-063790, 特開 2011-052204, 特開 2011-084714, 特開 2011-084715, 特開 2011-084716, 特開 2011-132488, 特開 2011-231158, 特開 2011-231159, 特開 2011-231160, 特開 2011-231161, 特開 2012-172019, 特開 2012-188766, 特開 2012-187624, 特開 2013-87196, 特開 2013-82804

Patent not included in this thesis

- 吉原秀輔、渡辺順次、戸木田雅利、特願 2012-176524、「有機部材の製造方法および当該製造方法により得られた有機部材」

III. Presentations

International Conference

- "New thermally conductive thermoplastic liquid crystal polyester"

  S. Yoshihara, K. Matsumoto

  AWPP2012, August 2012.

Domestic Conferences (Japanese)

- 「主鎖型液晶性ポリエステルの結晶ラメラの配向と熱伝導性」

  吉原秀輔、江﨑俊明、中村充、渡辺順次、松本一昭

  日本化学会第 92 春季年会、2012 年 3 月

- 「ベース樹脂の高熱伝導化による新しい射出成形用高熱伝導性樹脂を開発」

  吉原秀輔、江﨑俊明、中村充、坂口雅史、松本一昭、渡辺順次

  第 61 回高分子年次大会　記者発表、2012 年 5 月

- "Lamellar crystal alignment of main chain liquid crystal polyester and thermal conductivity" (Oral presentation in English.)

S. Yoshihara, T. Ezaki, M. Nakamura, J. Watanabe, M. Sakaguchi, K. Matsumoto

第 61 回高分子学会年次大会、2012 年 5 月

- 「高熱伝導性を示す新規熱可塑性液晶ポリエステル」

  松本一昭、吉原秀輔

  プラスチック成形加工学会第 23 回年次大会、2012 年 6 月

- 「カネカの熱対策材料」

  吉原秀輔

  第 241 回新規事業研究会月例研究会、2012 年 7 月

- 「樹脂分子鎖の配向が及ぼす樹脂複合材料の熱伝導率への影響」

  吉原秀輔

  環境・エネルギー材料熱物性シンポジウム 2012、2012 年 11 月

- 「主鎖型液晶ポリエステルの結晶ラメラの配向と熱伝導性」

  吉原秀輔、江﨑俊明、中村充、坂口雅史、松本一昭、渡辺順次

  第 20 回日本ポリイミド・先端芳香環高分子研究会、2012 年 12 月

- 「ベース樹脂の高熱伝導化技術とその応用展開」

  吉原秀輔

  技術セミナー、「パワーデバイス用高分子材料における高耐熱・高熱伝導化と開発技術動向」、サイエンス&テクノロジー株式会社主催、2013 年 4 月

- 「植物由来原料を用いた熱伝導性液晶ポリマーの開発」

  吉原秀輔、坂口雅史、松本一昭

  第 2 回 JACI/GSC シンポジウム、2013 年 6 月

- 「等方性複合材料における主鎖型液晶性ポリエステルマトリックスの高熱伝導性」

  吉原秀輔、戸木田雅利、坂口雅史、松本一昭、渡辺順次

  第 62 回高分子討論会、2013 年 9 月

- 「ベース樹脂の高熱伝導化技術の開発と熱伝導のメカニズム」

  吉原秀輔

  技術セミナー、「樹脂、フィラーの両面から見た高熱伝導樹脂の低フィラー化～ベース樹脂の分子デザインとフィラーの配向制御～」、技術情報協会主催、2013 年 9 月

Domestic Conferences not included in this thesis (Japanese)

- 「主鎖型液晶性ポリエステル表面に現れるマイクロオーダー凹凸周期構造」

  奥田周平、吉原秀輔、姜　聲敏、戸木田雅利、渡辺順次

  平成 24 年度繊維学会秋季研究発表会、2012 年 9 月

- 「主鎖型液晶性ポリエステル表面に現れるマイクロオーダー凹凸周期構造」

  奥田周平、吉原秀輔、姜　聲敏、戸木田雅利、渡辺順次

  第 61 回高分子討論会、2012 年 9 月

IV. Press Releases

第 61 回高分子学会年次大会記者発表（2012/5/16）、化学工業日報（2012/5/18）、石油化学新聞（2012/5/21）、TechOn（2012/5/21）、日経産業新聞（2012/5/22）、日刊工業新聞（2012/5/25）、ゴムタイムス WEB（2012/5/28）、コンバーテック(2012 年 6 月号 P132)、日経ものづくり（2012 年 7 月号 P26）、プラスチックスタイムス（2013 年 1 月号 P1）

Materials Views (Wiley-VCH)　(http://www.materialsviews.com/)

V. Awards Received

- GSC Poster award, 2nd JACI/GSC Symposium, June 2013.